Tevhide Ayça YILDIZ

A Ph.D.Thesis

AGU 2023

THE SIMULATIONS OF AMORPHOUS BORON MATERIALS

A THESIS
SUBMITTED TO THE DEPARTMENT OF MATERIALS SCIENCE AND MECHANICAL ENGINEERING
AND THE GRADUATE SCHOOL OF ENGINEERING AND SCIENCE
OF ABDULLAH GUL UNIVERSITY
IN PARTIAL FULFILLMENT OF THE REQUIREMENTS
FOR THE DEGREE OF
DOCTOR OF PHILOSOPHY

By
Tevhide Ayça YILDIZ
January 2023

THE SIMULATIONS OF AMORPHOUS BORON MATERIALS

A THESIS
SUBMITTED TO THE DEPARTMENT OF MATERIALS SCIENCE AND MECHANICAL ENGINEERING
AND THE GRADUATE SCHOOL OF ENGINEERING AND SCIENCE OF ABDULLAH GUL UNIVERSITY
IN PARTIAL FULFILLMENT OF THE REQUIREMENTS
FOR THE DEGREE OF
DOCTOR OF PHILOSOPHY

By
Tevhide Ayça YILDIZ
January 2023

SCIENTIFIC ETHICS COMPLIANCE

I hereby declare that all information in this document has been obtained in accordance with academic rules and ethical conduct. I also declare that, as required by these rules and conduct, I have fully cited and referenced all materials and results that are not original to this work.

Tevhide Ayça YILDIZ

REGULATORY COMPLIANCE

Ph.D.Thesis titled “The Simulations of Amorphous Boron Materials” has been prepared in accordance with the Thesis Writing Guidelines of the Abdullah Gül University, Graduate School of Engineering & Science.

Prepared By	Advisor
Tevhide Ayça YILDIZ	Prof. Murat DURANDURDU

Head of the Materials Science and Mechanical Engineering Program

Asst. Prof. Çağatay YILMAZ

ACCEPTANCE AND APPROVAL

Ph.D.thesis titled “The Simulations of Amorphous Boron Materials” and prepared by Tevhide Ayça YILDIZ has been accepted by the jury in the Materials Science and Mechanical Engineering Graduate Program at Abdullah Gül University, Graduate School of Engineering & Science.

11 / 01/ 2023

JURY :

Advisor : Prof. Murat DURANDURDU .....

Member : Prof. Mehmet ŞAHİN .....

Member : Prof. Ercan KARAKÖSE .....

Member : Prof. Zeki BÜYÜKMUMCU .....

Member : Prof. Hakan USTA .....

APPROVAL:

The acceptance of this Ph.D. thesis has been approved by the decision of the Abdullah Gül University, Graduate School of Engineering & Science, Executive Board dated ….. /….. / 2023 and numbered ……..…… .

…….. /…….. / ……..

Graduate School Dean

Prof. İrfan ALAN

ABSTRACT

THE SIMULATIONS OF AMORPHOUS BORON MATERIALS

Tevhide Ayça YILDIZ
Ph.D. in Materials Science and Mechanical Engineering
Advisor: Prof. Murat DURANDURDU

January 2023

Boron-based materials and their technological applications have great interests in many scientific and technological areas from materials science to medicine. This doctorate thesis was prepared for the purpose of investigating the atomic structure, electrical and mechanical properties of different boron based amorphous materials by using an ab-initio molecular dynamics technique. The results obtained via a computational method were presented in three main chapters. In the Chapter 3, the influence of hydrogenation on the atomic structure and the electronic properties of amorphous boron nitride (*a*-BN) was examined. The structural evaluation of *a*-BN and the hydrogenated (*a*-BN:H) models revealed that their short-range order was mainly similar to each other. Hydrogenation suppressed the formation of twofold coordinated chain-like structures and tetragonal-like rings and leaded to more sp^2 and even sp^3 bonding. Furthermore, hydrogenation was found to have an insignificant impact on the electronic structure of *a*-BN. Secondly, in the Chapter 4, an amorphous boron carbide (a-B_4C) model was generated. The pentagonal pyramid-like motifs were found to be the main building units of B atoms in a-B_4C and some of which yielded the development of B_{12} icosahedra. On the other hand, the fourfold-coordinated units were the leading configurations for C atoms. a-B_4C was a semiconducting material and categorized as a hard material. In the Chapter 5, amorphous boron carbides (B_xC_{1-x}, $0.50 \leq x \leq 0.95$) were systematically created. With increasing B/C ratio, more closed packed materials having pentagonal pyramid motifs form. All models were semiconducting materials. Some amorphous compositions were proposed to be hard materials.

Keywords: *Amorphous, Hydrogenation, Boron Nitride, Boron Carbide, Ab-initio molecular dynamics technique*

ÖZET

AMORF BOR MALZEMELERİN SİMÜLASYONU

Tevhide Ayça YILDIZ
Malzeme Bilimi ve Makine Mühendisliği Anabilim Dalı Doktora
Tez Yöneticisi: Prof. Dr. Murat DURANDURDU

Ocak 2023

Bor esaslı malzemeler ve teknolojik uygulamaları malzeme biliminden tıp alanına kadar birçok bilimsel ve teknolojik alanda büyük bir ilgi görmektedir. Bu doktora tezi, ab-initio moleküler dinamik tekniğini kullanarak farklı amorf bor malzemelerin atomik yapısını, elektronik ve mekanik özelliklerini incelemek amacıyla hazırlanmıştır. Hesaplamalı metot aracılığıyla elde edilen sonuçlar üç ana bölümde rapor edilmiştir. Bölüm 3'te, amorf bor nitrürün (*a*-BN) atomik yapısı ve elektronik özelliklerine hidrojen eklemenin etkisi incelenmiştir. *a*-BN ve dört farklı hidrojen konsantrasyonuna sahip *a*-BN:H modellerinin yapısal değerlendirmeleri kısa erim düzenlerinin esas olarak birbirleriyle aynı olduğunu göstermiştir. Hidrojenasyon, iki kat koordinatlı zincir benzeri yapıların ve dörtgen benzeri halkaların oluşumunu baskılar ve daha fazla sp^2 ve hatta sp^3 bağı oluşmasına sebep olur. Ayrıca, hidrojenasyonun *a*-BN'nin elektronik yapısı üzerinde önemsiz bir etkiye sahip olduğu görülmüştür. İkinci olarak, bölüm 4'te, amorf bor karbür (a-B_4C) modeli oluşturuldu. B atomları için beşgen piramit benzeri motifler, a-B_4C'deki ana yapı birimleridir ve bazıları B_{12} ikosahedralarının oluşumuna sebep olur. Öte yandan, dört kat koordinatlı birimler C atomları için önde gelen konfigürasyonlardır. a-B_4C yarıiletken bir malzemedir ve sert malzeme olarak kategorize edilebilir. Bölüm 5'te, farklı B oranlarına sahip amorf bor karbür bileşikleri (B_xC_{1-x}, $0.50 \leq x \leq 0.95$) oluşturulmuştur. Artan B/C oranıyla, beşgen piramit motiflerden oluşan daha kompakt malzemeler oluşur. Amorf bor karbür modellerin hepsi yarı iletken malzemelerdir. Bazı amorf bileşiklerin sert malzemeler olduğu önerilmiştir..

Anahtar Kelimeler: *Amorf, Hidrojenleşme, Bor Nitrür, Bor Karbür, Ab-initio moleküler dinamik tekniği*

Acknowledgements

I would like to extend thanks to many people who so generously contributed to the work presented in this thesis.

First of all, special mention goes to my respectable supervisor Prof. Murat DURANDURDU for providing me with the oppurtinity to do research under his supervision. I would like to express gratitude to him for the guidance, caring, patience, enlighting comments and insprising advices during the years of my PhD.

Similar, I would like to profoundly thank the members of my thesis committee throught my research, Prof. Mehmet ŞAHİN, Prof. Ercan KARAKÖSE, Prof. Zeki BÜYÜKMUMCU and Prof. Hakan USTA for their valuable contributions and advices.

I acknowdledge the Council of Higher Education (YÖK) to provided financial support via 100/2000 Doctorate Scholarship during my PhD study. This dissertation was also supported by The Scientific and Technological Research Council of Turkey (TÜBİTAK) under 117M372 project number and 2211-C National PhD Scholarship Program in the Priority Field in Science and Technology. The calculations were run on the TÜBİTAK ULAKBİM, High Performance and Grid Computing Center (TRUBA) resources.

I also would like to show my appreciation to great people who my team members, Dr. Ayşegül Özlem KARACAOĞLAN and Dr. Duygu TAHAOĞLU for their supporting and intellectual friendships.

Last, but not the least, I would like to my deepest appreciation to my family: my beloved parents Nuran and Köksal ÜÇHÖYÜK, and my brother Muhammed Ünsal ÜÇHÖYÜK for their endless love, supports and encouragement during whole my life.

Eventually, my innermost thanks go to the meanings of my life: my husband Mehmet YILDIZ and my little girl Arya YILDIZ. Life is much more beautiful and meaningful with you.

TABLE OF CONTENTS

LIST OF FIGURES

LIST OF TABLES

LIST OF ABBREVIATIONS

μ	: Shear Modulus
a- B_4C	: Amorphous Boron Carbide
a-BN	: Amorphous Boron Nitride
a-BN:H	: Amorphous Hydrogenated Boron Nitride
B	: Boron
B_2O_3	: Boron Oxide
B_4C	: Boron Carbide
BADF	: Bond Angle Distribution Function
BN	: Boron Nitride
C	: Carbon
c-BN	: Cubic Boron Nitride
CG	: Conjugate Gradient
CNs	: Coordination Numbers
CRN	: Continuous Random Network
DFT	: Density Functional Theory
DZ	: Double-ζ
DZP	: Double-ζ Polarized
E	: Total Energy
E	: Energy
E	: Young Modulus
EDOS	: Electron Density of States
EOS	: Equation of State

GGA	: Generalized Gradient Approximation
h-BN	: Hexagonal Boron Nitride
HEFs	: Hybrid Exchange Functionals
H_v	: Vickers Hardness
K	: Bulk Modulus
LDA	: Local Density Approximation
MD	: Molecular Dynamics
N	: Nitrogen
N	: Number of Atom
NAO	: Numerical Atomic Orbitals
NMR	: Nuclear Magnetic Resonance
P	: Pressure
PCF	: Pair Correlation Function
PDF	: Pair Distribution Function
PDOS	: Partial Density of States
PECVD	: Plasma Enhanced Chemical Vapor Deposition
PPDFs	: Partial Pair Distribution Functions
r-BN	: Rhombohedral Boron Nitride
RDF	: Radial Distribution Function
SIESTA	: Spanish Initiative for Electronic Simulations with Thousand Atoms
T	: Temperature
TDOS	: Total Density of States
w-BN	: Wurtzide Boron Nitride
ν	: Poisson Ratio

To my beloved family

Chapter 1

Introduction

1.1. Why Boron?

As many scientists studied on boron said that *'Boron is a unique and essential element for life and living'*. When considering the capacity of structure and bonding of boron, as if it looks like that boron wrote the rules of the game itself. For a long time, there have been prevalent discussions across different areas of science and technology all related to the simple element of boron. So, what is exciting about boron for scientists and researchers? There are many striking considerations behind these. Now let us explain the reasons, first of all, as importance of boron for countries, especially Türkiye, and then give brief information of historical process, physical and chemical properties and usage areas of boron to understand its importance of boron scientifically.

1.2 Boron Sources

The cosmic abundance of boron is relatively low compared to hydrogen, carbon, nitrogen and oxygen[1]. Although it has low abundance, it is found in soil (10-20 ppm), rocks (0.5-9.6 ppm) and water (0.01-1.5 ppm)[2]. However, it is never found as a free element naturally because it is eager to form compound with C and other elements owing to its high chemical affinity character. Its mineral forms such as borax, kernite, pandermite and hydrated sodium borates are fundamental commercial boron minerals[2].

1.2.1 The Shining Star of Türkiye: Boron

The essential boron deposits, which are described by scientists as the energy source of 21st century, are found in Türkiye with a fraction of approximately 73% of the world's total reserve. The most abundant boron reserves in Türkiye are tincal and

colemanite and these deposits are placed at Kütahya-Emet, Balıkesir-Bigadiç and Bursa-Kestelek[2].

Türkiye is known as the leader country that produces the refined boron products. As shown in Figure 1.1, boron products are commonly used in Türkiye for necessities such as glass, ceramic, cleaning-detergent, adhesive, etc.

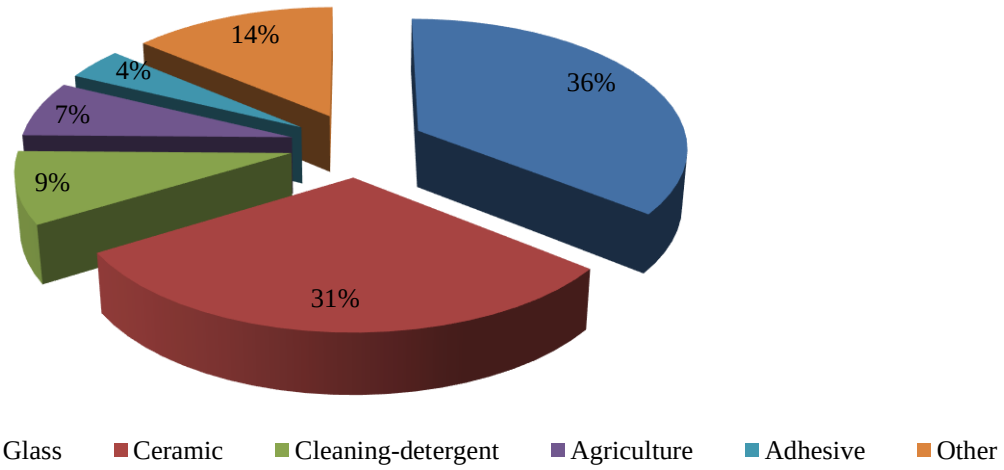

Figure 1.1 Distribution of usage areas of boron in Türkiye[2].

Boron, which should be used in many important areas as well as domestic requirements and versatile material, has potentials to play key roles in the development of significant technological innovations, especially in advance technology products. Hence, it is important to develop necessary research projects on boron and boron-based compounds for the future of Türkiye.

1.2.2 The Situation of Boron in the World

The importance of boron is gradually increasing all over the world due to the decrease in raw material and energy sources each day. Türkiye is followed by Russia and USA with 7.7% and 6.2%, respectively, in terms of total reserve of boron as presented in Figure 1.2.

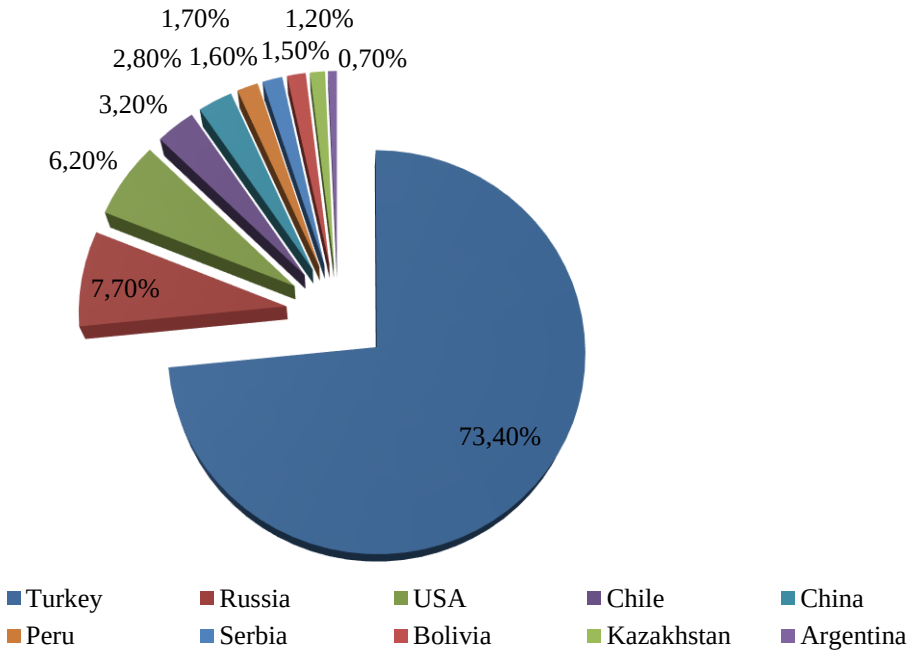

Figure 1.2 Distribution of the total boron oxide(B_2O_3) reserves of the world by country[2].

The consumption of boron products and the usage areas on industrial basis in the world exhibit substantial differences by countries. From general perspective, glass sectors with a fraction of 47% are the highest ratio whereas the cleaning-detergent products with a fraction of 2% are the lowest one on sectoral basis as shown in Figure 1.3.

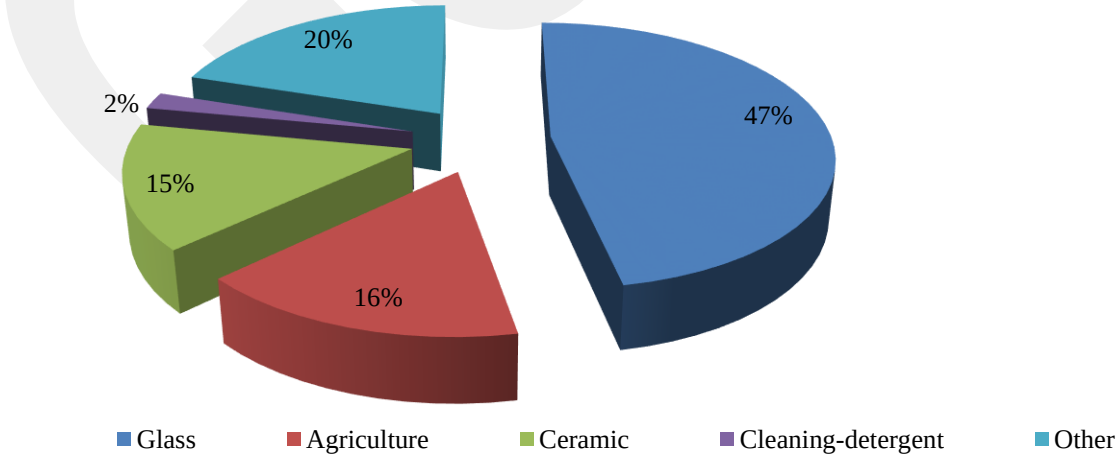

Figure1.3 Distribution of usage areas of boron in the world[2].

1.3 Application Areas of Boron

It is known that the chemistry of boron owns multi facets. Boron has numerous application areas ranging from medicine sectors to space technologies as depictured in Figure 1.4.

Figure 1.4 The versatility of boron in all areas of application.

The boron compounds have been used by pharmacologist for several decades and some boron compounds which are called as caged-boron compounds (carboranes) are widely used in medicinal chemistry[3]. As known, boron has two essential isotopes: ^{10}B and ^{11}B. ^{10}B isotope appears to be a high absorption cross section and hence it is categorized as a good neutron absorber. It can have applications in nuclear reactors in order to control nuclear reactivity and to shutoff rods[4]. In 1936, four years later after the discovery of neutrons, Locher[5] suggested, for the first time, the possible usage of boron compounds as well, in boron neutron capture therapy for the purpose of detecting cancer cells. Because of the electron-deficient character of boron, it can find possible applications in energy-conversion devices, for example, organic light emitting diodes, organic photovoltaics and organic field effect transistors[6]. Thanks to the lightness of boron and the capacity of forming B-H bonds, boron-based materials can be thought as alternative materials[7] for chemical hydrogen storage. The combination of compelling properties of boron such as high melting point, oxidation resistance etc. suggest its possible applications in aerospace technology[4,8–11] as well.

1.4Boron Chemistry

1.4.1 A Brief History of Boron Element

The name of boron is coined from the Arabic ‘buraq’, that was the name for borax[12]. The history of boron, similar to other light elements such as lithium and beryllium, dates back to the early phase of the universe, which is called Big Bang nucleosynthesis[1]. Boron was not identified as an element until 1808. For the first time, two French chemists Joseph Louise Gay-Lussac and Louise Jacques Thenard, and a British chemist, Sir Humphry Davy, individually separated boron during the heating processes of B_2O_3 with potassium metal[12]. In 1824, boron is defined as an element by Swedish chemist Jöns Jacob Berzelius, who discovered modern chemical notation and considered to be one of the fathers of modern chemistry[13]. In 1892, a purer form of boron (containing ~90% boron) was isolated by Henry Moisson[12]. In 1909, a major breakthrough for boron chemistry was accomplished by American chemist Ezekiel Weintraub by producing pure boron with ~99% impurity by sparking a mixture of boron chloride and hydrogen[12].

1.4.2 Physical and Chemical Properties of Boron Element

Boron is one of the closest neighbors to carbon and the lightest member of the IIIA group, which is called as the aluminum family, in the periodic table. However, it is an intriguing member of family. All other members of the group are metal whilst boron is the sole nonmetallic element[14]. Boron exhibits novel and splendid chemical and physical features: it has low densities ranging from ~2.34 to 2.52 g/cm^3, quite high bulk modulus (~185-227 GPa) and high melting points (>2000 °C) and hence hardness and neutron-capturing capability[15–18]. In addition to these superior characteristics, one of the essential properties of boron is that it shows electron deficiency nature. As known boron has three valence electrons, however it must be occupied four orbitals. By means of this situation, boron can have ‘*two-center-two-electron bonds (2c2e)’* and exceptional *‘multi-center-two-electron bonds’*. Via multi-center bonds concept, boron has large numbers of allotropes, 16 in total[19,20], four of which α-rhombohedral[21–23], β-rhombohedral[24], γ-orthorhombic[25,26] and β-tetragonal boron structures[27], are accepted to be thermodynamically stable. Now, let us mention them concisely.

1.4.2.1 α-Rhombohedral Boron Crystals

The name of α-rhombohedral boron comes from a space group of R-3m. Amongst boron allotropes, α-rhombohedral crystal presents the simplest structural motif and it is generally symbolized with α-B_{12} since the unit cell possesses 12 boron atoms in the rhombohedral settings. Namely, α-rhombohedral boron holds one icosahedron in each rhombohedral unit cell[28]. Figure 1.5 presents the unit cell in a hexagonal (a) and rhombohedral (b) structure[28]. As exhibited in Figure 1.5, the boron atoms are positioned on two six-fold sites and each one is also crystallographically independent of each other.

α-rhombohedral boron can have different color, red and maroon color and it exhibits the different electronic structure at room temperature. Its direct band gap was anticipated to be 1.94 eV whereas its indirect band gap was found to be 1.54 eV[29]. The bulk modulus of α-rhombohedral boron was anticipated as 208 GPa and 213-224 GPa theoretically and experimentally, respectively[29,30]. α-rhombohedral boron possesses several remarkable qualities, for example, self-healing from radiation damages and a high hole mobility. By means of its extraordinary characters, it is suitable to be an excellent candidate for novel electronic devices such as direct energy conversion devices and neutron detectors[31].

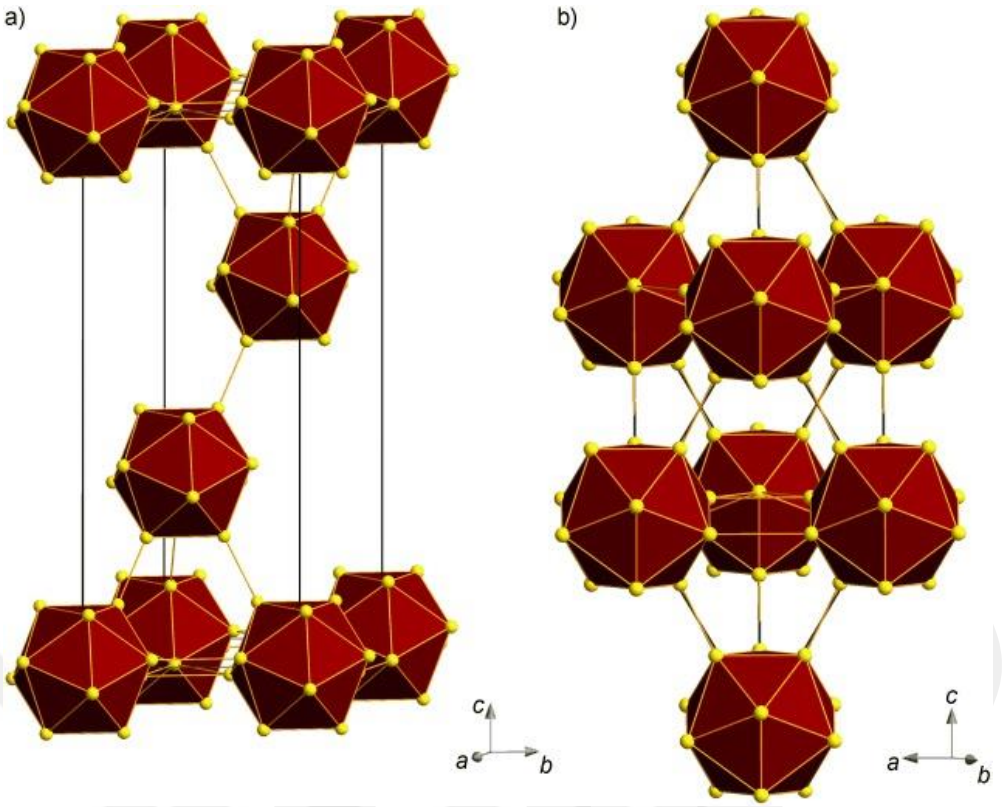

Figure 1.5 Unit cells of α-boron: in different settings a) hexagonal settings, b) rhombohedral[28]. Copyright 2009 John Wiley and Sons

α-rhombohedral boron can be procured using different protocols. The crystallization amorphous boron is the well-known technique to get high quality α-rhombohedral boron samples[32,33]. Another possible and effective method of synthesizing α-rhombohedral boron is pyroltic decomposition of boron trihalogenides on surfaces[34].

1.4.2.2 β-Rhombohedral Boron Crystals

The crystal arrangement of β-rhombohedral boron is based on different forms. The first basic description of β-rhombohedral boron was provided by Kolakowski in 1962[35]. Figure 1.6(a) illustrates its unit cell. The more modern view on the structure of β-rhombohedral boron was enhanced by Geist et al. and Hoard et al. in 1970[36,37]. β-rhombohedral boron owns the space group R-3m, parallel to α-rhombohedral boron, however its rhombohedral unit cell is considerably larger than that of α-rhombohedral boron[28].

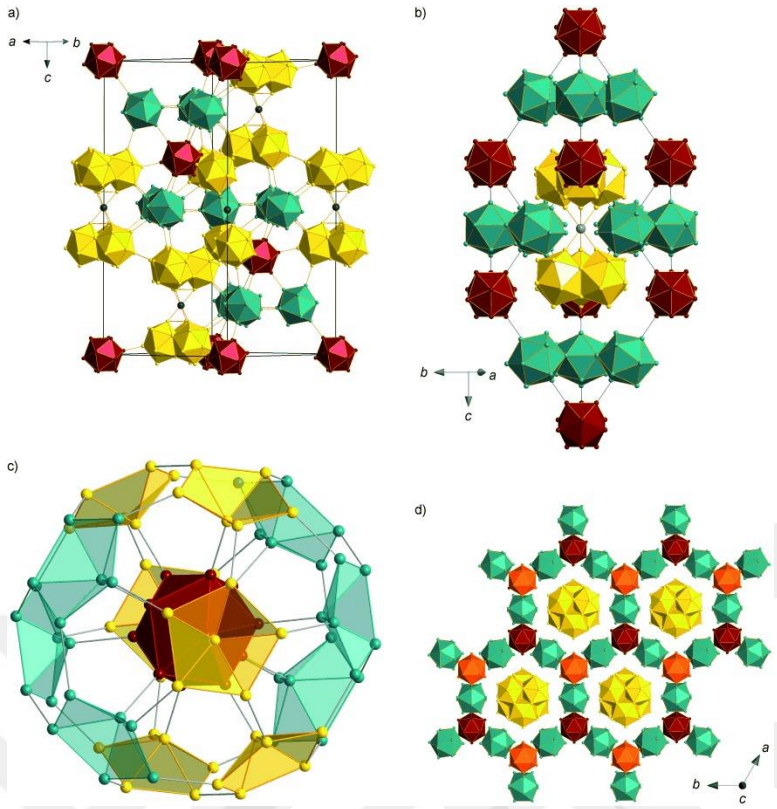

Figure 1.6 Different descriptions of the unit cells of β-boron: a) hexagonal settings, b) rhombohedral settings, c) B_{84} unit, d) Kagome net of icosahedra[28]. Copyright 2009 John Wiley and Sons

In a rhombohedral structure, as given in Figure 1.6(b), the icosahedra are located at the corners and in the middle of the edges. In other words, the unit cell has four icosahedra in total. Two B_{28} units are positioned on the body diagonal, which compose of three icosahedra and connected with boron atom in the middle of the rhombohedral unit cell[28]. The B_{84} units are shaped by combining twelve boron atoms of a central icosahedron with twelve half-icosahedra and identified as super-icosahedra[38]. These super-icosahedra in β-rhombohedral boron follow the arrangements of the cubic close packing of spheres. The B_{84} unit (Figure 1.6(c)) is formed three shell sub-nanoparticles: B_{12} icosahedron with a usual diameter (nearly 0.8 nm) is located inside and it is surrounded by a B_{12} sheath[28]. Lastly, in the Figure 1.6(d), the crystal structures of β-rhombohedral boron are illustrated via Kagome nets, which is a lattice motif found in a crystal arrangement and consists of corner-connected triangles of atoms. The Kagome nets of icosahedra possess an ABC stacking that is vertical to the c axis[39].

β-rhombohedral boron is a grayish black in color and has a semiconducting character[40]. The melting point is between 2450-2723 K and its bulk modulus is 185-210 GPa[41].

β-rhombohedral boron can be obtained by different chemical processes such as the crystallization of the boron melt[12] and purification by zone-melting[24].

1.4.2.3 γ-Orthorhombic Boron Crystal

The production of a new boron structure at pressure higher than 10 GPa and at temperatures nearly 1500 °C was reported by Wentorf in 1965[15]. However, the existence of this form has been contradictory until 2008[42,43]. This high pressure boron phase was studied both experimentally and theoretically[25,42,43]. According to these studies, the high-pressure crystal presents an orthorhombic crystal belonging to Pnnm space group. Its unit cell comprises just 28 atoms. Thus, the new boron form is called as γ-orthorhombic boron crystal and it is symbolized with γ-B_{28}[25]. The crystal arrangement of γ-orthorhombic boron can be defined as a distorted cubic packing of B_{12} clusters having B_2 pseudo pair motifs (dumbbells) positioned at the octahedral sites[44].

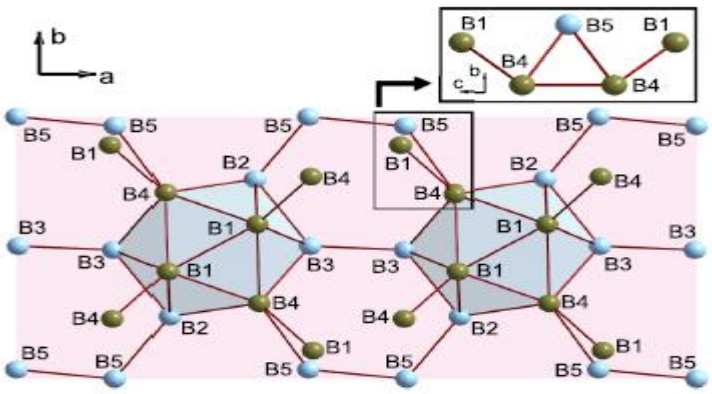

Figure 1.7 Perspective view of γ-orthorhombic boron crystal[44]. Copyright 2011 American Physical Society

Several experimental studies show that γ-orthorhombic boron can be synthesized under different pressure (7-20 GPa) and temperature (1500-2500 K) conditions depending on starting materials, like amorphous boron, α-B_{12} and β-B_{106}[45].

γ-orthorhombic boron is a semiconductor material with band gap energy of nearly 1.7 eV. Since it is optically transparent and thermally stable (beyond 1000 K in

the air), it can be categorized as an attractive material for materials science and technology[26].

1.4.2.4 β-Tetragonal Boron Crystal

Initially, two different tetragonal structures of boron were reported. The first tetragonal form recommended by A.W. Laubengayer et al., which is named α-tetragonal boron, was considered as a true adaptation of pure boron and was investigated by J.L. Hoard et al. in 1958[46–48]. A later study showed that this structure, actually, is related to the tetragonal phase of boron-rich forms with a three-dimensional structure of B_{12} icosahedra stabilized by small amount of impurities[49].

The second one, which has distinct denomination such as β-tetragonal, tetragonal II or tetragonal III, was first discovered by Tally et al. in 1960[50]. After nearly two decades, its structural investigation was executed by Vlasse et al.[51]. In the later years, various experimental studies on the β-tetragonal boron were subjected[52,53]. However, its physical characteristics have not exactly clarified in these studies. β-tetragonal boron was found to be stable in region between β-rhombohedral and γ structures[54] at high pressure. In addition to these experimental studies, there have been limited numbers of theoretical investigations on β-tetragonal boron[55,56]. Its theoretical band gap energy was calculated to be 1.16-1.54 eV[56], quite parallel to 1.29-1.50 eV reported for β-rhombohedral boron[57]. No experimental information about its band gap energy has been reported in the literature so far.

According to two different studies belonging to the same theoretical group, the unit cell of β-tetragonal crystal have 190 or 192 atoms[27,51]. Figure 1.8 demonstrates it[56]. The unit cell consists of 196 atoms. It has a tetragonal lattice and is a member of $P4_1$ or $P4_3$ space groups. The crystal comprises of two particular subunits. The first one is a double icosahedron B_{21}. The second one is a single icosahedron B_{12}. These are depicted in different colors in the Figure: grey ones represent the icosahedra while orange ones denote as double icosahedra. The single and double icosahedra are connected to each other as well.

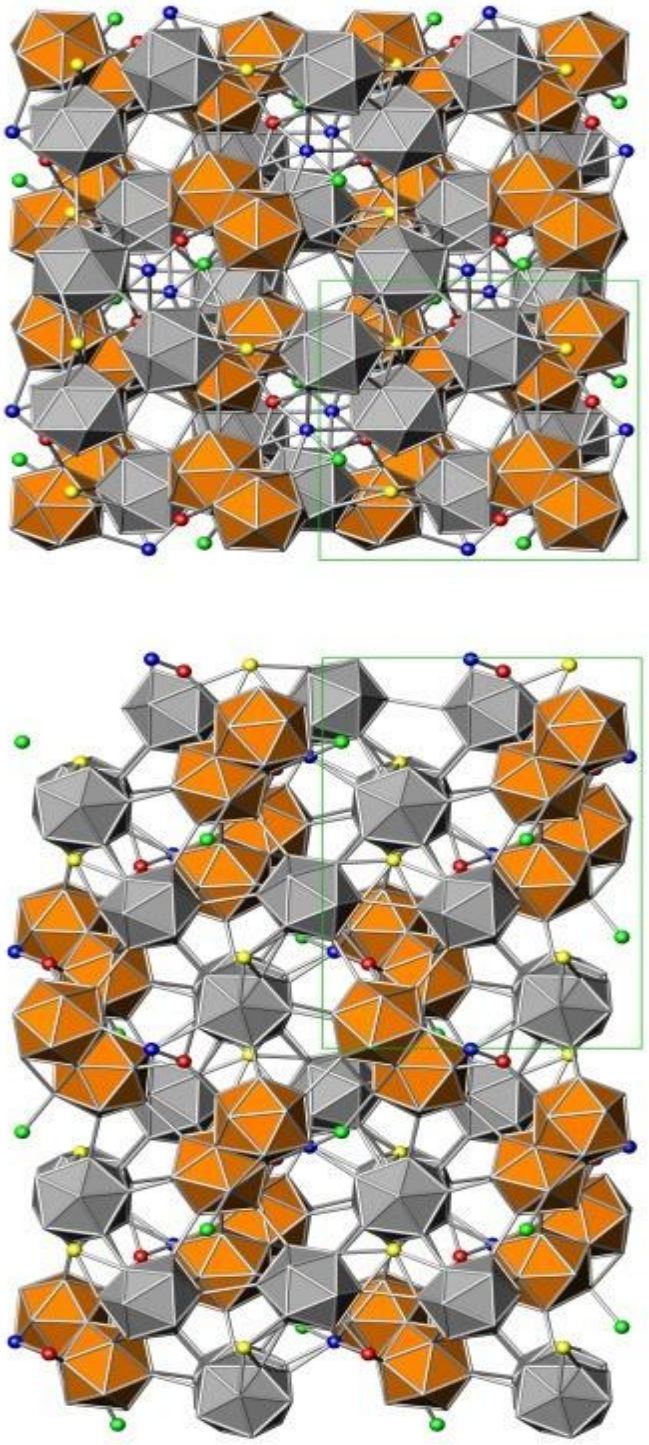

Figure 1.8 Presentationβ-tetragonal boron viewed along two different directions, <001> (upper panel) and <100> (lower panel)[56]. Copyright 2015 Elsevier

On account of the complex bonding and varied crystal structures, the investigations of boron allotropes still will continue to be a charming, however, challenging research issue for researchers and scientists.

1.5 Boron-Based Materials

As well as the studies on boron allotropes, the characteristics of boron make it possible to produce boron-based materials with other elements such as carbon, nitrogen and hydrogen. The created different boron-based materials have been contributing to materials science by providing opportunities to explore and pioneer improver and innovator materials. Before presenting our studies in detail, let's provide some information on boron-based materials studied in this thesis.

1.5.1 Boron Nitride

Boron nitride (BN) is considered as one of the essential ceramics and is distinctive among the III-V materials in its capacity to form strong covalent bonds. BN has been of great interest across a wide range of research areas in materials science for long years in so far as its doozy specialties, for example, good thermal conductivity, a wide band gap and the capacity of hydrogen uptake[58–68]. In virtue of these features, BN is a likely candidate for many areas and can be used various high technological applications. BN own four different crystal arrangements which will be explained below briefly. The structures of boron nitride are depicted in Figure 1.9[69].

1.5.1.1 Hexagonal Boron Nitride (h-BN)

The primarily synthesized form of BN is a hexagonal arrangement (h-BN), that is akin to graphite[70]. h-BN has a rather excellent chemical stability even in monolayer form[71]. Monolayer h-BN is sometimes denotes '*white graphene*' and can be obtained from bulk BN[72]. In two-dimensional layered structure of BN, in the layers, between boron and nitrogen atoms forms hexagonal rings and the B-N bonds are quite strong covalent bonds whilst the layers are hold together by weak Van der Waals force, similar to graphite. Thus, h-BN can effortlessly squeezable under external stresses[73].

The melting point of h-BN is quite high and it is nearly 3000 K. It is insulator and a good thermal conductor[74]. It can be obtained under different protocols. Some of these techniques are chemical reaction between boron and nitrogen compounds[75], hot pressing[76], and chemical vapor deposition methods[77].

h-BN exhibits remarkable electronic properties. Hence, it can be used in a broad range of optoelectronic areas[71] like optical[61,78,79], electro-optical[80,81] and

quantum optics[82]. Because of some physical characters of h-BN, it is favorable in the usage of vacuum technology[83] as well.

There are some discrepancies about the electronic structure of h-BN, specifically, its band gap was reported between 3.0 and 7.5 eV[61,84–86].

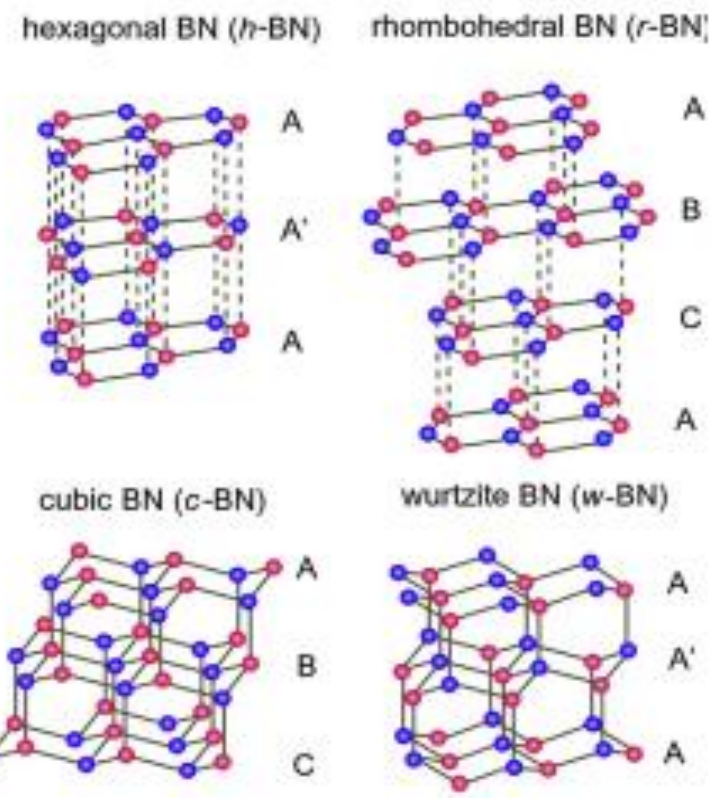

Figure 1.9 The structures of boron nitride[69]. Copyright 2019 Elsevier

1.5.1.2 Rhombohedral Boron Nitride (r-BN)

The second two-dimensional structural form of BN is the rhombohedral one (r-BN)[87]. When the crystal structure of r-BN is investigated, it is seen that its structure is akin to the h-BN arrangement and similarly consists of hexagonal layers with sp^2 bonding. However, the stacking sequence of them is different each other: r-BN occurs a three-layered stacking sequence (ABCABC) whilst h-BN has two-fold stacking arrangement of ABAB[88].

r-BN has a distinctive property from the rest three BN polymorphs. Namely, it can easily transforms into any other BN structures[88] depending on experimental pressure and temperature conditions. r-BN is the least studied BN phase until recent years since

it could be fabricated by just two forms: in a mixture with h-BN or/and small whiskers[89,90].

1.5.1.3 Cubic Boron Nitride (c-BN)

The cubic arrangement of BN (c-BN), which is the diamond-like structure of BN, was synthesized by Wentorf at high temperature and pressure conditions in 1957[91,92]. c-BN owns the zinc blende arrangement and it comprises of fourfold coordinated boron and nitrogen atoms in a three-layered packing arrangement of ABCABC.

c-BN is the most attractive and studied phase amongst of the BN crystals. The most distinguishing characteristic of c-BN is that it is second hardest material[93]. Due to its useful characteristics, c-BN can be thought as a good alternative to diamond[94]. It is known that c-BN is stable at high temperatures relative to diamond. In addition, it does not exhibit any reaction with ferrous metals[95]. Considering all these features, it is a suitable candidate for cutting tool applications.

Similar to diamond, it is a good insulator having band gap energy of ~6 eV and hence it is considered as a perfect material for electronic applications[94]. Unlike diamond, it has not only p-type but also n-type dopant[95]. Due to its wide band gap and capability of n- and p-type doping, it is a desirable material for high temperature and high-power applications in electronic and optical devices.

1.5.1.4 Wurtzide Boron Nitride (w-BN)

The other crystal structure of BN arrangement is the wurtzide boron nitride (w-BN). In 1963, it was reported that w-BN could be obtained in the range of 300-2500 K temperature and under static pressure above 1100 kbar[96]. In addition, a few years later, some studies reported about the formation of w-BN as well as zinc-blende structure under shock compression[97,98]. Namely, in analogy to c-BN, w-BN can form at high temperature and high pressure environments[99–101] but it is a metastable phase of BN[102,103]. Therefore it is rather challenging to achieve its pure phase using common growth methods[104].

w-BN has an isostructural character with other nitrides in group III such as GaN, AlN and InN, for using optoelectronic devices[102]. The optical band gap of w-BN is

investigated for compacted nanoscale w-BN powder and it is found to be nearly 8.7 eV, which is quite coherent with theoretical prediction of 8.5 eV[105,106].

w-BN demonstrates remarkable mechanical features as well. Its hardness is in the range of 24-54 GPa[101,105]. Moreover, some studies speculated that w-BN might be almost as hard as or even harder than diamond[104,107]. Therefore, in recent years, the attention of mechanical properties of w-BN is increasing. As a result of not only micro structural features of w-BN but also mechanical properties for the single phase, w-BN has been exposed[108].

1.5.2 Boron Carbide

Boron carbide is a prominent composition among the carbides due to its notable characters. By combining its properties, it can be adapted for various usages in different technological areas. Let's give some examples about its properties and usage areas. Its high melting point and thermal stability yield the application of boron carbide as a refractory material[109]. Due to its high hardness and low density, it is an model material in ballistic uses[110,111]. Boron carbide is well-known as a good neutron absorber. Therefore, it can be used in nuclear applications[112]. Moreover, it has a semiconducting nature. Thus, it is a good candidate for novel electronic devices[111].

Boron carbide was exposed by Wöhler in the mid 19^{th} century while he was studying pure boron[113]. The material was synthesized with different stoichiometric phases as B_3C and B_6C by Joly in 1883 and by Moisson in 1894, respectively[114]. Until 1934, the stoichiometric B_4C was identified[115] and the investigations about boron carbide were relatively limited. After that time, the studies related to boron carbide including many different boron-carbon compounds have started to attract attentions by scientists. At the beginnings, the researchers mainly focused on determining the phase diagram of complex boron-carbon systems[116,117]. Later, exhaustive studies were done on the purpose of the exploring features of boron carbide[111,118–120]. Nowadays, due to its extraordinary properties, boron carbide has been extensively studied and still continues to arouse curiosity.

The crystal arrangement of boron carbide is one of the fundamental issues of different studies in the literature[111,120–124]. Its primary crystal consists of 12-atom icosahedra located at the vertices of a rhombohedral lattice of trigonal symmetry, belonging to R-3m space group, and the linear chains having 3 atoms. Figure 1.10

illustrates the crystal phase of boron carbide[121]. Because of the elemental boron's affinity to shape cage-like structures of different sizes, the icosahedra within boron carbide form[120,123–126].

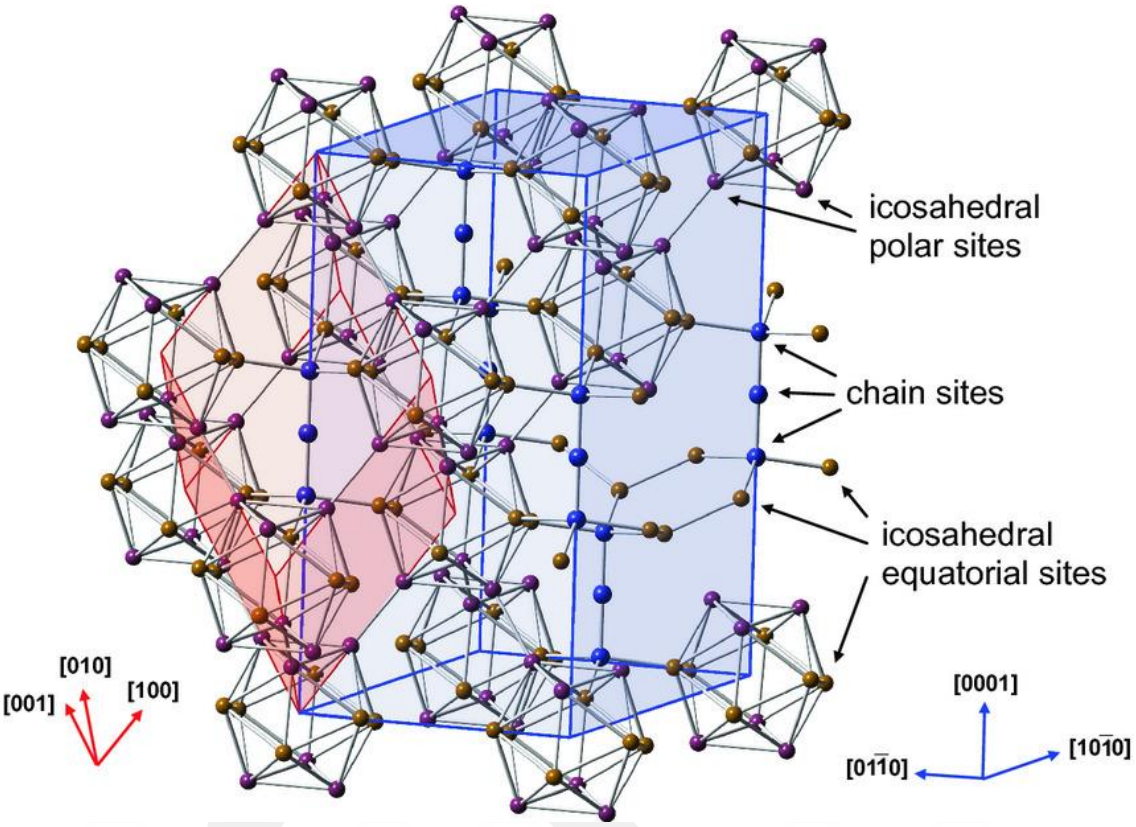

Figure 1.10 The crystalline phase of boron carbide. Its lattice shows the association between the rhombohedral (red) and the hexagonal (blue) unit cells[121]. Copyright 2011 John Wiley and Sons

In fact, by using diffraction measurement methods, information about the crystal arrangement of boron carbide can be obtainable. However, owing to the similarities of boron and carbon atoms in terms of electronic and nuclear scattering cross-section (^{11}B and ^{12}C isotopes), it is pretty hard to separate these two atoms via characterization protocols.

Scientists started from the question '*What is the true stoichiometrical phase for boron carbide?*' in order to determine its phase diagram. The phase diagram of boron carbide has been controversy amongst scientists for years. After meticulous studies, different types of the B-C phase diagram were propounded in the literature[127–132]. Figure 1.11 exhibits commonly used ones[129,130]. It is most recognized that the stable phase of carbon atom is in the range of ~8% C and ~20% C[111,131,132], although single crystal ($B_{3.2}C$ which correspond to ~24% C) was reported[110]. Boron carbide

has a mixture of stable phase beyond ~20% C. Low C content phases, equaled to below nearly 8% C content, are usually accepted to be the stable phase of boron carbide. It is clearly seen that from Figure 1.11, as C content increases (roughly 16% C), similarly, the melting temperature increases.

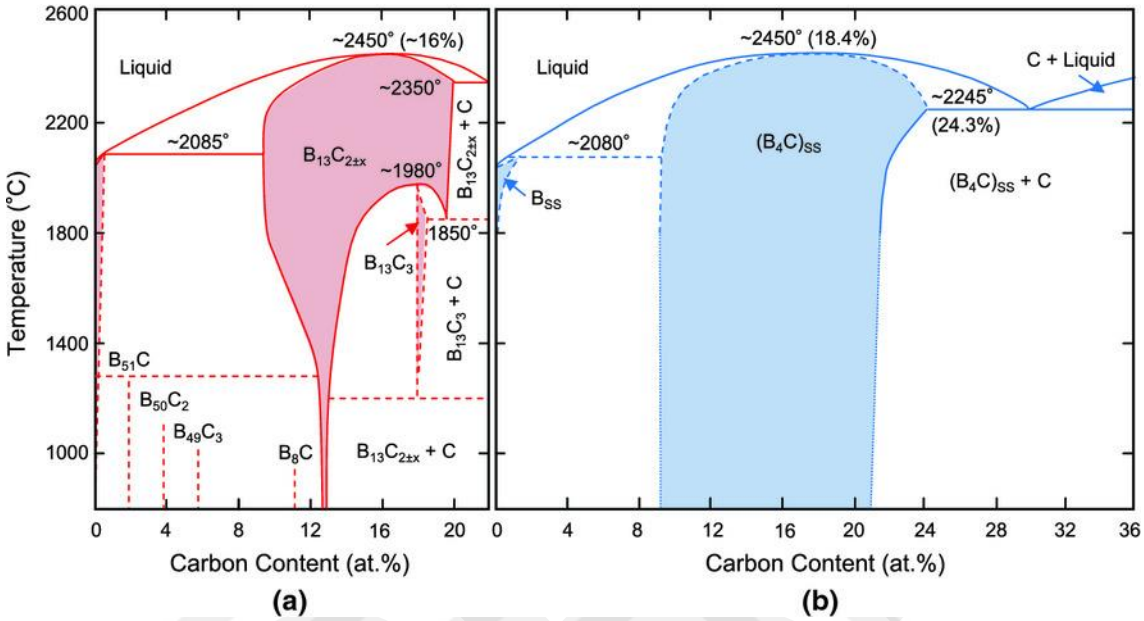

Figure 1.11 Phase diagram of boron carbide[121]due to (a) Ekbom and Amundin,[129]and (b) Beauvy,[130]. Copyright 2011 John Wiley and Sons

1.6 Motivation of the Study

The motivation of this study is based on two pillars. The first one is the technology vision project including 2023 targets of Türkiye offered by The Scientific and Technological Research Council of Türkiye (TÜBİTAK) in 2003[133]. In this report, it is aimed for Türkiye to create its own technologies. In order to achieve this target, making important breakthroughs in the field of technology and focusing on technological innovations are essential. Some of the recommendations expected to accomplish in the 2023 vision of Türkiye are as follows:

- To generate new materials based on technologies related to the production of boron minerals and to model new materials by using ab-initio method,
- To create new energy technologies such as hydrogen and boron fuels alternative to fossil fuel,

- To develop the semiconducting technology,
- To product nanotechnology and advanced ceramic materials (including semiconductor materials),
- To enhance materials technologies (especially ceramic technology based on boron materials).

Considering all these purposes, it is seen that this thesis is quite overlap with the technology vision project of TÜBİTAK.

The second source of the motivation of this study is that Türkiye is a leader country to produce the refined boron products having extraordinary properties. Research on boron-based materials have aroused great interest over many decades for scientists due to their prodigious properties such as high hardness, chemical resistance, low density, superconductivity, high melting temperature, neutron scattering and thermoelectricity. Amongst of the boron-based solids, boron nitride, boron carbide, boron oxide and boron lithium are commonly studied not only experimentally but also theoretically. By virtue of their unique features, they are used in the latest technology areas like power electronic devices, superconductors, heat resistance applications, nuclear reactor coatings, body armor vests, neutron capture therapy method, lithium-ion batteries, and especially semiconductor technology.

Boron-based materials, especially boron carbide, own quite complex structures. Moreover, the crystal structures of some boron-based solids have been debated for many years. In order to understand their local structures, knowing the relationships between physical properties and crystal structures are essential. Although there are some experimental studies as well as limited number of theoretical investigations on their atomic structures, the correlation between their physical properties and crystal structures is not wholly explained yet.

Experimental studies also suggest that boron-based materials can be obtained in amorphous forms under different environments. However, the fundamental questions regarding their amorphous forms are still unsolved e.g., their physical properties, atomic structures, electrical and mechanical characters are not known clearly yet and current experimental protocols cannot provide clear evidence at the atomistic level. Additionally, there are limited numbers of theoretical investigations in the literature, which focus only specific stoichiometries and shed light onto the experimental studies on disordered forms of boron-based materials.

As a result of, taking into all considerations mentioned above, it is seen that there are still some properties to be discovered for boron-based materials to contribute both 2023 vision of Türkiye and materials science.

1.7 Overview

The remainder of this thesis is structured as follows:

After giving some fundamental information about boron and its applications, the importance of boron for Türkiye and world, boron-based materials in studied this thesis in chapter 1, we provide a brief knowledge of computational science and theoretical bases of density functional theory (DFT) in chapter 2.

In chapter 3, the impact of hydrogenation on the microstructure and the electronic behavior of amorphous boron nitride (*a*-BN) is examined via first principles simulations.

In chapter 4, an amorphous boron carbide (a-B_4C) structure is modeled and its physical and chemical properties are revealed in details.

We have modeled amorphous boron carbide compositions with different B concentration (B_xC_{1-x}, $0.50 \leq x \leq 0.95$) and their structural, electrical and mechanical characters are meticulously inspected in chapter 5.

Finally, in chapter 6, the thesis is concluded with a brief summary and a few final remarks for future outlook.

Chapter 2

Theoretical Framework

Computational science is a multi-discipline field combining some branches of science such as physics, applied mathematics and materials science, etc. The aim of scientists who specially focus on the computational science is to examine realistic physics, engineering or mathematics problems by modeling them and then try to comprehend their behaviors. The existence of this scientific area has been the result of the considerable developments in high performance computing over the last few decades and a developing necessity for novelty perspective for scientists in areas where not only theories but also experimental techniques are of limited capability. The limitations of experiments and theories are completely independent of each other. The restrictions of experiments might be caused owing to the high cost of executing experiments, absence of the capability of devices or instruments. On the other hand, the limitations of the theories generally depend upon the lack of analytical solutions of the complex systems.

The developments of computer and computational systems have gained advantages and facilitated to scientists for many improvements in materials science. The computational science used in various physics main fields like atoms and molecular physics, quantum physics and condensed matter physics are commonly categorized with two main topics as direct and inverse methods. In the first method (in direct method), in other words unbiased protocols, as the name suggests, while a material is modeled, there is no needed any prior knowledge from experiments, out of some basic parameters such as its chemical compositions, physical constants, and density. The point to be noted in such an approach requires the usage of an accurate potential. Another important point is to create a model, which is coherent with experiments. Traditional Monte Carlo and Molecular dynamics are two good examples for the direct method. In other respects, in inverse method, the concept is to use important experimental data in order

to generate a model. The reverse Monte Carlo technique is a good example for inverse method[134–137].

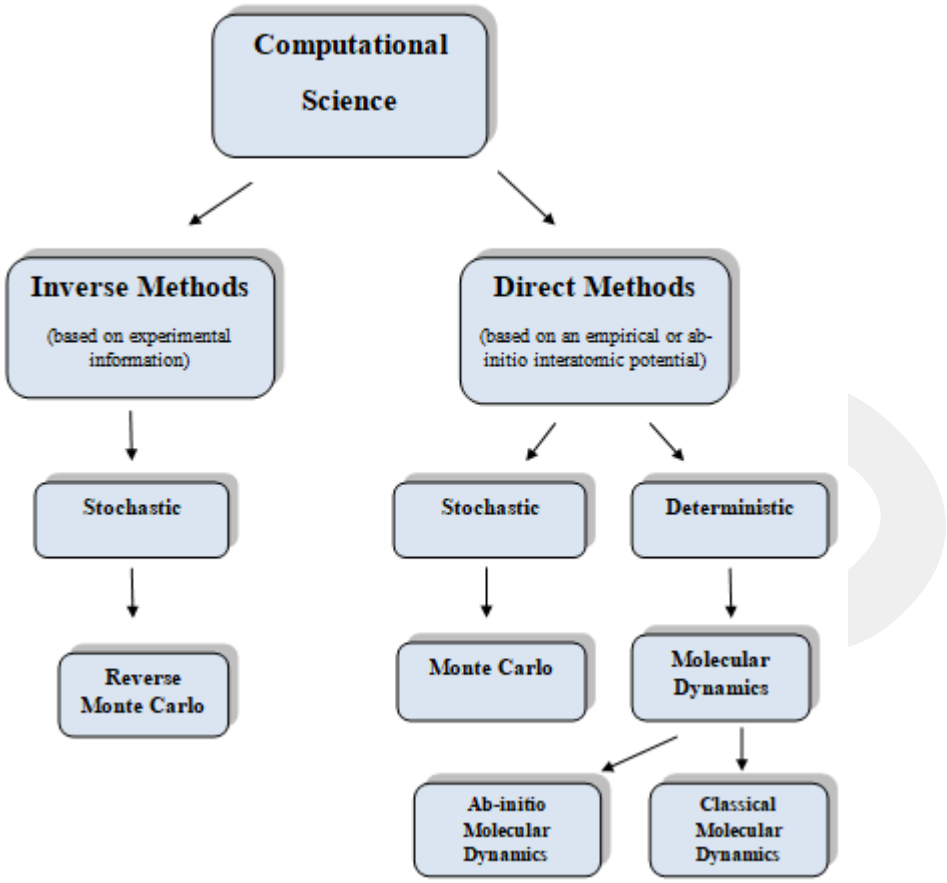

Figure 2.1 Scheme of some computational methods used in materials science.

In this thesis, amorphous models are contracted by using an ab-initio molecular dynamics approach. Before giving the elaborated information of our studies, we purpose to issue a clear, brief, introductory presentation of the most basic equations, important for theoretical bases of our calculations in this chapter.

2.1 Density Functional Theory

2.1.1 An Introduction the Density Functional Theory

Density functional theory (DFT) is known as the one of the most commonly used procedures for ab-initio simulations in order to explore the structure of solids and liquids. The basis of the DFT dates back to 1970s. However, DFT has been gained the essential popularity between physicists, chemists, and materials scientists since the

beginning of the 1990s[138,139]. The success of DFT was supported by the 1998 Nobel Prize to Walter Kohn, who made significant contributions in the development of DFT[140]. In a word, especially, for the past 3 decades DFT has been a fundamental technique for the quantum mechanical calculations of periodic or non-periodic structures. Consequently, what are the mathematical foundations of this method? Let's take a quick look at it now.

2.1.2 The Mathematical Background of Density Functional Theory

The Schrödinger wave equation, in shortly Schrödinger equation, is one of the most fundamental formulas of quantum mechanics, can be written as

$$i\frac{\partial \psi}{\partial t} = \hat{H}\psi \tag{2.1}$$

in the time-dependent form. Here ψ is the wave function for any system. As known, all matter consists of a large number of subatomic particles such as nuclei, electrons and their interactions with each other. Hence, in the atomic units, the Hamiltonian operator, $\hat{H}$, of a system can be given:

$$\hat{H} = -\frac{1}{2}\sum_{i=1}^{n}\nabla_i^2 - \frac{1}{2}\sum_{I=1}^{N}\frac{1}{M_I}\nabla_I^2 - \sum_{i,I}\frac{Z_I}{|\boldsymbol{r_i} - \boldsymbol{R_I}|} + \frac{1}{2}\sum_{i\neq j}\frac{1}{|\boldsymbol{r_i} - \boldsymbol{r_j}|} + \frac{1}{2}\sum_{I\neq J}\frac{Z_I Z_J}{|\boldsymbol{R_I} - \boldsymbol{R_J}|} \tag{2.2}$$

In this equation, the first two terms stand for the kinetic energy of electrons and nuclei, correspondingly, and M_I symbolizes the mass of the nucleus. The other terms denote the potential energy of charged particles, electron-nucleus, electron-electron and nucleus-nucleus, correspondingly. $\boldsymbol{r_i}$ and $\boldsymbol{R_I}$ represent the position vector of the electron and nucleus, correspondingly and Z_I indicates the charge number of the nucleus.

The solution of Equation 2.1 will be quite hard because a macroscopic structure consists of many particles, almost Avogadro's number and its wave function involves lots of parameters (degrees of freedom), and can be expressed as

$$\psi = \psi(\boldsymbol{r_1}, \boldsymbol{r_2} \ldots, \boldsymbol{r_n}, \ldots, \sigma_1, \sigma_2, \ldots, \sigma_n, \boldsymbol{R_1}, \boldsymbol{R_2}, \ldots, \boldsymbol{R_N}, t) \tag{2.3}$$

here σ_i signifies the spin of the electrons. There are several approaches to make the problem easier. The first approximation is the stationary ground state character of the system, which means that $\hat{H}$ depends just upon the state of the system. Hence, assuming that $\hat{H}$ is the time-independent, now let's rewrite the Schrödinger equation,

$$\hat{H}\psi = E_{tot}\psi \tag{2.4}$$

in which E_{tot} symbolizes the total energy of the system. In the circumstances, the wave function for the time-independent form can be defined as below,

$$\psi = \psi(\boldsymbol{r_1}, \boldsymbol{r_2}, \dots, \boldsymbol{r_N}, \dots, \sigma_1, \sigma_2, \dots, \sigma_n, \boldsymbol{R_1}, \boldsymbol{R_2}, \dots, \boldsymbol{R_N}) \tag{2.5}$$

2.1.3 Bohr-Oppenheimer Approximation

The second simplification is the Born-Oppenheimer approximation[141], which is one of the approaches to evaluate the Schrödinger equation of many particle systems having more complex structures than systems including one or two electrons. Let's try to explain this simplification. Since a proton is much heavier, roughly 2000 times, than an electron, the motion of the nucleus (including both proton and neutron) will be very slow compared to that of electrons. This situation is the key point where the Born-Oppenheimer approximation comes into play. The approach separates nucleus and electron motions from each other. It neglects the motion of the nucleus as it very little compared to the motion of the electrons and assumes that the electrons move in the potential caused by the nuclei whose position fixed in space. Consequently, in Equation 2.2, the kinetic energy of the nuclei can be separated out, and the expression based on between nucleus and nucleus interaction can be accepted as a constant which stands for E_{II}. The system just includes the electron-electron and electron-nucleus interactions any more. Now, the eigenvalue equation is expressed for the electronic system and is given by,

$$\hat{H}_{elec}\psi_{elec} = E_{elec}\psi_{elec} \tag{2.6}$$

where ψ_{elec} specifies the wave function including system of n electrons and their interactions in the external field of the fixed nuclei.

$$\psi_{elec} = \psi_{elec}(\boldsymbol{r_1}, \boldsymbol{r_2}, \dots, \boldsymbol{r_N}, \dots, \sigma_1, \sigma_2, \dots, \sigma_n) \tag{2.7}$$

$\hat{H}_{elec}$ presents electronic Hamiltonian and formulated by,

$$\hat{H}_{elec} = -\frac{1}{2}\sum_{i=1}^{n}\nabla_i^2 + \frac{1}{2}\sum_{i\neq j}\frac{1}{|\boldsymbol{r}_i - \boldsymbol{r}_j|} - \sum_{i,I}\frac{Z_I}{|\boldsymbol{r_i} - \boldsymbol{R}_I|} \tag{2.8}$$

The eigenvalue E_{elec} is responsible for the energy states of the system. The total energy, abbreviated E_{tot}, can be computed as:

$$E_{tot} = E_{elec} + E_{II} - \frac{1}{2}\sum_{I=1}^{N}\frac{1}{M_I}\nabla_I^2 \tag{2.9}$$

By means of Equation 2.9, the solution of the problem for the periodic systems like crystalline solids can be more practical.

In 1929, for the first time, purposed by Felix Bloch, Bloch's theorem[142] offered a different perspective for the solution of Schrödinger equation in a periodic potential. According to this theorem, it is accepted that the primitive unit cell has just a few particles, instead of a large number of particles in a crystal. For this situation, the wave functions ψ_{elec} can be converted into the following form

$$\psi_{n\boldsymbol{k}}(\boldsymbol{r}) = e^{i\boldsymbol{k}.\boldsymbol{r}}U_{n\boldsymbol{k}}(\boldsymbol{r}) \tag{2.10}$$

in which n signs the band index (n=1,2,3,….), and **k** refers to reciprocal vector in the first Brillion zone. $U_{n\boldsymbol{k}}(\boldsymbol{r})$ is a function related to periodicity of the crystal

$$U_{n\boldsymbol{k}}(\boldsymbol{r}+\boldsymbol{T}) = U_{n\boldsymbol{k}}(\boldsymbol{r}) \tag{2.11}$$

here $\boldsymbol{T}$ represents a translation vector of the lattice. $e^{i\boldsymbol{k}.\boldsymbol{r}}$ defines a plane wave.

Although the solution of the problem has become a little easier by dint of this approximation, there are still difficulties to straight evaluate the Equation 2.6 owing to the Schrödinger equation for a system having more than a few particles. We can overcome these difficulties by using electron density concept, which is defined in the Equation (2.12), instead of using the electron wave function.

$$n(\boldsymbol{r}) = N\int d\boldsymbol{r_2}\int d\boldsymbol{r_N}\,\psi^*(\boldsymbol{r_1},\boldsymbol{r_2},\ldots\boldsymbol{r}_N)\,\psi(\boldsymbol{r}_1,\boldsymbol{r}_2,\ldots,\boldsymbol{r_N}) \tag{2.12}$$

2.1.4 The Hohenberg-Kohn Theorems

In 1964, the basis of the DFT, Hohenberg-Kohn Theorems[143], were ingeniously proposed. The two theorems are fundamentally specified as follows [144]:

- **Theorem I**

'For any system including interactions of particles in an external potential $V_{ext}(\mathbf{r})$, the potential is uniquely identified via ground state particle density, which stands for $n_0(\mathbf{r})$. Even though, the first Hohenberg-Kohn theorem mindfully proposed that a functional of the electron density exists, the theorem states anything about the actual form of the functional'[145].

- **Theorem II**

'A universal functional for the energy of system E[n] can be determined in respect to the density $n(\mathbf{r})$. The exact ground state energy of the system defines with global minimum value of the functional E[n]. In addition, the density $n(\mathbf{r})$ minimizing the functional is the exact ground state density $n_0(\mathbf{r})$.The two theorems clearly state that, if the exact form of the total energy functional E[n] was described, it could be used by way of the minimization process to accurately find the ground state density $n_0(\mathbf{r})$, from which, in theory, all ground state features could be determined'. Thus, the total energy functional in theory can be written as

$$E[n] = T[n] + E_{int}[n] + \int d^3\, r V_{ext}(\boldsymbol{r}) n(\boldsymbol{r}) + E_{II} \tag{2.13}$$

here T[n] represents the kinetic energy of the interacting electrons, in the meantime, the other terms are the potential energies. The second term signifies electron-electron interaction. The third term is the Coulomb interaction between the electron density n(**r**) and the external field $V_{ext}(\boldsymbol{r})$. The last term is the nuclei-nuclei interaction.

Nevertheless, there is an obstacle to solve the problem for the system of n-interacting electrons' system: The main question here is to define the form of T[n] and E_{int}[n]! Thankfully, this impediment can be overcome by help of the Kohn-Sham approach[146]. Just now, let's take a look at this approximation.

2.1.5 Kohn-Sham Equations

Kohn and Sham propounded a useful approximation to find a solution for the difficulties which mentioned above in 1965. The general concept of the theorem is to substitution of a real system of interacting particles in Equation 2.6 by an artificial system of non-interacting particles having the same charge density n(**r**) of the real system. Now, in addition to the external potential V_{ext}(**r**), all non-interacting particles

depend upon another potential called as the effective potential $V_{eff}(\mathbf{r})$ and is formulated as

$$V_{eff}(\boldsymbol{r}) = V_{ext}(\boldsymbol{r}) + \int \frac{n(\boldsymbol{r}')}{|\boldsymbol{r} - \boldsymbol{r}'|} d\boldsymbol{r}' + V_{xc}(\boldsymbol{r}) \tag{2.14}$$

The second term in the equation presents Hartree potential, which related to the Coulomb correlation between the electrons. $V_{xc}(\boldsymbol{r})$ stands for exchange-correlation potential.To evaluate the Kohn-Sham equation, it is essential to determine the exchange-correlation potential.$V_{xc}(\boldsymbol{r})$ can be computed from the exchange-correlation energy functional $E_{xc}[n(\mathbf{r})]$ by

$$V_{xc}(\boldsymbol{r}) = \frac{\partial E_{xc}[n(\boldsymbol{r})]}{\partial n(\boldsymbol{r})} \tag{2.15}$$

For the non-interacting potential, ψ_i (Kohn-Sham wave functions) can be defined as

$$\left(-\frac{1}{2}\nabla^2 + V_{eff}(\boldsymbol{r})\right)\psi_i(\boldsymbol{r}) = \in_i \psi_i(\boldsymbol{r}) \tag{2.16}$$

Equation 2.16 is referred as the Kohn-Sham equation, which is the single-particle Schrödinger-like equation. The eigenvalue of the non-interacting single particle is defined with $\in_i$, which is related to the Kohn-Sham eigenstate ψ_i. For a system including N-non-interacting particles, the particle density $n(\mathbf{r})$ can be practically calculated via

$$\mathrm{n}(\mathbf{r}) = \sum_{\mathrm{i}=1}^{\mathrm{N}} \left|\psi_{\mathrm{i}}(\mathbf{r})\right|^2 \tag{2.17}$$

The total energy functional is formulated by

$$E_{KS}[n] = T_s[n] + \int d^3r V_{ext}(\boldsymbol{r}) n(\boldsymbol{r}) + E_{Hartree}[n] + E_{XC}[n] + E_{II} \tag{2.18}$$

here $T_s[n]$ is the kinetic energy functional of the non-interacting particles and can be obtained as follow:

$$T_s[n] = -\frac{1}{2}\sum_{i=1}^{N} < \psi_i|\nabla^2|\ \psi_i > \tag{2.19}$$

$E_{Hartree}[n]$ is the typical Coulomb energy functional owing to the particle density n(**r**). The representation of the $E_{Hartree}[n]$ functional is tendered by

$$E_{Hartree}[n] = \frac{1}{2}\int \frac{n(\boldsymbol{r})n(\boldsymbol{r}')}{|\boldsymbol{r}-\boldsymbol{r}'|}d\boldsymbol{r}d\boldsymbol{r}' \tag{2.20}$$

2.1.6 Exchange-Correlation Functional

The accuracy of DFT calculations for the lowest-state energy and density distributions of a real system can be developed via better approximations for exchange-correlation functional $E_{XC}[n]$ since in the Kohn-Sham formula which is identified in equation (2.16), $E_{XC}[n]$ is not accurately known. Now, the exchange-correlation functional, which is used in this thesis, will be introduced in the next sections.

2.1.6.1 The Local Density Approximation for $E_{XC}[n]$

The local density approximation (LDA) is not only easiest method but also practical one to obtain$E_{XC}[n]$. The LDA was proposed in the same year as the Kohn-Sham equation was formulated[146]. The background view of the LDA is quite apprehensible: The exchange correlation energy per electron, in other word, the value of energy density $\in_{XC}^{LDA}(n(\boldsymbol{r}))$, at that point can be thought of the same as that for a homogeneous electron gas ($\in_{XC}^{hom}(n)$), of the same charge density[147]. By this way, $E_{xc}^{LDA}[n]$ could be approximated as the following

$$E_{xc}^{LDA}[n] = \int \mathrm{n}(\mathbf{r}) \in_{XC}^{hom}(n(\boldsymbol{r}))d\boldsymbol{r} \tag{2.21}$$

The LDA, which is the majorly basic approximation, has been demonstrated to give rather good results for many atomic, molecular and crystalline interacting electrons systems, even in the systems the density of electrons is rapidly varying.

In addition, for the open-shell atoms and molecules, an advanced version of the LDA which is known as local spin density approximation can be exploited[148]. In the extended form of LDA, electron spins are adjusted distinct Kohn-Sham orbitals and can be obtained bit much accurate results.

2.1.6.2 Generalized Gradient Approximation for $E_{XC}[n]$

In LDA, as mentioned above, a system is considered as homogeneous. However, as known, in the real system, there is in homogeneity with spatially changing electron field. Therefore, an improved form of LDA, called as generalized gradient approximation (GGA), is enhanced to approximate $E_{XC}[n]$[149–151]. The main concept of the GGA within the DFT framework is that depending upon both electron density n(**r**) and its gradient $\nabla n(\boldsymbol{r})$ at the same point **r**.

The general form of the GGA functional is expressed as

$$E_{XC}^{GGA}[n] = \int n(\boldsymbol{r}) \in_{xc}^{GGA} (n(\boldsymbol{r}), \nabla n(\boldsymbol{r}))\mathrm{d}\mathbf{r} \tag{2.22}$$

Even though various exchange and correlation functional types can be used in different combinations together, just some of them are usually preferred in the studies. The calculations in this thesis are accomplished using the GGA, offered by Becke (for gradient exchange functional)[149] and by Lee, Yang and Parr (for correlation functional)[152] to predict the exchange correlation energy.

2.2 Molecular Dynamics

Molecular dynamics (MD) is a useful computer simulation scheme to inspect dynamical and structural characters of materials at the atomistic level. MD is commonly used in various scientific disciplines such as theoretical physics, materials science, even in the interdisciplinary like biophysics and biochemistry. MD method can be separate two sub-categories: classical MD and ab-initio MD. Both of these methods own comparatively the pros and cons. This part aims to give a brief knowledge about classical MD and ab-initio MD.

2.2.1 Classical Molecular Dynamics

The theoretical fundamental of the MD method is formed on the statistical thermodynamic rules. The classical MD approach is conceptually accepted to be the simplest one[153–157]. Because, it is clearly known that the a system which has interacting many-particles such as atoms and molecules interacting can be numerically solved via Newton's popular law, which is called equations of motion. Therefore, the basis of this approach is considered to be practical and utilizes classical mechanics.

Now the basic concept is that time averages of the observables can be taken through this path and based upon the statistic mechanics (the ergodicity hypothesis). This idea enounces that the time averages are equaled to ensemble averages of the suitable micro canonical (NVE) ensemble. It is known that Newton's equation of motion preserves the total energy (E). Thermodynamics changeable like temperature and (T) and pressure (P) can be deduced from circuitously and they show oscillations due to the limited number of atoms (N). Therefore, it is needed to straightforwardly define other ensembles of statistical mechanics, including constant volume and constant temperature (NVT) or another form (constant pressure and constant temperature, NPT)[158]. Sometimes, it is an advantageous to directly identify the ensembles. However, in physics of condensed matter, modern physics and chemistry, many fundamental phenomena have non-classical rules, in other words quantum effects. For this reason, it is required to apply approximations. The most common methodology is the ab-initio MD or Car-Parrinello method [159]. Now, let's qualify the current status of the theory of ab-initio MD from a modern view.

2.2.2 Ab-initio Molecular Dynamics

The methodology called as ab-initio MD, in which finite-temperature dynamical trajectories, are created via forced computed 'on the fly' from electronic structure calculations[160]. Due to the elimination of drawbacks of classical MD, ab-initio MD has had extensive effects in modern theoretical research. ab-initio MD enables structural arrangements including bond breaking or formation of new bonds, etc.[161].

This approach can be stated in terms of Lagrange

$$L = T - V = \frac{1}{2}\sum_{i=1}^{3N} m_i V_i^2 - E[\psi(\boldsymbol{r}_1, \boldsymbol{r}_2, \dots, \boldsymbol{r}_{3N})] \tag{2.23}$$

According to the Lagrange equation, the calculations can be performed consecutively. Namely, initially, the lowest energy state is computed. Later, the location of nuclei is altered by dint of a MD step. And then, the new lowest state is once more determined, and so on.

2.2.2.1 Car-Parrinello Method

In mid 1980s, R. Car and M. Parrinello[159] reformulated ab-initio MD in the form of a two-component classical dynamic system. The fundamental concept of an

efficient and precise ab-initio scheme is the combined the dealing with nuclear and electronic degrees of freedom. In other saying, the Car-Parrinello method holds not only classical MD of nuclei but also electronic character of ab-initio MD. Thence, it can be seen as a key-stone of up to date simulation techniques in many computational scientific fields[162]. Almost, until mid 1990s, ab-initio MD simulations were preponderant by the Car-Parrinello technique and thus this method had a synonym for ab-initio MD[163].

This method determines the extended Lagrangian technique and the equation is given as follows:

$$\frac{1}{2}\sum_{i=1}^{3N} m_i V_i^2 - E[\psi(\boldsymbol{r}_1, \boldsymbol{r}_2, \dots, \boldsymbol{r}_{3N})] + \frac{1}{2}\sum_j 2\mu \int d\boldsymbol{r} \left|\psi_j(\boldsymbol{r})\right|^2 + L_{ort} \qquad (2.24)$$

As obviously seen, the first two terms are same as in Equation 2.23. In addition to them, the third one presents the kinetic energy of fictitious mass which is signified with μ. The term L_{ort} is due to the orthogonality for one –electron functions.

2.2.2.2 Parrinello-Rahman Method

The first version was suggested by Andersen[164] in 1980. According to this method, the volume of the cell can change whereas its shape cannot alter. In other words, the shape is conserved by permitting the cell to change isotopically. Hence, this approach is more convenient for liquid simulations, not materials under non-isotropic stress or phase transitions. And one year later, the method was extended by Parrinello and Rahman[165,166] to allow changes not only cell lengths but also cell angles. By means of the Parrinello and Rahman method, both pressure and stress can be controlled in the simulation of a molecular system under externally applied stress. Moreover, the Lagrangian of the system is revised with a term symbolizing the kinetic energy of the cell depending upon a fictitious mass (*W*). Thuswise, the Parrinello-Rahman Lagrange for a simulation box having lattice vectors **a**, **b** and **c** is described by

$$L = \frac{1}{2}\sum m_i \dot{\boldsymbol{S}}_i^t \boldsymbol{G}\dot{\boldsymbol{S}}_\iota - \sum_i \sum_{i>j} \varphi(\boldsymbol{r}_{ij}) + \frac{1}{2} W T_r\left(\dot{\boldsymbol{h}}^t \dot{\boldsymbol{h}}\right) - P_{ext}\Omega \qquad (2.25)$$

in which **h** is a matrix contracted by lattice vectors. The volume of simulation box is defined by $\Omega = \det \mathbf{h} = \mathbf{a}.\mathbf{b}\mathrm{x}\mathbf{c}$, $\boldsymbol{S}_\mathrm{i}$ represents the position vector in fractional coordinate

for atom i. **G** is equal to $\boldsymbol{h^t h}$ and is a metric tensor, where $\boldsymbol{h}^t$ is the transpose of the matrix **h**. The second term is a pair potential. The fictitious mass is represented by W in the third term. P_{ext} stands for the hydrostatic pressure applied.

By using Equation (2.25), the equations of motion are practically got

$$\ddot{\boldsymbol{S}} = m_i^{-1} \sum_{i \neq j} \chi(\boldsymbol{r}_{ij})(\boldsymbol{S}_i - \boldsymbol{S}_j) - \boldsymbol{G}^{-1}\dot{\boldsymbol{G}}\,\dot{\boldsymbol{S}}_i \tag{2.26}$$

$$W\ddot{\boldsymbol{h}} = (\pi - P_{ext})\sigma \tag{2.27}$$

where $\chi(r)$ is the $-{}^{d\varphi}/_{rdr}$. The matrix σ has elements$\sigma_{ij} = {}^{\delta\Omega}/_{\delta \boldsymbol{h}_{ij}}$, and the matrix π is given in dyadic tensor notation via,

$$\Omega\pi = \sum_i m_i \boldsymbol{v}_i . \boldsymbol{v_i} + \sum_i \sum_{j>i} \chi(\boldsymbol{r}_{ij})(\boldsymbol{r}_i - \boldsymbol{r}_j)(\boldsymbol{r}_i - \boldsymbol{r}_j) \tag{2.28}$$

where $\boldsymbol{v_i} = \boldsymbol{h}\dot{\boldsymbol{S}}_{\boldsymbol{i}}$. Equation 2.26 and 2.27explore the dynamic of a simulation cell having N particles with periodic boundary conditions. Equation 2.27 presents the connection between the variation of **h**, microscopic tensor π and external pressure.

In the DFT calculations, the Kohn-Sham wave function which stands for $\psi_i(\boldsymbol{r})$ are fixed on **h** cell and it is known that not only $\psi_i(\boldsymbol{r})$ but also **h** depends on fields since **h** are Lagrangian degree of freedom. Now, the wave function can be determined with denominated the scaled coordinate (**S** = $\mathbf{h}^{-1}\mathbf{r}$). The orbital $\psi i(\mathbf{r})$ as described by unscaled cell **h** are converted as follows

$$\psi i(\mathbf{r}) = \frac{1}{\sqrt{\Omega}}\psi(\mathbf{h}^{-1}\mathbf{r}) = \frac{1}{\sqrt{\Omega}}\psi(\mathbf{s}) \tag{2.29}$$

In this situation, the resultant charge density in the unit cell is represented via

$$n(\boldsymbol{r}) = \frac{1}{\Omega} n(\boldsymbol{s}) \tag{2.30}$$

Both scaled fields $\psi(\mathbf{s})$ and charge density $n(\boldsymbol{s})$ do not rest on the dynamical variables due to the cell degrees of freedom. Nevertheless, original $\psi(\mathbf{r})$ depends upon **h** owing to the normalization of the cell volume which is defined Ω=det**h**.

Now, the Lagrangian can be written for ab-initio molecular dynamics by pressure control

$$L = \mu \sum_i \int d\boldsymbol{S} \left|\psi_i(\boldsymbol{S})\right|^2 + \frac{1}{2}\sum_j M_j(\dot{\boldsymbol{S}}_{\boldsymbol{J}}^{\boldsymbol{t}} G\dot{\boldsymbol{S}}_J) - E[\{\psi_i\},\{\boldsymbol{hS_j}\}$$
$$+ \sum_{il} \Lambda_{il}\left(\int d\boldsymbol{S}\ \psi_i^*(\boldsymbol{S})\psi_i(\boldsymbol{S}) - \delta_{ij}\right) + \frac{1}{2}WT_r(\dot{\boldsymbol{h}}^{\boldsymbol{t}}\dot{\boldsymbol{h}}) - P_{ext}\Omega) \tag{2.31}$$

In Equation 2.31, nine dynamical degrees of freedom are correlated with **h**, namely the lattice parameters of the simulation box, and the integrals are integrated on the scaled simulation box. In the formula, the third term gives the DFT-LDA energy functional. δ is the identity matrix. The fourth term defines the orthonormality constraint on the Lagrangian multipliers which stand for ψ_i and Λ_{il}. W is the fictitious mass similar to in the classical Parrinello Rahman method and μ is inertia parameters which control the time scale of electronic motion. M_j typifies the mass of nuclei.

The equation of motion in DFT-LDA method is given by

$$\mu\ddot{\psi}_i(\boldsymbol{S}) = -\frac{\delta E}{\delta\psi_i^t(\boldsymbol{S})} + \sum_l \Lambda_{il}\ \psi_i(\boldsymbol{S}) \tag{2.32}$$

$$\ddot{\boldsymbol{S}}_{\boldsymbol{J}}^{\boldsymbol{\alpha}} = -\frac{1}{M_j}\frac{\partial E}{\partial \boldsymbol{S}_j^{\beta}}\boldsymbol{G}_{\alpha\beta} - \boldsymbol{G}_{\alpha\beta}\ddot{\boldsymbol{G}}_{\beta\alpha}\dot{\boldsymbol{S}}_j^{\gamma} \tag{2.33}$$

$$\ddot{\boldsymbol{h}}_{\alpha\beta} = \frac{1}{W}\left(\pi_{\alpha\gamma} - P_{ext}\delta_{\alpha\gamma}\right)\Omega(\boldsymbol{h}^t)_{\gamma\beta}^{-1} \tag{2.34}$$

in which $\pi_{\alpha\gamma}$ is,

$$\pi_{\alpha\gamma} = \frac{1}{\Omega}\left(\sum_j M_j\dot{\boldsymbol{S}}_j^t\ \boldsymbol{G}\dot{\boldsymbol{S}}_j\right)_{\alpha\gamma} - \frac{\partial E}{\partial h_{\alpha\beta}}\boldsymbol{h}_{\delta\gamma}^t \tag{2.35}$$

The differences of the above Equations (2.33 and 2.34) from the classical Parrinello Rahman method are that quantum mechanical terms are replaced for the classical forces on ions and the internal stress.

2.3 Modeling Amorphous Structures

Before expressing the common techniques for modeling amorphous materials, let's designate the meaning of the word amorphous.

The word amorphous is stemmed from Greek. The word comprises of combination of two words: without and morphe (shape, form)[167]. Namely, the amorphous word refers to being shapeless or formless. The crystalline solids exhibit a definite and regular geometry whereas amorphous forms have irregular geometric shapes. The most important differences between crystalline and amorphous solids, an ordered form consists of long-range order while a disordered form owns a shorter range order.

Though there are lots of obscurities about the physical and chemical properties of amorphous systems, they continue to draw interest of scientists due to their discovered distingue characters day by day. There are different techniques to construct models of amorphous materials based on the specific chemistry and order of materials. Now, let's clarify some general methods for production of amorphous materials.

2.3.1Continuous Random Network

The continuous random network (CRN) is a favorable protocol for the definition atomic character of strongly covalent bonded amorphous materials. This method, firstly, was introduced by Zachariasen[168]. The underlying insight of this procedure is that the materials are accepted to include of building blocks of tetrahedral, as their crystalline structure do. However, the atoms are randomly oriented and connected. In the modeling disordered arrangements, CRN method is quite useful as well as impressively simple. The substantial advantage of the model is that each atom wholly performs its bonding characters. In other word, all atoms are ideally coordinated. The eligibility of CRN is commonly specified by means of the amount of strain. By dint of this model, convincing definitions of the topology of elemental amorphous semiconductors can be provided.

2.3.2 Quenching from Melt

Another alternative method for constructing a disordered network is the quenching from melt. This scheme is a well-known process used for producing an

amorphous material from a crystal structure. While producing of an amorphous arrangement, MD conducts like an experimental protocol. The process of the traditional MD method (as used in this study) is fundamentally as follows: In the first step, the initial crystal structure is exposed to temperature, higher than its melting temperature. Thus, the structure converts into a liquid phase. In the second step, a simulated annealing protocol is carried out to the system in order to relax a local minimum energy state. And then the material is cooled from its liquid phase at the certain time scale for its chemical ordering. Lastly, the final configuration at room temperature is relaxed via suitable geometry optimization technique.

2.4 Simulation Conditions

In this dissertation, the calculations are based on the SIESTA package program. Therefore, in this section, some general information about SIESTA will be introduced.

2.4.1 SIESTA

SIESTA is not only a method but also computational code, to fulfill impressive electronic character calculations and ab-initio MD simulations of solids, liquids or molecules[169]. The word SIESTA consists of the initial letters of *'Spanish Initiative for Electronic Simulations with Thousand Atoms'.* The method enables strongly quick simulations via minimal basis sets and quite exact calculations with complete multiple-zeta and polarized bases. By means of its useful performance, the usage of the computational code is preferred a wide different of systems, such as metallic surface, nanotube, nanocluster, amorphous semiconductors, ferroelectric films, and biomolecules. The method has showed as citation more than 12000 times so far. The essential advantages of SIESTA are showing excellent performance for finite systems, dealing with computationally demanding system (>10000 atoms) which are out of the plane-wave codes and it is an open-source.

The calculations in this dissertation were employed by using the version 3.2 and 4.1 of SIESTA.

2.4.2 Pseudopotentials

The pseudopotential concept has owned a deep effect on the comprehending of the electronic behavior of semiconductors. In the beginnings of 1980s, the combining DFT method with pseudopotential resulted in remarkable advance for perceptive electronic characters of materials. In the beginnings, there were some uncertainties the exactness of DFT method for determining electronic and structural energies. However, the direct numerical application of structural energies to problems including bond lengths, compressibility and phase stability exhibited conclusively the capability of pseudopotential methods to these problems[170].

A norm-conserving pseudopotential method is used in SIESTA to estimate the electron-ion interaction. Pseudopotentials, in other words, effective core potentials are used to disregard the inactive core electrons from an explicit treatment in quantum chemical calculations. These potentials are suitable techniques to incorporate the essential scalar relativistic impacts into calculations[171]. In short, the idea of pseudopotential is linked to substituting the results of the core electrons with an effective potential. Consequently, a modified effective potential term is used in the Schrödinger equation.

To define the ion-electron correlation, the norm-conserving Troullier-Martins pseudopotentials were adopted in this dissertation[172].

2.4.3 Basis Sets

In a theoretical calculation or modeling, the orbitals of a system can be defined a mathematical term which are called as a basis set, which consists of a simple functional building block. Any set of mathematical functions building the practical molecular orbitals can be preferred.

As known, an atomic orbital characterizes the wave-like behavior of an electron in an atom. The basis sets consist of numerical atomic orbitals (NAO). SIESTA employs NAO, a numerical solution of the Kohn-Sham equation for an isolated pseudo atom can be obtained by the Numerov scheme, which is feasible to linear ordinary differential equations as Schrödinger equation is. In order to define the basis functions, the choice of two points is important: the first one is changeable radial component and the second thing is well-identified spherical harmonic for a particular orbital. The radial part of an orbital consists of radial function such as single-ζ, double-ζ or triple-ζ. The advantages

of NAOs are that they can be produced with any shape with no extra computational cost, NAOs can be eliminated expensive long-range correlations, and they can be basically localized. In this dissertation, in the first study the double-ζ (DZ) or double-ζ (DZ) plus polarized (DPZ) and in the rest two studies the double-ζ (DZ) basis sets were chosen for valence electrons.

2.4.4 Periodic Boundary Conditions

In order to investigate properties of materials via computer simulation using a MD method, a simulation box is required. A unit cell in MD is commonly termed to as periodic box. When the large simulation box is used, the extremely extensive computational time is required to complete calculations. On the other hand, if a much smaller simulation box is used, most atoms can locate the edge of the simulation cell. Besides, in a simulation cell, for all atoms, homogeneity and ideal situations may not be continuously achieved. All these problems can be dealt with using periodic boundary conditions.

The essential aim of the usage of periodic boundary conditions to prevent the existence of surface and to evade enormous number of atoms or greater size of simulation cell. Shaping an infinitely large unit cell by repeating the simulation cell along space can be considered as periodic boundary conditions as shown Figure 2.2. The rules in a simulation cell are as follows: firstly, an atom moves off the cell, right after, one of its images come along the other side with precisely following the same direction. Hereby, the atoms in the simulation cell preserves and it is considered that there is no change and having no surface in the system.

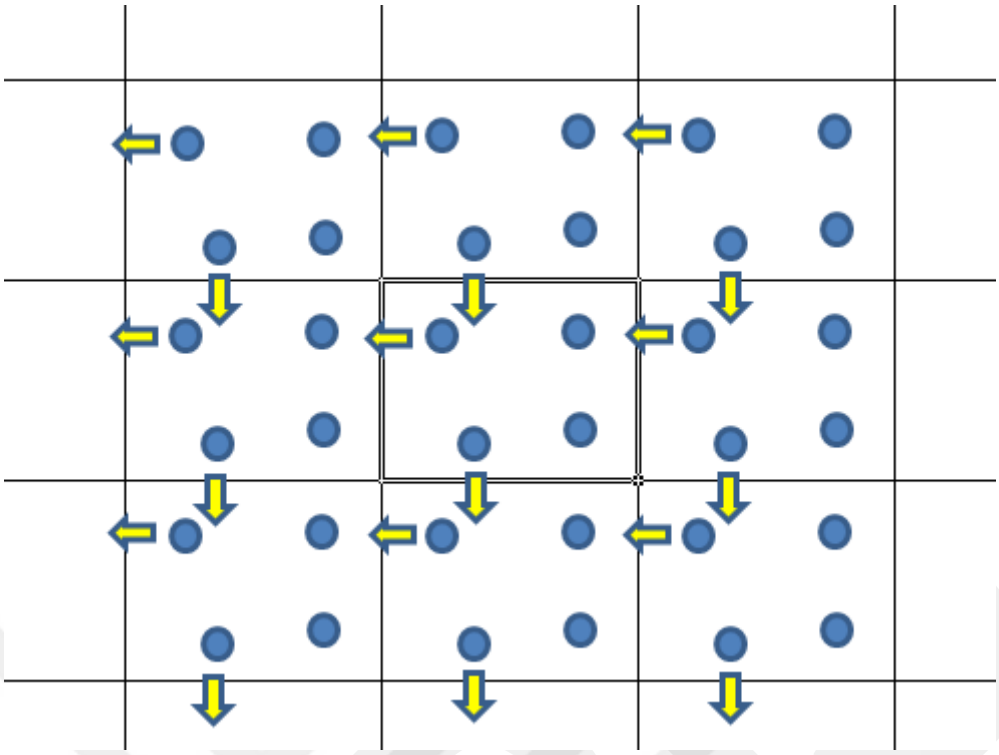

Figure 2.2 The schematic demonstration of periodic boundary conditions in 2D.

2.4.5 Geometry Optimization

The one of the best ways of the determining a molecular structure is the geometry optimization procedure, which is a useful theoretical tool. Moreover, by means of the geometry optimization, the structural changes in a molecular system can be identified. The general goal of the geometry optimization, in other saying, local optimization is to minimize the total energy of the systems.

In this dissertation, for all calculations, the geometry optimization was fulfilled via a conjugate gradient (CG) variable cell technique, which is a convenient protocol to solve unrestrained optimization problems like energy minimization, in which not only the atomic positions but also the volume of the simulation cell was optimized at zero pressure. In addition, in the all calculations, the force criteria of 0.01 eV/Å were accomplished for the purpose of optimization of the structures.

2.5 Structural, Electronic and Mechanical Analyses

In this part, it is aimed to complete the chapter 2 by tendering a brief knowledge about the structural, electronic and mechanical analysis techniques used in this study.

2.5.1 Pair Distribution Function

The pair distribution function (PDF) having several different definitions such as, radial distribution function (RDF) and pair correlation function (PCF) is a powerful analytical method to gain quantitative view into the structure of materials. The PDF offers the possibility of finding an atom at a distance 'r' from a given atom as demonstrated in Figure 2.3.

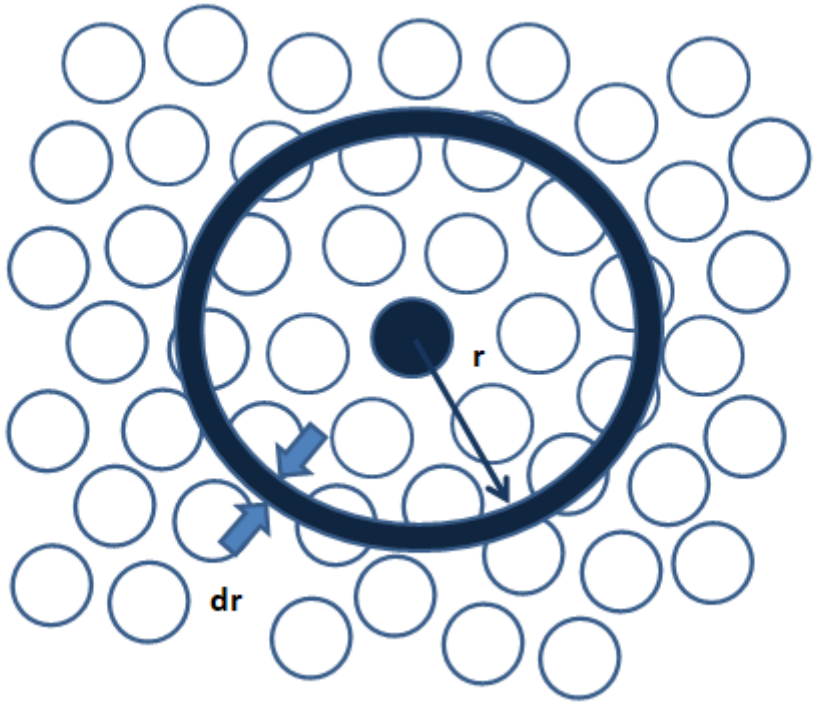

Figure 2.3 The spatial discretization for the evaluation of the radial distribution function.

The number of atoms dn(r) at a distance between r and r+dr can be computed,

$$dn(r) = \frac{N}{V}\rho(r)4\pi r^2 \tag{2.36}$$

in which N is the total numbers of atoms. V refers to the volume of the system. $\rho(r)$ stands for the PDF. In the Equation 2.36, the volume of the shell having dr width can be effortlessly computed,

$$V_{shell} = \frac{4}{3}\pi(r+dr)^3 - \frac{4}{3}\pi r^3 \approx 4\pi r^2 dr \tag{2.37}$$

The PDF is given by

$$\rho_{\alpha\beta}(r) = \frac{N}{4\pi r^2 \rho N_\alpha N_\beta} \sum_{i=1}^{N_\alpha} \sum_{j=1}^{N_\beta} \delta\left(r - \left|\overrightarrow{r_{ij}}\right|\right) \tag{2.38}$$

where N, N_α, and N_β represent the total number of atoms and the number of α and β type atoms, respectively, used in the simulation cell whose density is ρ.

2.5.1.1 Bond Properties and Coordination Numbers

The first peak position of PDFs can be practically used to determine the mean bond separation for each atom pair in the structures. The total and partial coordination numbers (CNs) are implemented to gain different perspectives onto the local structure of a material at the atomistic level and hence by way of cutoff distances (the first minimum) of PDFs, the CNs were estimated for all structures in this study.

2.5.2 Bond Angle Distribution Function

The bond angle distribution function (BADF) is performed to provide further information on local chemical structure of materials. The BADF $f(\theta)$, (θ is the angle between atoms) in the nearest neighbor coordination shell can be analyzed by the following equation

$$f(\theta) = 16\pi^2 \int_0^{d_1} \int_0^{d_2} R_1^2 R_2^2 \mathrm{g}(R_1)\mathrm{g}(R_2)\mathrm{g}_3(R_1, R_2, \theta)\, dR_1\, dR_2 \tag{2.39}$$

Here d_1 is the possible maximum bond length between two neighboring atoms.

2.5.3 Electronic Properties

The electronic structure of ordered and disordered materials can be probed via electron density of states (EDOS), and can be calculated

$$\rho_{EDOS}(E) = \frac{1}{N_f} \sum_{i=1}^{N_f} \delta(E - \varepsilon_i) \tag{2.40}$$

where N_f stands for the total number of occupied electronic states. ε_i represents the energy eigenvalues.

2.5.4 Mechanical Properties

The equation of state (EOS) involving thermodynamic rules is commonly used formula by physicist, chemists and materials scientist. The equation identifies the state of materials under some physical conditions such as pressure (P), volume (V) and temperature (T).

In this thesis, for the purpose of inspecting reaction of a material to external stress, the EOS, was used. Now, let's try to express the EOS via not only practical but also useful equations. For a solid under isothermal conditions, the basic form of EOS can be defined in terms of bulk modulus (K), which measures the compressibility of a solid under uniform pressure.

$$K_0 = -V\left(\frac{\partial P}{\partial V}\right)_T \quad K_0' = \left(\frac{\partial K_0}{\partial P}\right)_T \tag{2.41}$$

in where, the equilibrium bulk modulus of a solid stands for K_0, K_0' represents the first derivative of K with respect pressure. Meanwhile, pressure can be expressed as a function of volume, namely,

$$P(V) = -\left(\frac{\partial E}{\partial V}\right)_S \tag{2.42}$$

By means of Equation 2.37, the bulk modulus can be rewritten as

$$K(V) = V\left(\frac{\partial^2 E}{\partial V^2}\right)_{T,S} \tag{2.43}$$

Now, K can be calculated by fitting the energy-volume relation of materials to the third order Birch-Murnaghan EOS,

$$E(V) = E_0 + \frac{9V_0K}{16}\left\{\left[\left(\frac{V_0}{V}\right)^{\frac{2}{3}} - 1\right]^3 K' + \left[\left(\frac{V_0}{V}\right)^{\frac{2}{3}} - 1\right]^2\left[6 - 4\left(\frac{V_0}{V}\right)^{\frac{2}{3}}\right]\right\} \tag{2.44}$$

By using Equation 2.37, the third order Birch-Murnaghan EOS can be reformulated in terms of *P(V)*,

$$P(V) = \frac{3K_0}{2}\left[\left(\frac{V_0}{V}\right)^{\frac{7}{3}} - \left(\frac{V_0}{V}\right)^{\frac{5}{3}}\right]\left\{1 + \frac{3}{4}(K_0' - 4)\left[\left(\frac{V_0}{V}\right)^{\frac{2}{3}} - 1\right]\right\} \tag{2.45}$$

The advantage of writing the formula in terms of P(V) is that if the P-V values are known, bulk modulus and enthalpy can be also achieved by fitting the data to the third order Birch-Murnaghan EOS.

Named after Simeon Poisson, Poisson's ratio is the negative of the ratio of transverse strain to longitudinal strain computed by the application of a uniaxial strain along the principal axes. The ratio is practically calculated via following equation:

$$\nu_{ij} = -\frac{\Delta L_i / L_i}{\Delta L_j / L_j} \tag{2.46}$$

in which L_s are the magnitude of the supercell's vectors and i and j introduce the principal (x, y and z) directions.

Young modulus (E), also called as modulus of elasticity, is a quality of the material that expresses correlation between stress and strain in a material under a uniaxial deformation. E can be practically achieved by using the following equation:

$$E = 3K\,(1 - 2\nu) \tag{2.47}$$

Shear modulus (μ), also called as modulus of rigidity, gives the information about the ratio of shear stress to shear strain of the material within the restricted elastic deformation and can be calculated by means of the next formula,

$$\mu = \frac{E}{2\,(1 + \nu)} \tag{2.48}$$

Vickers hardness (H_v), a measurement technique of the hardness, is the denomination of the resistance of a material to deformation. H_v can be computed four different equations as follows[173–176],

$$H_v = 0.151\mu \tag{2.49}$$

$$H_v = 2\left(\frac{\mu}{n^2}\right)^{0.585} - 3\ (\mathrm{GPa}) \tag{2.50}$$

$$H_v = 0.92\left(\frac{1}{n}\right)^{1.137}(\mu)^{0.708} \tag{2.51}$$

$$H_v = 0.0635E \tag{2.52}$$

Chapter 3

Hydrogenated Amorphous Boron Nitride: A First Principles Study

The work presented in this chapter is published in T.A. Üçhöyük, and M. Durandurdu. "Hydrogenated amorphous boron nitride: A first principles study." *Journal of Non-Crystalline Solids* 502 (2018): 159-163.

3.1 Introduction

Boron Nitride (BN), a III-V compound, is a synthetic material having crystal structures similar to carbon. It is a wide band gap semiconductor. Due to its unique physical and chemical features, it has been attracted a great deal of scientific and advanced technological interests. It is one of promising candidates as a superhard material after diamond.

BN forms four different crystal structures: hexagonal (h-BN), rhombohedral (r-BN), cubic (c-BN) and wurtzite (w-BN)[177]. The ground state structure of BN is the h-BN phase being a two-dimensional layered material with a weak Van der Waals force [178]. h-BN has various superior features[179]. The rhombohedral BN (r-BN) also forms in a two-dimensional structure[87], similar to h-BN. Amongst the other phases, r-BN is the least understood one[180]. Cubic BN (c-BN) can be manufactured from h-BN and r-BN at high temperature and pressure conditions[92]. Due to its extreme hardness, it can be used as a protective coating of heavy-duty tools[181]. The high pressure and temperature treatments can possess a phase transformation from h-BN to a wurtzite structure (w-BN) as well[182], which can be classified as a superhard material.

Amorphous BN (*a*-BN) can be synthesized using various experimental techniques such as high frequency chemical vapour deposition and ball milling[183–185] but relative to the crystalline forms, it has been little explored and hence less understood

[186–191]. Amorphous materials have coordination defects and strained topologies, which significantly influence their electrical and physical properties. Their main coordination defect is undercoordinated atoms i.e. dangling bonds. Hydrogenation somehow not only passivates the dangling bonds but also breaks strained and weak bonds in amorphous materials and yields more ordered configurations[192]. Such hydrogenation induced structural changes improve significantly their physical and electrical properties. Consequently hydrogenated *a*-BN (*a*-BN:H) has been studied experimentally as well[193,194]. Although there are few theoretical studies on *a*-BN [73,195] to shed some light on its atomic structure and electronic properties, to our knowledge, there has been no attempt to investigate theoretically *a*-BN:H. Thus currently the impact of hydrogenation on the atomic structure and electric properties of *a*-BN is not well known. And hence in this work, we generate *a*-BN:H with four different hydrogen contents based on an ab initio technique and compare them structurally and electronically with pure *a*-BN to fill the gap in the literature. We find that hydrogenation induces drastic structural changes in the network compared to pure *a*-BN. Yet in spite of the changes, hydrogenation is found to have a small influence on its electronic properties.

3.2 Methodology

The SIESTA package[169] based on the density functional theory (DFT) was used to perform molecular dynamics (MD) simulations. The atomic orbital basis set was selected as a double-zeta plus polarized (DZP) orbital for the valance electrons. The pseudopotentials were produced by the Troullier and Martins approach[172]. The Becke gradient exchange functional[149] and Lee, Yang, and Parr correlation functional[152] were applied to estimate the exchange correlation energy. The MD simulations were performed within the NPT (isothermal-isobaric) ensemble in which temperature and pressure were controlled by the velocity scaling and the Parrinelo-Rahman techniques[166], respectively. The time step of each MD simulation was set to 1.0 fs. We chose a 216-atom liquid BN model (108 B atoms and 108 N atoms) at 3300 K as an initial structure. We removed arbitrarily 5 B and 5 N atoms from the melt, replaced 14, 22, 30 and 46 H atoms and created 220, 228, 236 252-atoms models that were labeled as model1, model2, model3 and model4, respectively. The hydrogen concentration is

about 6.4, 9.6, 12.7 and 18.2 % for the model1, model2, model3 and model4, correspondingly. Experiment[194] suggested the existence of 5–10% hydrogen in a-BN:H film. So the model1 and model2 consist of a H concentration in the experimental range. On the other hand, model2 and model3 have a higher H concentration than the experimental proposition and hence they can be considered as a hypostatical structure but they actually allow us to understand the impacts of excessive hydrogenation on the local structure of the amorphous network. All initial configurations were subjected to 3300 K for 50.0 ps and then the melts were gradually cooled to 300 K within 150.0 ps. Finally these structures were relaxed according to the force criteria of 0.01eV/Å. The relaxed structures' density is 2.0430 g/cm^3 for pure *a*-BN, 1.8033 g/cm^3 for model1, 1.9063 g/cm^3 for model2, 1.7055 g/cm^3 for model3, and 1.8345 g/cm^3 for model4. They are indeed reasonably comparable with the experimental value of 1.9 ±0.1 g/cm^3[193].

3.3 Results

In order to distinguish the short-range order of the *a*-BN:H configurations from that of pure (unhydrogenated) *a*-BN, we first consider the partial pair distribution functions (PPDFs) and plot them in Figure 3.1. The first peak position of all correlations of the *a*-BN:H models along with that of h-BN and pure *a*-BN model is summarized in Table 3.1.

Table 3.1 The first peak position of correlations.

	B-B (Å)	B-N (Å)	N-N (Å)	B-H (Å)	N-H (Å)	H-H (Å)
h-BN	2.50	1.57	2.50			
pure α-BN	2.51	1.46	2.54			
Model 1	2.50	1.43	2.51	1.17	0.98	1.95
Model 2	2.51	1.43	2.52	1.16	0.98	1.74
Model 3	2.49	1.43	2.50	1.17	0.97	1.65
Model 4	2.51	1.44	2.52	1.17	0.98	1.68

One can see that the distances estimated are quite close to each other, suggesting that the *a*-BN:H structures are locally similar to pure *a*-BN[73] and h-BN[196]. The B-H and N-H bond lengths are located at around 1.17 Å and 0.98 Å, respectively for the all *a*-BN:H networks. These values are comparable with 1.17 Å for B-H bond length and 1.03 Å for N-H bond distance reported in a neutron diffraction study of

BH_3NH_3[197]. The position of the H-H correlation at near 1.65 -1.95 Å indicates that the models are free from H-H bonds because H-H bond length is 0.74 Å. From the PPDFs, one can see that these models do not form any N-N bond as well but have a small amount of B-B homopolar bonds as denoted by a feeble peak at 1.70-1.74 Å in the B-B correlation, similar to what has been observed for pure *a*-BN[73]. The analyses suggest that the correlation distances are not affected by hydrogenation.

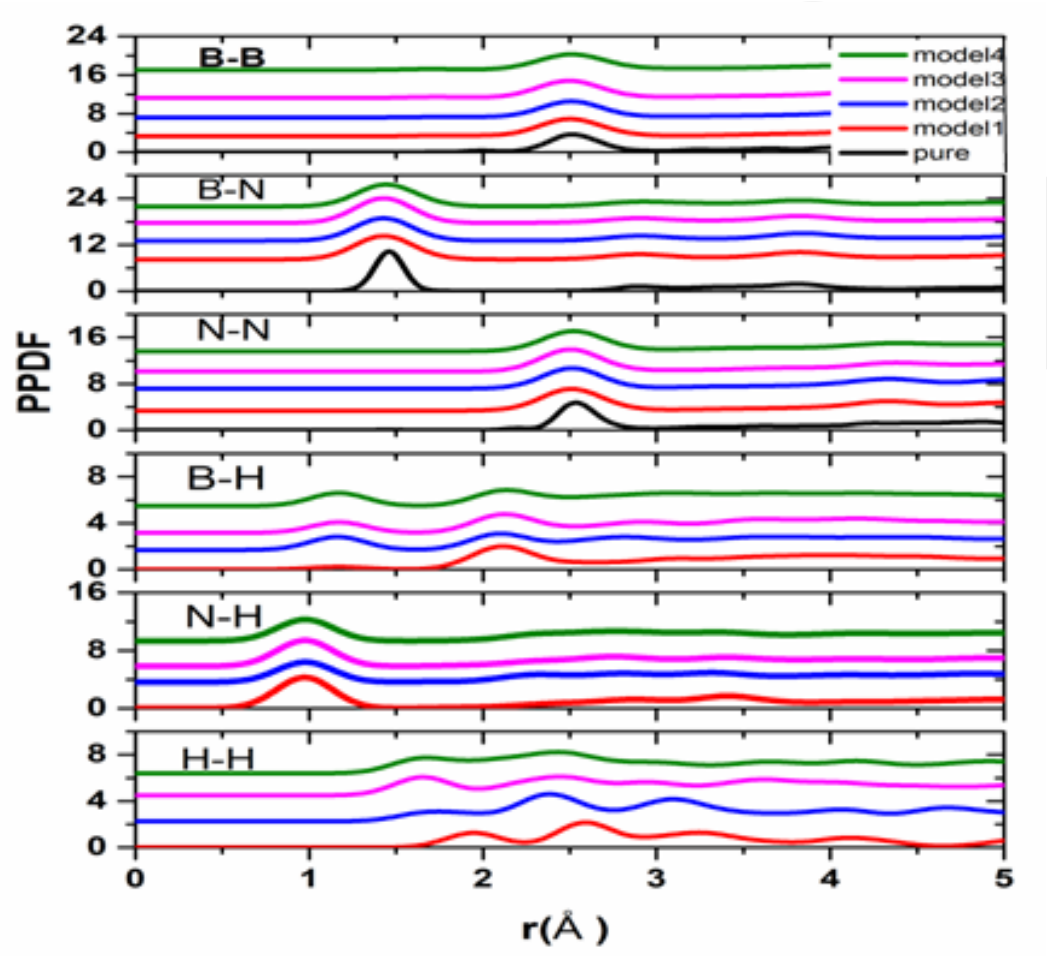

Figure 3.1 PPDFs of the pure *a*-BN and *a*-BN:H models.

The coordination number (CN) is an essential feature to describe the short-range order of disordered systems. Using the first minimum of the PPDFs (~1.86 Å for B-B, ~2.02 Å for B-N, ~1.57 Å for B-H and 1.49 Å for N-H correlations), we estimate the total and partial CNs. Figure 3.2 illustrates the coordination distributions of the *a*-BN:H models and the *a*-BN network.

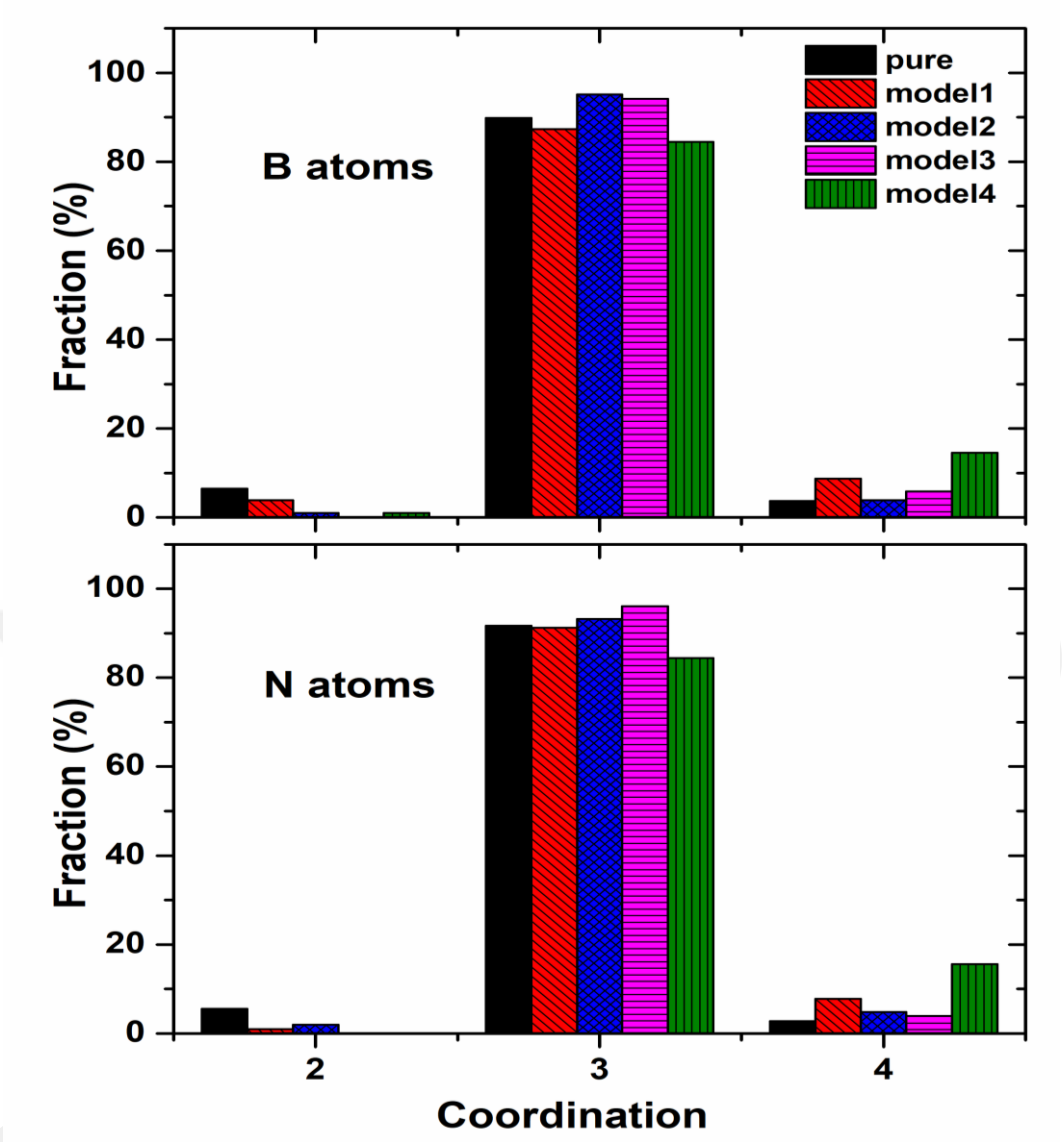

Figure 3.2 Coordination distribution of the pure *a*-BN and *a*-BN:H models.

For the pure *a*-BN configuration, the frequency of twofold, threefold, and fourfold-coordinated atoms is 6%, 91%, and 3%, correspondingly. The subsequent average CN is 2.97. By hydrogenation, one can perceive a decrease in the number of dangling bonds (twofold chain-like configurations) and almost no twofold coordinated atoms for the model3 and model4. Hydrogenation leads to more sp^2 and even sp^3 hybridizations in the first three models, relative to pure *a*-BN. Their mean CN is about 3.03-3.06. The situation for model4 is slightly different: 85% of atoms are threefold coordinated and about 15% of atoms (15% of B atoms and 16% of N atoms) are fourfold coordinated. The average B and N CNs are 3.13 and 3.15, correspondingly. For this model, we find that the at least 50% of sp^3 configurations involve at least one H atom while the rest occurs between B and N atoms. The B-N_4, B-N_3H, N-B_4, N-B_3H

and N-B_2H_2 configurations are the main sp^3 hybridization units in the model. For intermediate hydrogen concentration, similar trend has been reported for hydrogenated amorphous carbon (*a*-C:H) called as hydrogenated diamond-like carbon (DLC) films, in which hydrogenation yields more sp^3 C-C bonding[198].

All H atoms are onefold coordinated and a close investigation reveals the fact that there are more N-H bonding than B-H bonding in the all *a*-BN:H models; about 65-93% of H atoms form a bond with N atoms. The model1 presents the highest fraction of N-H bonds (93%) while model4 shows the lowest one (65%). Actually, we find a correlation between H concentration and the number of N-H bonds (or B-H bonds) formed in the amorphous systems: the frequency of N-H bonds decreases with increasing H concentration.

To further understand the atomic structure of *a*-BN:H in details, we explore the bond angle distribution functions (BADFs). The B-N-B and N-B-N angle distributions are provided in Figure 3.3. The main peak of the all *a*-BN:H models are located at around 116^o-119^o, indicating that *a*-BN:H has an atomic arrangement related to that of h-BN. Note that the hydrogenated configurations (model1, model2 and model3) produce a sharper peak around 120^o than the pure *a*-BN model, suggesting that hydrogenation yields a more ordered local structure in the system. We also note here that while the pure *a*-BN network has a subpeak at about 80^o for the B-N-B and 95^o for N-B-N because of the presence of the tetragonal rings[194], the *a*-BN:H models do not present such peaks in the BADFs, indicating that hydrogenation suppress the development of tetragonal rings as well. This is further supported by the rings analysis as shown in Figure 3.4. Four membered rings exist in pure *a*-BN but the fraction of such rings is negligibly small in the *a*-BN:H models.

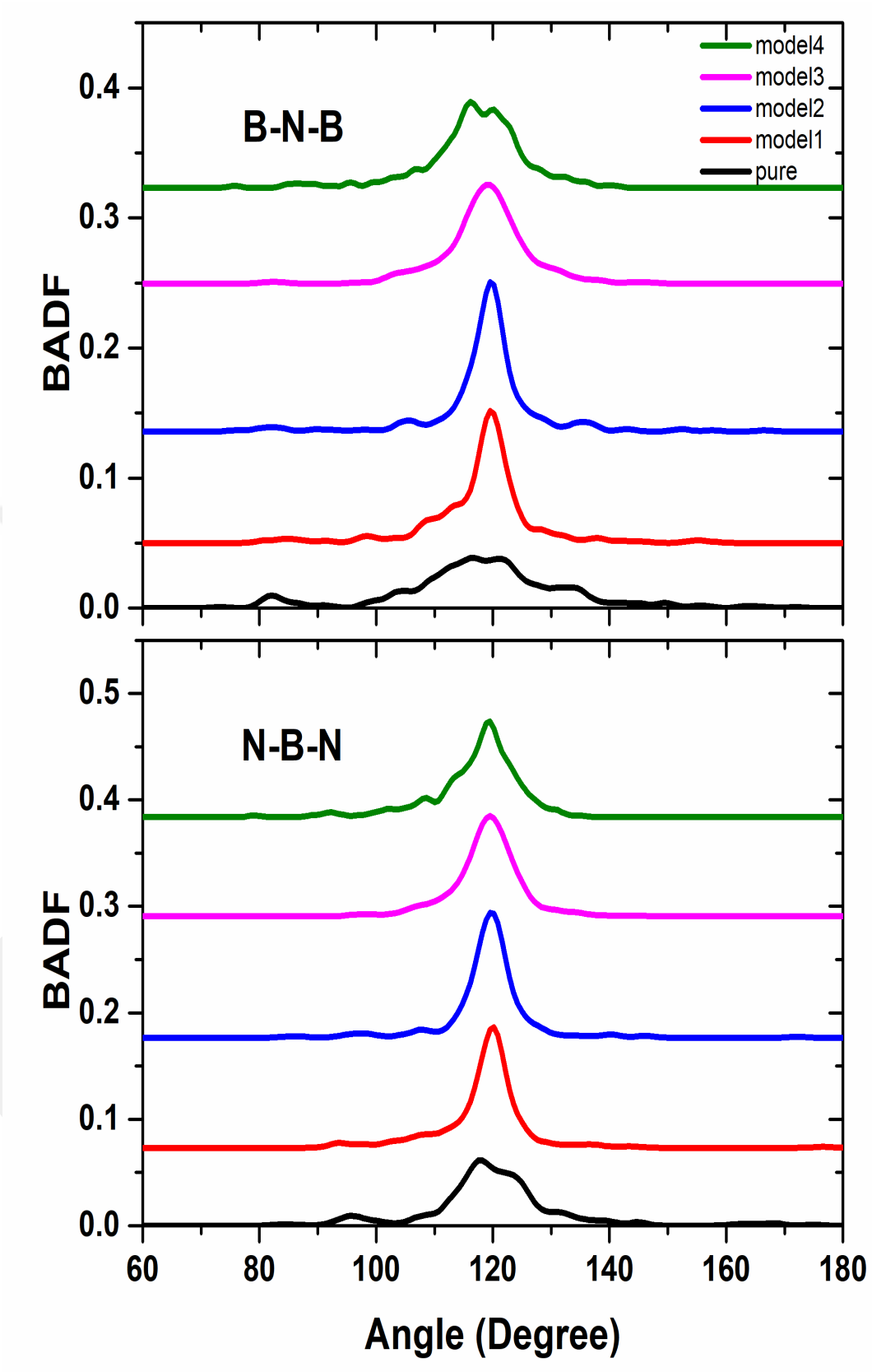

Figure 3.3 BADF of the pure *a*-BN and *a*-BN:H models.

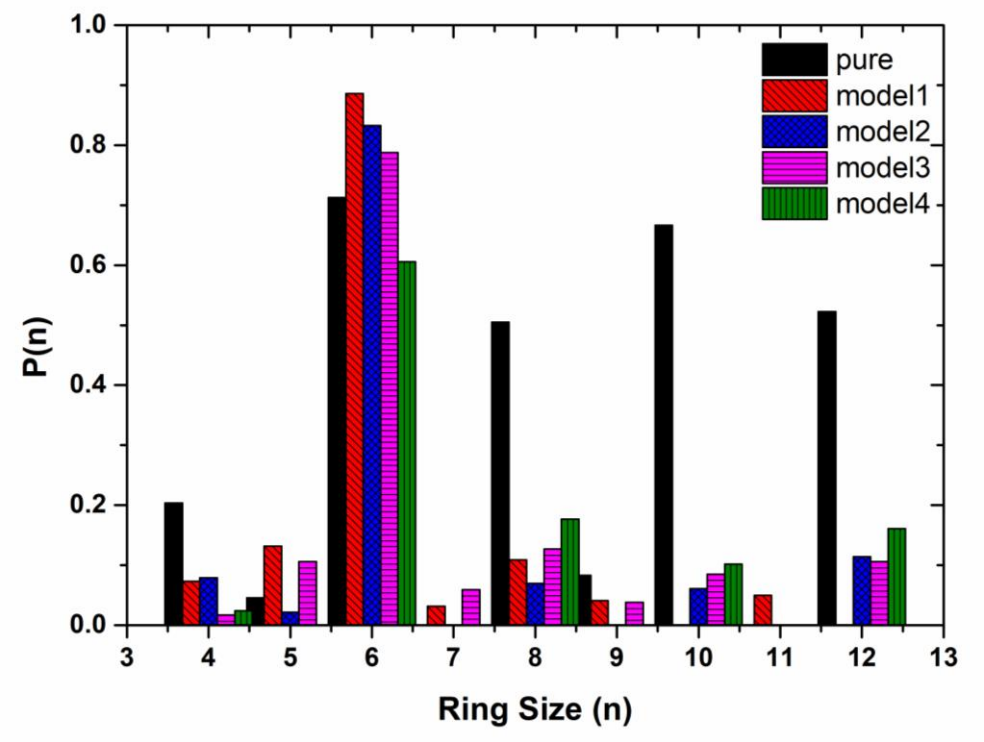

Figure 3.4 Ring distribution of the pure *a*-BN and *a*-BN:H models.

To understand the effects of hydrogenation on the electronic properties of *a*-BN, we lastly compute the electronic density of states (EDOS) of the models and demonstrate them in Figure 3.5.

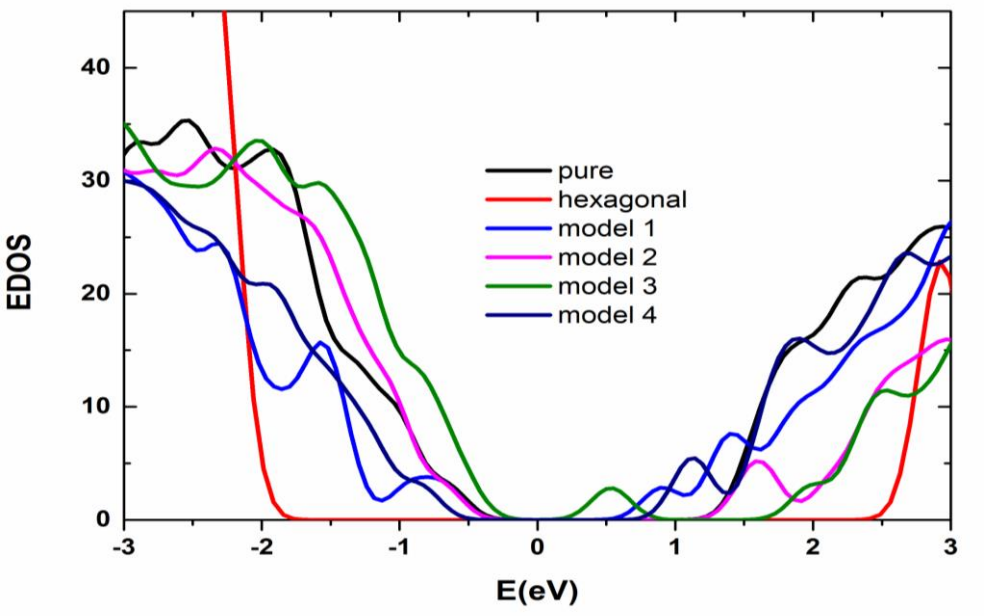

Figure 3.5 EDOS around the Fermi level for h-BN, *a*-BN and *a*-BN:H models.

We also provide the EDOS of pure *a*-BN and h-BN in the figure for comparison purpose. The band gap energy defined as the difference of HOMO-LUMO states is found to be about 4.5 eV for h-BN and ~2.0 eV for pure *a*-BN. It should be pointed out here that DFT-GGA calculations underestimate band gap widths and hence they are not comparable with experimental values. For the *a*-BN:H models, we do not perceive a drastic modification in the band gaps except that a midgap state is presented in model3. The band gap of the *a*-BN:H configurations is close to that of pure *a*-BN and about 1.8-2.0 eV. A close analysis of the midgap state using the localization of wavefunctions reveals that it is indeed due to a chain-like B-B structure formed in model3 (see Figure 3.6). We should note here that such a chain-like structure does not exist in other models although they present a small amount of B-B homopolar bonds.

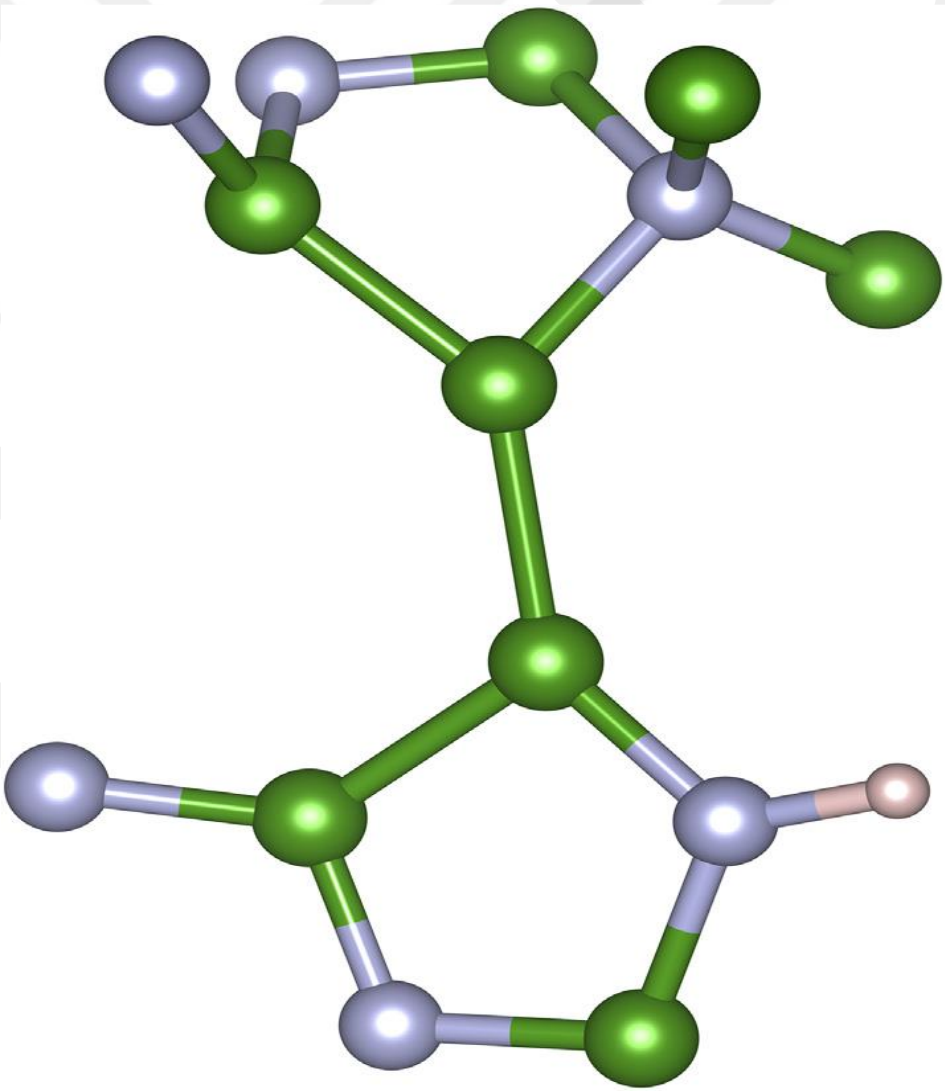

Figure 3.6 Chain-like B-B structure produces the midgap state in model3.

To shed additional lights on the electronic properties of the *a*-BN and *a*-BNH models, we probe the partial density of states (PDOS) provided in Figure 3.7.

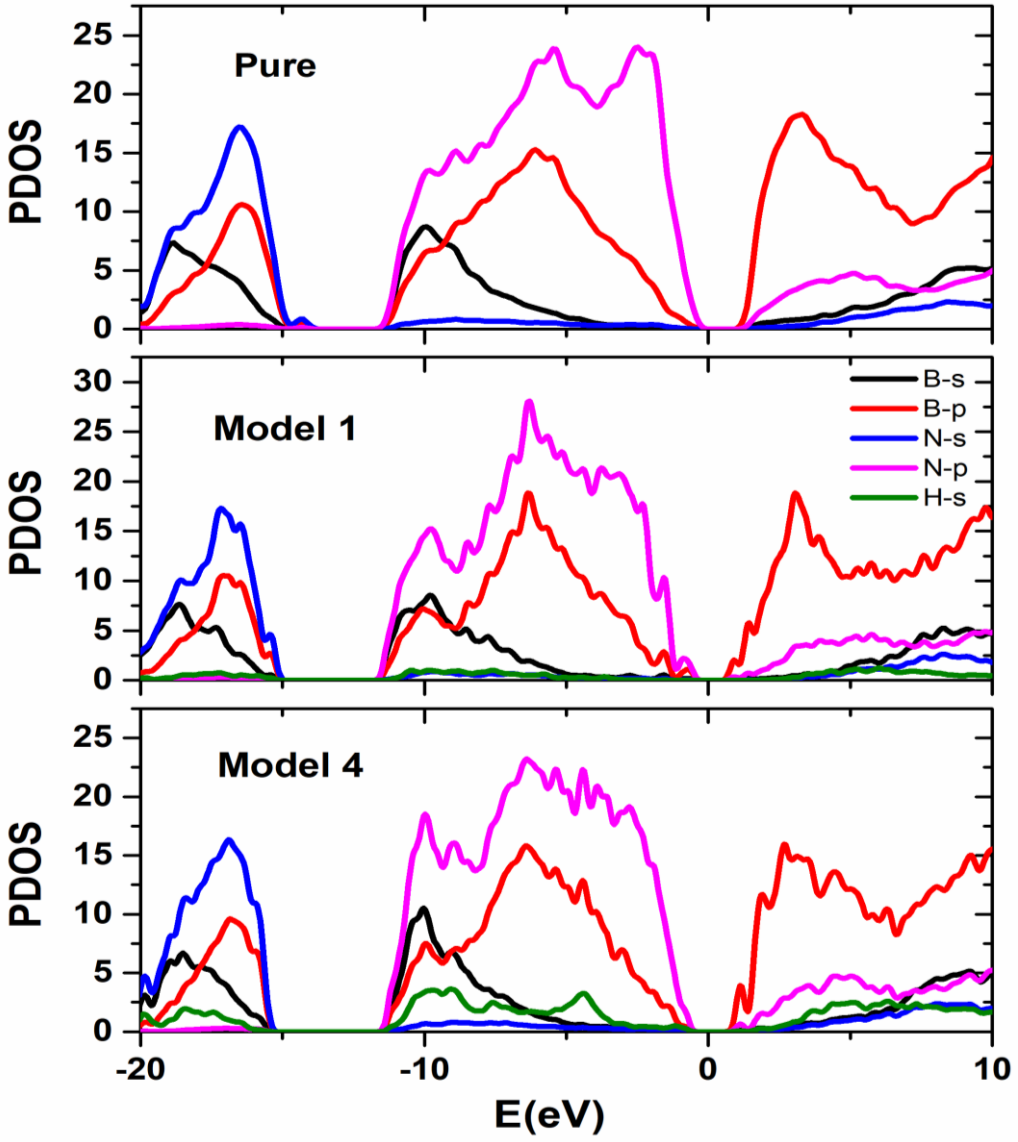

Figure 3.7 PDOS of selected models.

The eigenstates near −20 eV are mainly due to N-s states. B-s and B-p states have some contributions to these energy levels as well. The valance band has contributions from B-s, B-p and essentially N-p states. The conduction band near Fermi level is controlled by B-p states. Our observations are quite similar to what have been stated for h-BN in a previous simulation[199]. The contribution of H atoms to the PDOS is significantly small.

3.4 Discussion

On the basis of the structural analyses, we suggest that the main building unit of both *a*-BN:H and pure *a*-BN is hexagonal rings similar to h-BN. Yet there are some noticeable structural differences between *a*-BN:H and *a*-BN. As expected, hydrogenation passivates twofold-coordinated configurations and yields more sp^2 bonding. In addition, it induces a few sp^3 bonding in the models. Yet as for the hydrogenated content of 18.2%, a noticeable increase in the fraction of sp^3 hybridization is observed in the network. Here based on the observation of the sp^2-to-sp^3 transition in BN at high temperature and pressure treatments, we speculate that the physical origin of such a behavior is probably due to the high degree of stress caused by the excessive hydrogen content in the network. However, further investigations are needed to fully clarify this issue. The development of more sp^3 bonding can be interpreted as some improvement to the mechanical properties of the amorphous configurations because the BN crystals having sp^3 hybridization are a superhard material.

We observe that the formation of N-H bonding is more favorable than that of B-H bonding in all models. This behavior might be unsurprising and can be simply explained by bond energy. Based on bond energy[200], N-H bonding (347±13 kj/mol) is energetically more favorable than B-H bonding (289 ±38 kj/mol).

Since the bonding nature of BN has significant impacts on its physical, chemical, mechanical and electronic properties, perhaps by changing hydrogen content, *a*-BN:H with different features can be engineered.

3.5 Conclusions

We have generated *a*-BN:H models with four different hydrogen concentrations by means of a first-principles MD approach. The comparison of the *a*-BN:H configurations with *a*-BN reveals that although they are locally parallel to each other, hydrogenation yields some noticeable changes on the local structure of *a*-BN. Due to the H passivation of dangling bonds, the *a*-BN:H models do not form the twofold coordinated chain-like structures. Furthermore, it suppresses the development of tetragonal-like rings. All these structural modifications lead to more sp^2 and even sp^3 hybridizations. Because of higher sp^3 bonding, *a*-BN:H is anticipated to possess better

mechanical properties than pure *a*-BN. Additionally we witness the formation of more N-H bonds than B-H bonds in the hydrogenated models. Considering the electronic properties, hydrogenation is found to have minor impact on the electronic structure of *a*-BN.

Chapter 4

Amorphous Boron Carbide from ab initio Simulations

The work presented in this chapter is published in T. A. Yıldız, and M. Durandurdu. "Amorphous boron carbide from ab initio simulations." *Computational Materials Science* 173 (2020): 109397.

4.1 Introduction

Strong covalent solids like diamond and cubic boron nitrite (BN) are superhard materials. Boron carbide (B_4C), the most stable B-C compounds[201], is known as the third hardest crystal after diamond and cubic BN. B_4C has been attracted considerable attentions in recent years because its high hardness, lightweight and refractory features as well as superlative thermo mechanical and electrical properties[109]. It can be fabricated easily, for example, by means of plasma enhanced chemical vapor deposition (PECVD)[202]. B_4C has various practical applications and can be used, for example, as cutting tools, wear resistant gears, and ballistic armors[111,203]. It can also find applications in some devices as diodes and transistors[111]. Since it is a good neutron absorber, it can be used to control reactivity in nuclear reactors[112]. Another functional application area of B_4C is the treatment of cancer by using neutron capture therapy[204].

B_4C can form crystal (polycrystals or single crystal) and amorphous phases. The atomic structure of the B_4C crystal is rather unique and comprehensively discussed in the literature throughout long years[120,122–125,205,206]. At the beginning, it was believed that it consisted of just B_{12} icosahedrons and C-C-C linear chains[207,208]. In later years, however, the Raman and NMR spectra analyses revealed that B_4C did indeed have $B_{11}C$ icosahedrons with C-B-C intericosahedral chains[122,201]. Nonetheless, there have still been some uncertainties about how B and C atoms are

arranged in the B_4C unit cell. In order to develop its scientific and technological investigations, a greater understanding of its local structure is indeed crucial.

Amorphous boron carbide (a-B_4C), of an interest material, can form under diverse experimental techniques, for instance, irradiations[209], shock compression[210], scratch test[211,212], electric field[213], depressurization from high pressure[214] and shear deformations[215,216]. Yet, its local structure is far more complicated than the crystal since it is a random icosahedral network. The earlier studies proposed that the B atoms in the amorphous configuration have two type motifs such as $B_{11}C$ icosahedrons and C-B-C chains associated with the icosahedrons[217,218], similar to the crystal. However, the C-B-C chains were not observed in deposited amorphous films[219,220]. Consequently, depending on experimental preparation protocols, different local structures might exist for a-B_4C. As revealed by experiments, the diverse local structure can lead to the distinct mechanical properties for a-B_4C, for example, its hardness was reported to be between 20.8 and 33.8 GPa depending on deposition temperature[220].

Two theoretical efforts can be found in the literature to model a-B_xC (x=4 and ~2.5) so far. They proposed a dissimilar coordination distribution for these amorphous configurations. In the first study, the models having 120 and 135 atoms (a-B_4C) and different starting structures were generated by using a quite fast quench rate (840 K/ps) [112]. In the second computational study[109], the amorphous model consisting of 216 atoms (154 B atoms and 62 C atoms, namely a-$B_{2.5}C$) was created using cooling rates of 41.25 K/ps and 165 K/ps in different temperature ranges. Consequently, different stoichiometries, starting structure, quenching rates and size of supercells used in these studies are probably the main factors to observe a distinct microstructure in these amorphous systems.

The main objective of this study is to generate a slightly larger a-B_4C model (320 atoms) using a slow cooling rate (66 K/ps), to focus on its short-range order and its electrical and mechanical features and to compare them with available data in the literature.

4.2 Computational Method

In the present study, the SIESTA package program[169] within a pseudopotential method[172] was carried out to perform molecular dynamics (MD) simulations. The double zeta (DZ) as atomic orbital basis set for valence electrons was preferred. The Becke gradient exchange functional[149] and Lee, Yang, and Parr correlation functional[152] were chosen to guess the exchange correlation energy. The grid mesh cutoff was applied as 120 Ry and the Brillouin zone integration was restricted to Γ-point. The MD calculations were executed within the constant number of atom (N), pressure (P) and temperature (T). T and P were controlled by the velocity scaling and the Parrinelo-Rahman[166] approaches, separately. The MD time step was chosen to be 1.0 fs. Our initial configuration was a randomly distributed structure with 320 atoms (256 B atoms and 64 C atoms.) Firstly, the initial configuration was exposed to a temperature of 3200 K for 40 ps. Secondly; the temperature applied was decreased step by step from 3200 K to 300 K with a cooling rate of 66 K/ps. Finally, the structure was relaxed using a conjugate gradient technique. The crystalline form, a supercell having 120 atoms, was constructed based on $B_{11}C$ and C-B-C chains as suggested in Ref. 201. In the present work, the density of amorphous and crystalline phases of B_4C is estimated to be 2.2493 g/cm^3 and 2.4471 g/cm^3, respectively, which are slightly less than 2.47 g/cm^3 (amorphous) and 2.52 g/cm^3 (crystal) reported in experiment obtained by using helium pycnometry[109]. It should be noted that in both studies, amorphization leads to a decrease in the density of B_4C,which is however contradict to Ref. 216 in which it was proposed that shear-induced or quenched amorphous phases have a larger density than the crystal.

4.3 Results

4.3.1. Local Structure

The partial pair distribution functions (PPDFs) investigation is one of the convenient approaches to distinguish the microstructure of materials. Hence, firstly, we study PPDFs of the amorphous and crystalline forms of B_4C and illustrate them in Figure 4.1. Since the bonding natures (B-B, B-C and C-C) play a crucial role in

determining the structure and properties of a-B_4C, the first peak of all pairs is carefully examined.

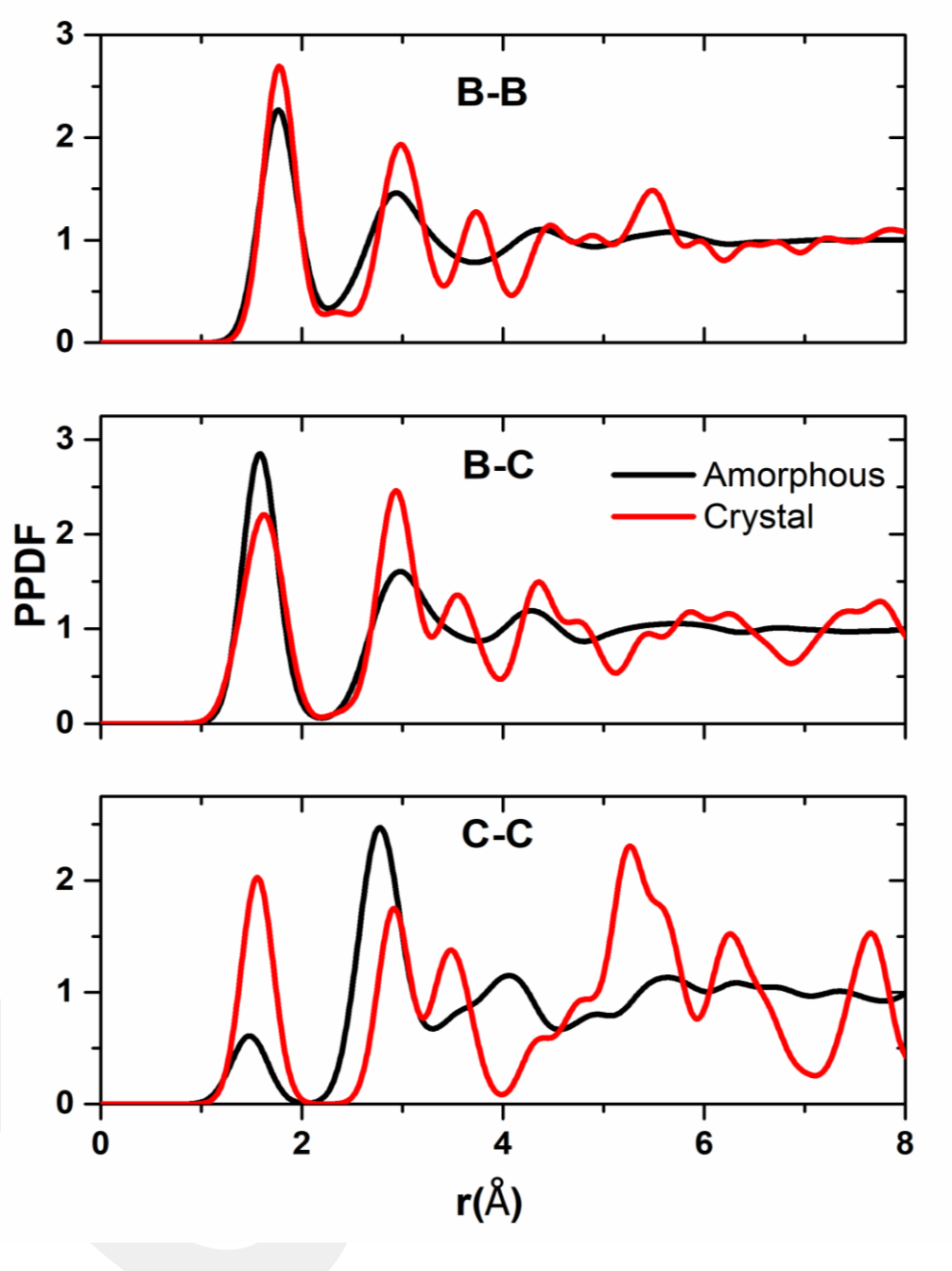

Figure 4.1 Partial pair distribution functions of a-B_4C and B_4C crystal.

The first peak of the B-B, B-C and C-C correlations of a-B_4C (B_4C crystal) is located at nearly 1.77 Å (1.77 Å), 1.58 Å (1.62 Å) and 1.49 Å (1.56 Å), respectively. So, one can see a slight shortening in the B-C and C-C bond lengths by amorphization. Our values logically agree with the computational results of 1.75 Å (B-B), 1.57 Å (B-C) and 1.54 Å (C-C) reported for a-$B_{2.5}C$[109]. The strength of the first C-C peak is relatively smaller than that of first B-B and B-C peaks because of the presence of the

limited number of C-C bonds in the amorphous arrangement, meaning that the formation of C-C bonds is not very favorable in the amorphous network (see below for the chemical environment analysis). The visible second and third peaks of B-B correlation are a result of pentagonal pyramids/B_{12} icosahedral molecules formed in the noncrystalline structure.

The total and partial coordination numbers (CNs) and chemical distribution analyses are very crucial to expose the microstructure of materials in details. Therefore, we secondly estimate them for each species using the first minimum of PPDFs (~2.22 Å for B-B, ~2.19 Å for B-C and ~2.24 Å for C-C correlations). The coordination distribution of the atoms is shown in Figure 4.2.

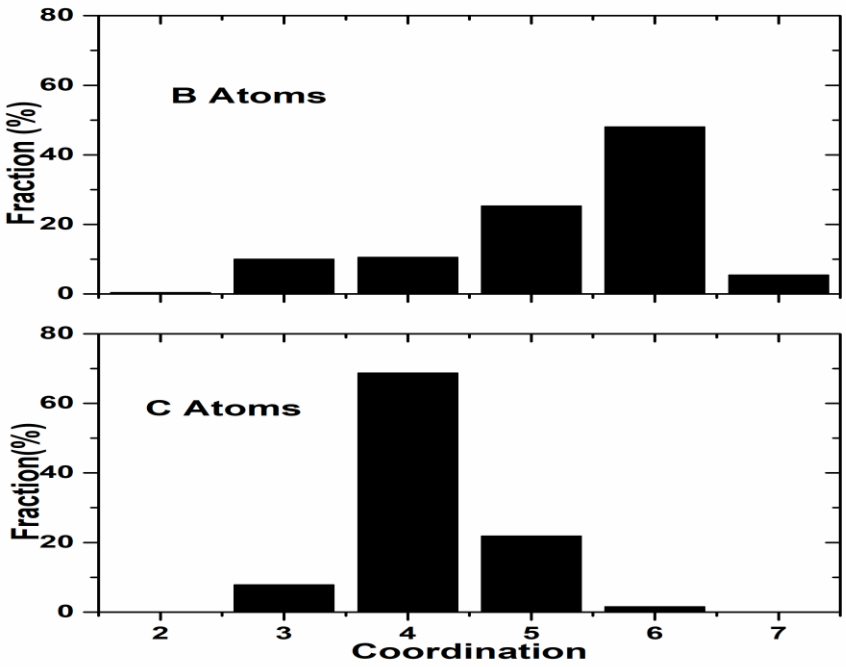

Figure 4.2 Coordination distribution of the amorphous model.

In the a-B_4C model, B atoms have a coordination distribution ranging from 2 to 7. Amongst them, six-fold coordination is the most dominated one with a fraction of nearly 48.0% (see also Table 4.1), which is slightly higher than the value of 42.90% reported in Ref. 109.

Table 4.1 Coordination distribution of B and C atoms in the a-B_4C.

1st Neighbors	2	3	4	5	6	7	References
B (%)	0.39	10	10.54	25.30	48.04	5.46	This study
	0	15	18.80	21.40	42.90	1.9	[109]
C (%)	0	7.80	68.75	21.87	1.50	0	This study
	0	4.90	61.30	29.00	4.80	0	[109]

Our amorphous arrangement has three-fold (10%) and four-fold (10.54%) coordinated B atoms, which are less than 15% and 18.80% recounted in Ref. 109. However, our disordered configuration demonstrates about 4% more five-fold and seven-fold coordinated motifs relative to the a-B_4C model of Ref. 109 (see Table 4.1). These coordination distributions result in an average CN of B atom to be 5.29, which is comparable with 5.66 in the crystal. For C atoms, the most prevalent cluster is the four-fold coordinated unit (68.75%) and its fraction is again comparable with 61.3% stated in the earlier study[109]. The second and third dominant ones are the five-fold (21.87%) and three-fold (7.80%) coordination, slightly different than 29% and 4.9% reported in Ref. 109. The mean CN of C atoms is 4.17, parallel to 4.66 in the crystal. All these observations reveal the striking similarities between our model and previously proposed amorphous network[109] and the crystal.

For a-B_4C, the chemical environments of B and C atoms demonstrated in Table 4.2 can provide more knowledge about the system at the microscopic level.

Table 4.2 Chemical identities around B and C atoms for a-B_4C.

a-B_4C			
B		**C**	
B_5C_1	23.83%	B_4	57.81%
B_6	20.31%	B_5	20.31%
B_4C_1	9.77%	B_3C_1	10.94%
B_5	7.03%	B_3	3.12%
B_3C_2	6.64%	B_2C_1	3.12%
B_1C_2	5.86%	B_4C_1	1.56%
B_4C_2	4.30%	B_1C_2	1.56%
B_3C_1	3.12%	B_6	1.56%
B_2C_2	3.12%		
B_7	2.73%		
B_4	2.34%		
B_2C_1	2.34%		
C_3	1.95%		
B_2C_3	1.95%		
B_1C_3	1.56%		
B_6C_1	1.56%		
B_3C_3	0.78%		
B_3	0.39%		
B_1C_1	0.39%		

As seen from Table 4.2, the most prevalent clusters for B atoms are B-B_5C_1 (23.83%) and B-B_6 (20.31%) type motifs. On the other hand, in the crystalline B_4C structure, B atoms have four kind motifs: B-B_5C_1 (50.00%), B-B_6 (25.00%), B-B_4C_2 (16.67%) and B-C_2 (8.33%). B-C_2 unit represents the intericosahedral linear C-B-C chain and as seen in Table 4.2, it does not exist in the noncrystalline network. Nonetheless one can see that nearly 50% of B atoms in the a-B_4C model form clusters (B-B_5C_1, B-B_6 etc.), similar to those of the crystal, suggestion partial local similarities between these two forms of B_4C. The first three common configurations for C atoms are C-B_4 (57.81%), C-B_5 (20.31%) and C-B_3C_1 (10.94 %) kind units. Likewise, the crystalline B_4C contains C-B_4 (33.33%), C- B_3C_1 (33.33%) and C-B_5C_1 (33.33%) type structures. The formation of more C-B_4, less C-B_3C_1 and lack of C-B_5C_1 type clusters in the amorphous model relative to the crystal can be interpreted as the tendency of C atoms to form more C-B bonds than C-C bonds in the amorphous model and their trend to form more tetrahedral configurations.

With aid of the Voronoi polyhedral approach[221], one can distinguish the type of clusters shaped around B and C atoms and thus have valuable information on the

structure at the atomistic level. In this method, the indices < n_3, n_4, n_5, n_6…> are used to identify polyhedrons, where n_i and $\sum n_i$ stand for the number of i-edge faces of a polyhedron and its CN, respectively. The principal structural unit of B and B-rich crystalline/amorphous materials are known as B_{12} molecules, which comprises of pentagonal pyramids[222]. In the crystalline B_4C phase, the most favorable polyhedron is characterized by < 2, 2, 2, 0 > index (92%), which represents the pentagonal pyramid. In other respects, we find eight distinct polyhedra for B atoms in the disordered structure. The two leading ones are denoted by the < 2, 2, 2, 0 > (47%) and < 2, 3, 0, 0 > (24%). The second one can be classified as defective pentagonal pyramid-like structures. Subsequently one can see that about 70% of B atoms have a tendency to form complete or incomplete pentagonal pyramid-like patterns in the amorphous network. On the other hand, we determine three diverse polyhedra for C atoms in a-B_4C. The most foremost ones are labeled as < 4, 0, 0, 0 > (68%) and < 2, 3, 0, 0 > (21%). In addition, we find < 2, 2, 2, 0 > (0.01%) type cluster, a part of $B_{12}C$ molecules. In the ordered form, on the other hand, there are just two types of polyhedrons for C atoms and they are characterized by the < 4, 0, 0, 0 > (66%) and < 2, 2, 2, 0 > (33%) indices. All these findings specify noticeable similarities in the local structure of amorphous and crystalline forms of B_4C. The earlier study[109] suggests the formation of B_{12}, $B_{11}C$ and $B_{10}C_2$ molecules for a-$B_{2.5}C$. Yet our model has just B_{12} and $B_{12}C$ molecules. The lack of the other clusters in our network might be associated with the size of simulation boxes or different cooling rates used in present and earlier studies.

To identify the structure features of a-B_4C in details, we further analyze the bond angle distribution functions (BADFs) and compare them with those of the crystalline structure. The B-B-B, B-C-B and C-B-C angle distributions for the crystal and a-B_4C are shown in Figure 4.3. The B-B-B angles produce two main peaks. The first peak is located at 59^o while the second peak is positioned at nearly 107^o, similar to the crystalline B_4C phase. These two sharp peaks are related to the intraicosahedral bonds of the pentagonal pyramids. The third sharp peak nearly 122^o in the crystal are associated with the intericosahedral bonds and weakly presented in the amorphous model due to the randomly distributed icosahedrons (or pentagonal pyramids).

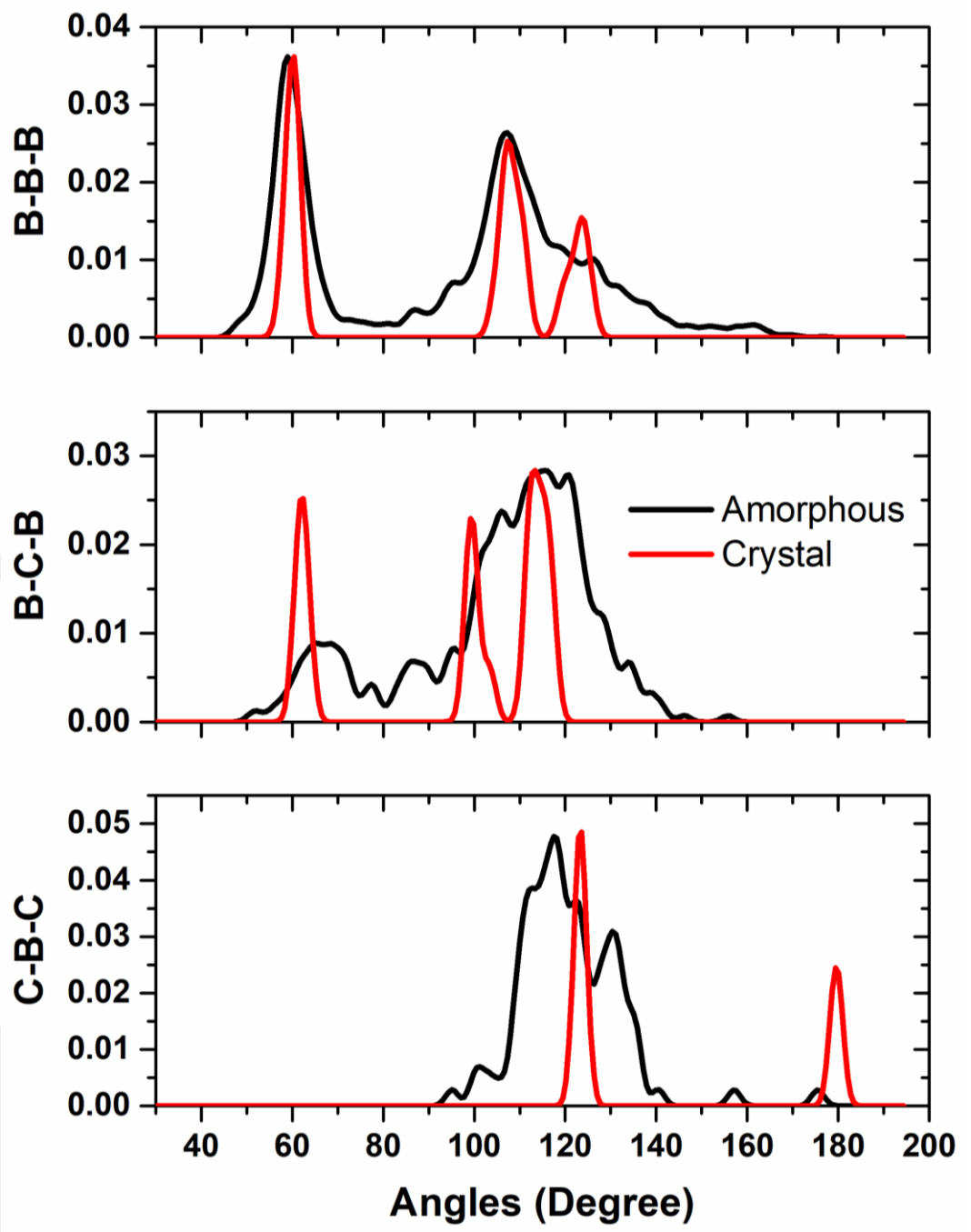

Figure 4.3 Bond angle distribution functions of a-B_4C and B_4C crystal.

The B-C-B angles of the crystalline structure have three sharp peaks at around 62°, 99° and 113°, which are again related to the intraicosahedral and intericosahedral bonds. These B-C-B angles show a broad distribution in our model but the peaks around 62°, 99° and 113° angles are roughly produced in our model. The C-B-C distribution in the noncrystalline network ranges from 90° and 180° and has a foremost peak at nearly 120°, which slightly deviates from 123° presented in the crystal. The C-B-C at 180° is not captured in the amorphous network. The occurrence of these peaks suggests the

existence of C-B-C bonds in the amorphous configuration but the intericosahedral linear C-B-C chain does not exist since B-C_2 motif does not form in the model (see Table 4.2), which is also confirmed by visualizing the model given in Figure 4.4.

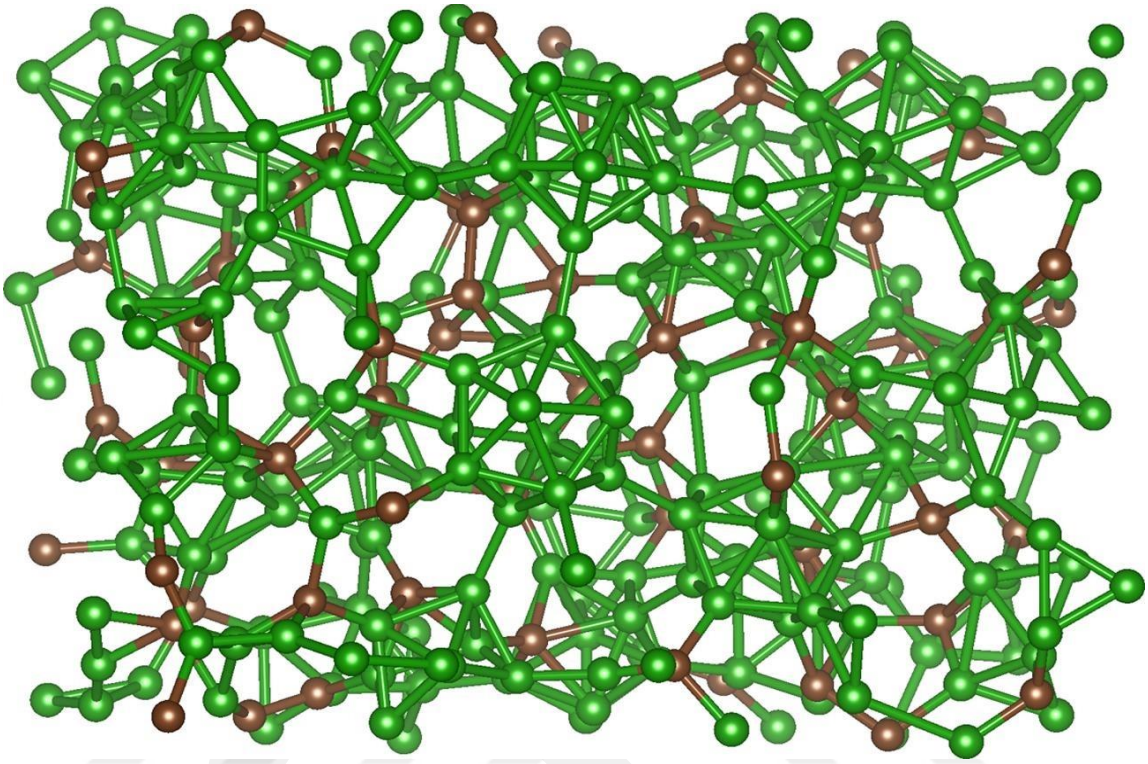

Figure 4.4 Ball-stick representation of a-B_4C.

4.3.2. Electronic Properties

Boron-rich materials such as the crystalline and amorphous boron carbides are of great interest for numerous technological applications, particularly, in the semiconductor devices. For that reason, revealing the electronic behaviors of ordered and disordered B_4C structures is significant in this study. Firstly, the electronic properties of a-B_4C and the crystal are investigated via the total electron density of states (TDOS). Secondly, in order to get more detailed contribution about their electronic features, their partial electron density of states (PDOS) is calculated. Figure 4.5 illustrates them.

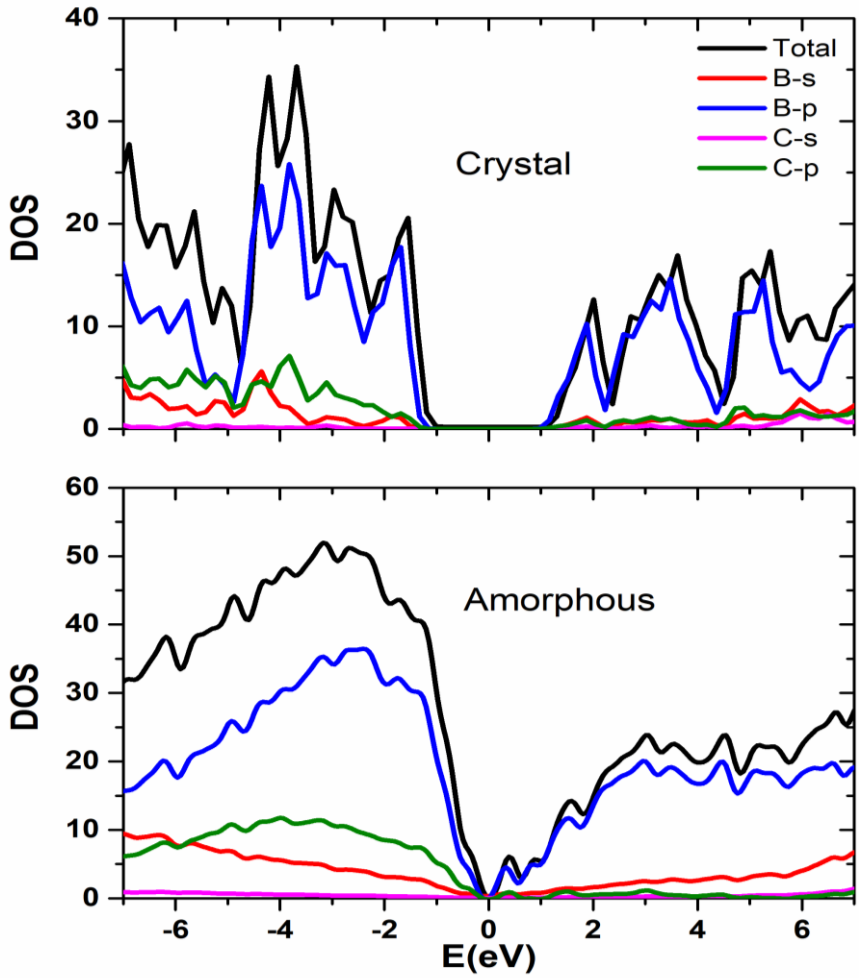

Figure 4.5 Total electron density of states (TDOS) and partial density of state (PDOS).

The band gap energy for the B_4C crystal is nearly 2.9 eV, parallel to the previous DFT-GGA (LDA) band gap of 2.6-3.0 eV[112,123,223–225]. It should be noted here that GGA calculations lead to smaller energy band gaps relative to experiments due to the self-interaction error in DFT-GGA computations. Such a limitation can be eliminated by using DFT-GGA+U, DFT-GWA or DFT-hybrid exchange functionals (HEFs). Indeed, using a HEF, the band gap energy of the crystal was estimated to be 3.84 eV[226]. In other respect, the energy band gap of a-B_4C is found as 0.15 eV. Thus, a drastic band gap closure is observed by amorphization but not metallization as suggested in Ref.112. According to the PDOS analysis, B-p states are more prevailing for both valence and conduction bands for the amorphous and crystalline phases. Additionally, B-s and C-p states also have some contributions to the valence band for both structures. However, C-s states have minor effect on both conduction and valance bands for the noncrystalline network, similar to that of the crystal.

4.3.3 Mechanical Properties

As a beginning, the relation between energy (*E*) and volume (*V*) for the crystalline and amorphous states is determined via a variable cell optimization technique. We estimate their bulk modulus (K), and equilibrium volume (V_0) and energy (E_0) by fitting the *E*-*V* values given in Figure 4.6 to the third-order Birch-Murnaghan equations of states via Equation 2.44.

As deduced from the Figure 4.6, the crystal has lower energy than the amorphous state. The relative energy difference between them is predicted to be around 0.25 eV/atom. The equilibrium volume of the crystal is 7.49 $Å^3$/atom whereas that of the amorphous structure is about 8.16 $Å^3$/atom. Thus, one can notice about 9% volume expansions by amorphization.

In Table 4.3, we list the mechanical properties of a-B_4C and the crystal along with the data available in the literature. The K value of a-B_4C is estimated to be about 162.61 GPa while that of the crystalline form is nearly 245 GPa, in good agreement with the earlier predictions of 248-274 GPa[201,227–230]. Consequently, amorphization leads to a noticeably decrease in the bulk modulus which is related to the disorder nature (coordination defects, chemical defects etc.) of the amorphous model.

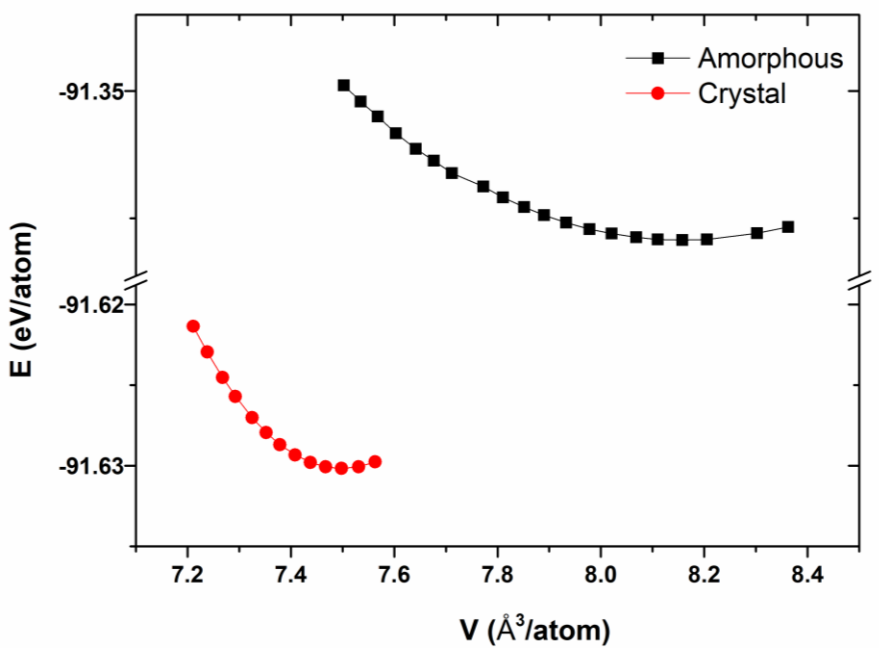

Figure 4.6 Energy volume relation of a-B_4C and B_4C crystal.

We apply a uniaxial stress along the principle axes of the supercells and optimize the atomic coordinates and their volume to predict the Poisson's ratio (ν) defined by Equation 2.46.

Poisson's ratio is predicted from the slope of the best fitting straight line and six different values between 0.16 and 0.21 are obtained for the noncrystalline network. The calculated average Poisson's ratio for the amorphous and crystalline forms of B_4C is estimated to be about 0.18 and 0.17 respectively, which is quite in agreement with the results of the earlier studies as presented in Table 4.3[227,228,231].

Table 4.3 Bulk modulus (K), Young's modulus (E), shear modulus (μ), hardness (H) and Poisson ratio (ν) in the crystalline and amorphous structures.

	K(GPa)	E(GPa)	μ (GPa)	K/μ	ν	H (GPa)	References
Crystal	245	470	200	1.22	0.17	~32(Chen)	This study
						~30(Teter)	This study
						~31(Tian)	This study
	248, 274						[201]
						~40, 41	[211]
		402				~42	[220]
	235	462	197		0.17		[227]
	247	472	200		0.18		[228]
		448			0.21		[231]
		441	188				[232]
	239					~45	[229]
	238		199				[230]
				1.20		~32	[233]
Amorphous	162.61	312.22	132.29	1.23	0.18	~24(Chen)	This study
						~20(Teter)	This study
						~23(Tian)	This study
		255-351				~21-34	[220]

Knowing K and ν is enough to calculate the Young's modulus (elastic modulus) (E) using Equation 2.47.

E is estimated to be 312 GPa for a-B_4C, which is reasonably in the range of experimental values of 255-351 GPa reported for a-B_4C at different temperatures[220]. For the ordered form, it is 470 GPa that again coincides with the 402-441 GPa[220,227,228,231,232].

The shear modulus (μ) is another important mechanical property of a material and can be obtained by using Equation 2.48.

The calculated shear modulus for a-B_4C is about 132 GPa. For the crystalline form, the modulus is calculated to be around 200 GPa, which is quite akin to the available results of 188-200 GPa[227,228,230,232] in the literature.

In the last step, the Vickers hardness (H_v) is calculated using three different empirical equations. The first formula, called as Teter's equation, is given by Equation 2.49[173]. The second equation, known as Chen's equation[174], is given by Equation 2.50. The Chen's equation appears to have some limitation and was revised by Tian [175] as Equation 2.51.

By using these three useful equations, the Vickers hardness of the disordered model is projected to be between 20 and 24 GPa, reasonably in the range of previous results of 21-34 GPa reported for a-B_4C[220]. On the other hand, for the crystal, we calculate the Vickers's hardness to be about 30-32 GPa, which are slightly smaller than previous experimental data of 40-42 GPa[211,220,233].

Pugh's ratio can be used to reveal the brittle or ductile behavior of a material. The critical value of n is equal to 1.75. If n is higher (lower) than 1.75, then the material is ductile (brittle). n is 1.23 for a-B_4C and 1.22 for the crystal, showing their brittle character. These values are in quite good agreement with earlier result of 1.20[233] as seen in Table 4.3.

4.4 Conclusions

We have carried out a comprehensive investigation on the local structure, electronic properties, and mechanical features of a-B_4C via quantum mechanical MD simulations. The values of structural parameters are found to be close to the previous investigations. The local structure of the amorphous model is partially similar to that of the crystal. The C-C bonds are found to be less favorable in the noncrystalline network. The mean coordination number of B and C atoms for a-B_4C is 5.29 and 4.17, correspondingly. The amorphous configuration shows an energy band gap of 0.15 eV, strikingly smaller than 2.9 eV estimated for the crystal. Softening of the mechanical properties is observed by amorphization. Nonetheless, due to the high Vickers hardness, a-B_4C can also serve as a hard material.

Chapter 5

Ab-Initio Study of Boron-Rich Amorphous Boron Carbides

The work presented in this chapter is published in T. A. Yıldız, and M. Durandurdu. "Ab-initio study of boron-rich amorphous boron carbides." *Journal of the American Ceramic Society* (2023).

5.1. Introduction

Boron (B), carbon (C) or nitrogen (N) compounds form covalently bonded solids and they are recognized as hard materials[234]. One of which is boron carbide[210,219,235] and is a semiconducting system possessing a wide band gap depending on the B to C stoichiometry[236,237]. Boron carbide compounds are promising materials for several high-technology industrial applications due to their distinguished features such as good chemical inertness, high hardness, low wear coefficient, high melting point and low density[111,238–242]. Because of their unique electronic properties[238,243], they can be used in photovoltaic and beta-voltaic devices [238,244], diodes and transistors [111], and neutron detectors[112,245–248] as well. In addition, combining their attractive properties such as lightweight and high hardness, they can be also used in body armor applications[111,121,249].

The first boron carbide material was synthesized in 1858. However, it was not attained enough considerations until 1934[114]. The stoichiometric ratio as B_4C was studied in the mid-1930s[115]. Up to today, boron carbide with different B/C ratios has been fabricated using numerous experimental procedures, such as plasma enhanced chemical vapor deposition[202], magneton sputtering[219,220,235,250], pulsed laser

deposition[251–253], ion beam synthesis[254], hot pressing, spark plasma sintering etc. [255–257].

The atomic structure and mechanical characteristics of boron carbide materials appear to be relatively sensitive to B/C ratios. The studies suggested that B substation first modified C atoms in the $B_{11}C$ icosahedra transforming $B_{11}C$ to B_{12} molecules and then excess B atoms revised C-B-C chains[255]. For the B/C<4 materials, on the other hand, the existence of free C atoms in the microstructure and the formation of B_4C and graphite like structures at a C concentration of >20 at.%. were suggested[256]. As expected, the change in the local structure has noticeable impacts on the mechanical properties of boron carbide. The maximum fracture toughness and hardness was observed for the stoichiometric composition (B_4C) and they surprisingly decreased for nonstoichiometric B_4C (B/C>4 and B/C<4) compositions[258]. For B/C>4 materials, the decrease was attributed to the weakening of the bond strength (substitution of the stronger B–C bonds with weaker B–B bonds) while the decrease for B/C<4 compositions was dedicated to free C atoms in the microstructure[258].

Amorphous state of boron carbides has also drawn attention due to their unique properties and has been considered both experimentally and theoretically[109,112,259]. An experimental investigation confirmed that pentagonal pyramids were the most preferable clusters in amorphous B_4C (a-B_4C)[259]. The atomic and electronic behaviors of a-B_4C were investigated at ab initio level using two different systems (containing 120 and 135 atoms) and several important findings were exposed. This computational study proposed that both amorphous configurations consisted of a random icosahedral network without linear chains and a-B_4C owned a semimetal character[112]. Later, the combination of experimental and theoretical studies provided useful information regarding the local structure of a-$B_{2.5}C$ and revealed that it consisted of B_{12}, $B_{11}C$ and $B_{10}C_2$ icosahedrons[109].

Hydrogenated amorphous boron carbide films having several B/C ratios[260,261] were also prepared. The basis of these studies is about their compositional, structural, physical, electrical optical, and mechanical properties. a-B_xC:H_y thin films ($3.4 \leq B/C \leq 4.9$ and H concentration changing from 10% and 45%) were fabricated via PECVD technique and thin films were found to have density from 0.9 to 2.3 g/cm^3, Young's modulus from 10 to 340 GPa and band gap between 1.7 and 3.8 eV[260]. In a different study, a-B_xC:H_y thin films ($3.4 \leq B/C \leq 4.9$ and H content varying from 37.5% and 50.5%) were synthesized by PEVCD process and it was found that the thin films had a

good thermal conductivity (0.31±0.03 $Wm^{-1}K^{-1}$) and a Young's modulus of 12±3 GPa[261].

Although there are some investigations on the microstructure and mechanical descriptions of B-rich boron carbides, there is no elaborated information about their structural, electrical and mechanical features of their amorphous form(s). In the current study, possible B-rich amorphous boron carbides with ten different B/C ratios (B_xC_{1-x}, $0.50 \leq x \leq 0.95$) are modeled via ab initio molecular dynamics (MD) simulations and some important properties (structural, electrical and mechanical) are exposed in details.

5.2 Computational Method

All calculations were executed by using the SIESTA ab initio code [169] within a pseudopotential method[172] and a generalized gradient approximation (GGA) proposed by Becke gradient exchange functional[149] and Lee, Yang, and Parr correlation functional[152]. A double-zeta (DZ) was adopted as the atomic orbital basis set for the valence electrons. The grid mesh cut-off was set to 120 Ry and Γ-point sampling of k-mesh was applied for the Brilliouin zone integration. The time step was selected as 1 femtosecond (fs). All simulations were done within the NPT (constant number of atoms, constant pressure, and constant temperature) ensemble. The controlling of temperature and pressure was managed by the velocity scaling and the Parrinelo-Rahman[166] techniques, correspondingly. We used a BN melt consisting of 200 atoms as an initial structure and replaced all N atoms with C atoms. Later, the structure was equilibrated at 3400 K for 40 picoseconds (ps). To achieve a definite amount of B concentration (55%-95%), C atoms were randomly replaced by B atoms. Depending on B content, then each configuration was explored to 3400 K (50 at. %B)-2500 K (95 at. %B) for 40 ps in order to get a well equilibrated melt and then the melts were quenched to 300 K in ~155-110 ps. Eventually, the resulting structures at 300 K were relaxed via a conjugate gradient (CG) technique until the maximum force was less than 0.02 eV/Å. In the present study, the density of c-B_4C is estimated to be about 2.45 g/cm^3, fairly parallel to 2.52 g/cm^3[36]. On the other hand, the density of amorphous materials ranges from ~1.97 to 2.24 g/cm^3, less than 2.47 (±0.01) g/cm^3 reported for a-$B_{2.5}C$ in an experimental study[109]**.** The VESTA[262] program for visualization of the

random structures was used. Figure 5.1 reveals the ball stick demonstration of some selected amorphous arrangements.

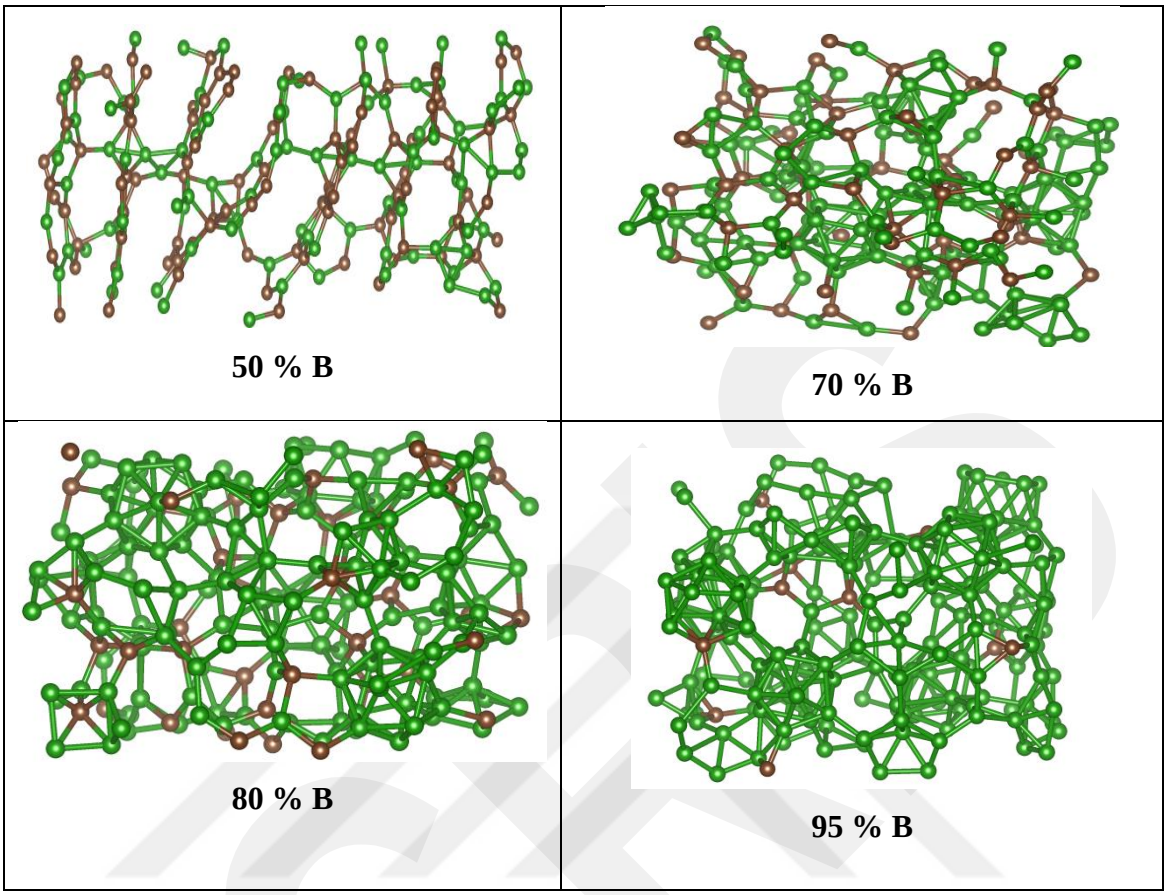

Figure 5.1 Ball stick representation of some amorphous models.

5.3 Results

5.3.1 Local Structure

The partial pair distribution functions (PPDFs) investigation is one of the effective schemes to offer valuable descriptions about the characteristic of a structure at the atomistic level. Figure 5.2 shows the PPDFs of some amorphous boron carbide configurations. There are some notable changes in the distributions with changing B content as expected. As B/C ratio increases, the intensity of the first and, similarly, second B-B peaks increases, due to the formation of more pentagonal pyramid-like motifs. For the B-C pairs, the intensity of the first peak moderately decreases with increasing B content. C-C bonds exist only between 50 and 80 % B concentrations.

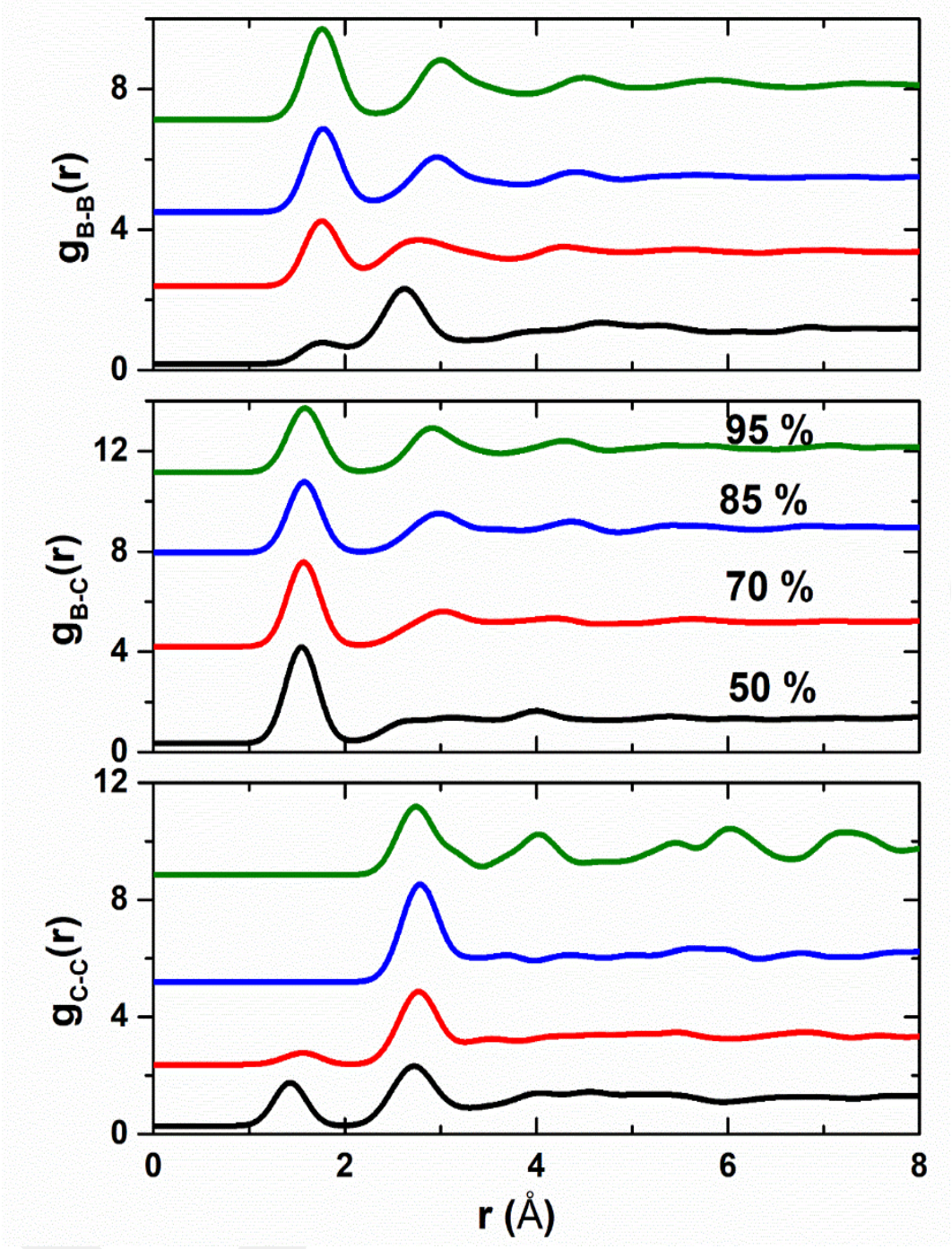

Figure 5.2 Partial pair distribution functions at some B concentrations.

The first peak position of PPDFs can be used to determine the mean bond separation for each pair. The average B-B bond length has the values of 1.75-1.77 Å, indicating that B content has almost no effect on this bonding. The range perceived is reasonably coherent with previously reported data of 1.75 Å in a-$B_{2.5}C$[109], 1.74-1.80 Å in c-B_4C[207], 1.73-1.79 Å in c-B_4C having different chains (B_{12}-CCC, B_{12}-CBC and $B_{11}C$-CBC)[263] based on a DFT calculation, and 1.73-1.80 Å formed in the liquid, amorphous and crystalline phases of B[264–266]. The mean B-C bond distance is

estimated to be 1.55-1.58 Å. Again, it appears that B content does not have a significant impact on this bonding as well. Our B-C estimations are also comparable with 1.57 Å in a-$B_{2.5}C$[109], 1.56-1.66 Å in c-B_4C[207,263] and 1.60 Å in c-$B_{13}C_2$[267]. The C-C bond distance is predicted to be in the range of 1.43-1.56Å, which are comparable with1.54 Å reported for a-$B_{2.5}C$[109], 1.39-1.45 Å in c-B_4C[207], 1.42 Å in graphite and 1.54 Å in diamond[268]. Relative to the other separations, C-C bond seems to be sensitive to B content, which is probably correlated with the formation of different motifs (from threefold to sixfold coordinated) around C atoms having homopolar bonds.

In order to validate our results, we compare atomic structure factor S(Q) and reduced pair distribution function $G_{PDF}(r)$ of two compositions [a-$B_{70}C_{30}$ and a-$B_{75}C_{25}$] with the neutron diffraction data of a-$B_{2.5}C$[109] and provide them in Figure 5.3. One can see that in spite of the small size of simulation boxes and different composition ratios, our results fairly agree with the experiment.

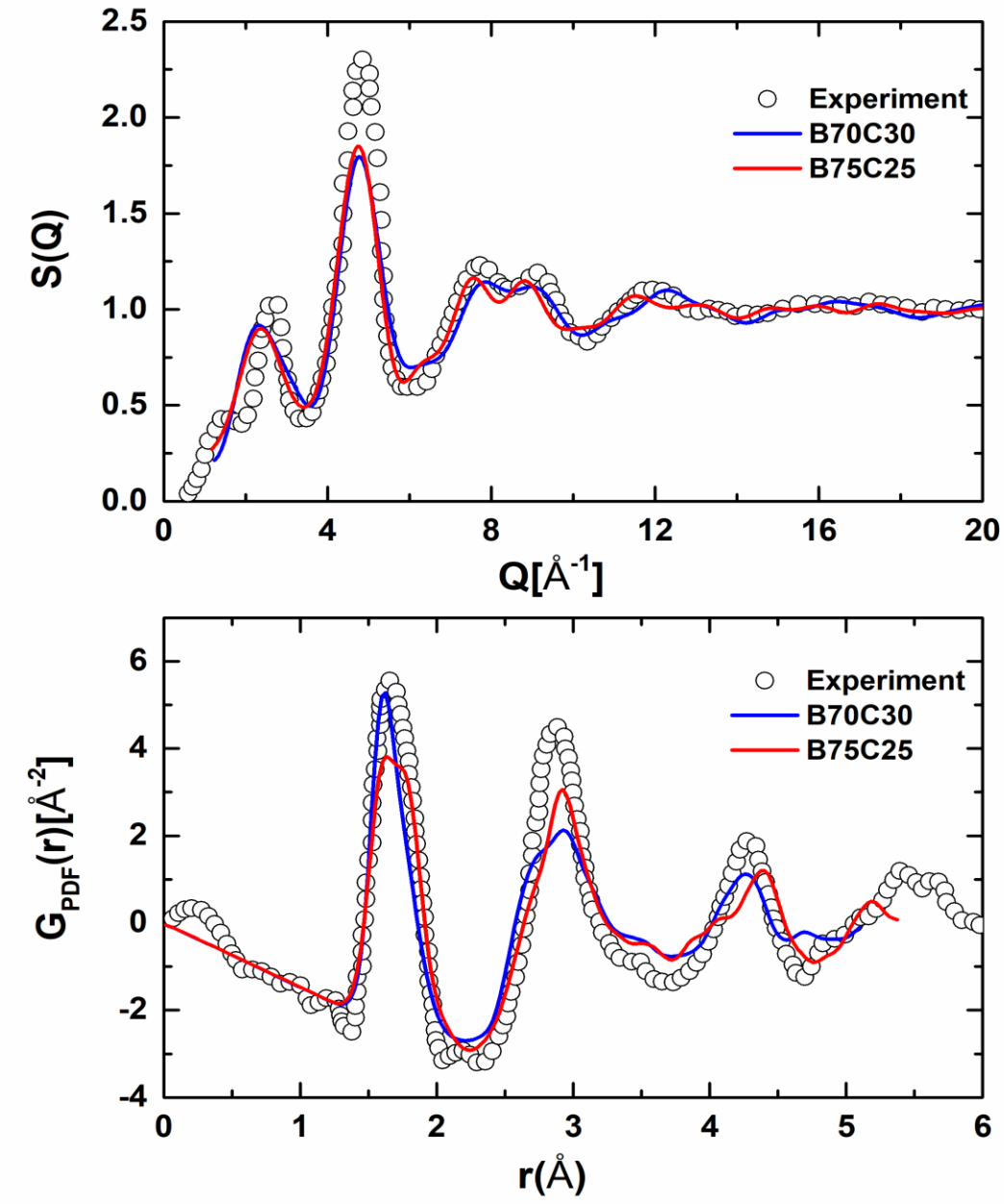

Figure 5.3 Atomic structure factor S(Q) and reduced pair distribution function $G_{PDF}(r)$ of two compositions [a-$B_{70}C_{30}$ and a-$B_{75}C_{25}$]. Empty circles: neutron diffraction data of a-$B_{2.5}C$.

The total and partial coordination numbers (CNs) are positively needed to shed some lights onto the local structure of a material at the atomistic level and hence in the second step, we estimate them by way of cutoff distances (the first minimum) of PPDFs (2.04-2.33 Å for the B-B correlation, 2.10-2.17 Å for the B-C distribution and 1.91-2.07 Å for the C-C pairs depending upon B concentration). As shown in Figure 5.4, the average CN of B atoms increases continuously from 3.22 to 5.70 while that of C atoms changes steadily from 3.46 to 4.30. As we will discuss below, B atoms have a strong tendency to form sixfold-coordinated pentagonal pyramid-like motifs. As B content increases, more B atoms are able to form sixfold coordination and hence the mean CN of B atoms gradually increases. We also see the development of pentagonal pyramid-like motifs around some C atoms (see Voronoi analysis below) as in c-B_4C[201] and a-$B_{2.5}C$[109].Thus, such a development leads to high mean coordination for C atoms. We specifically focus on the 80% B content because it is a well-studied material and find the mean CN of a-B_4C to be 4.15, which is comparable with 4.66 in c-B_4C.

In order to have more knowledge on the atomic structure of the networks, the coordination distribution is considered and provided in Figure 5.5. As seen from the figure, threefold-coordinated B atoms, supporting sp^2 hybridization, are prevailing at 50% B concentration and quickly decreases with increasing B content while the sixfold coordination rapidly increases. Fourfold-coordination, on the other hand, remains almost null up to 80% at which point it starts to decrease. Fivefold-coordination becomes noticeable at 60 at. %B and remains practically unchanged thereafter. Sevenfold-coordination develops at 65% B concentration and its fraction reaches a maximum value of 17%. On the other side, for C atoms, threefold and fourfold coordinated structures with a fraction of 56% and 42% respectively, are dominant at 50 at. %B. With the increase of B content, threefold coordination decreases drastically and parallel to this decreases, fourfold coordination increases initially, remains nearly unaffected between 60% to 85% B contents and then begins to decrease again. Fivefold-coordinated configuration gradually increases from 2% to 30%. Sixfold coordinated motif first develops at 70% B content and reaches a maximum value of 10% at 90 at. %B. We specifically focus on the 80% B ratio because it is a well-studied material and find the mean CN of a-B_4C to be 4.15, which is comparable with 4.66 in c-B_4C.

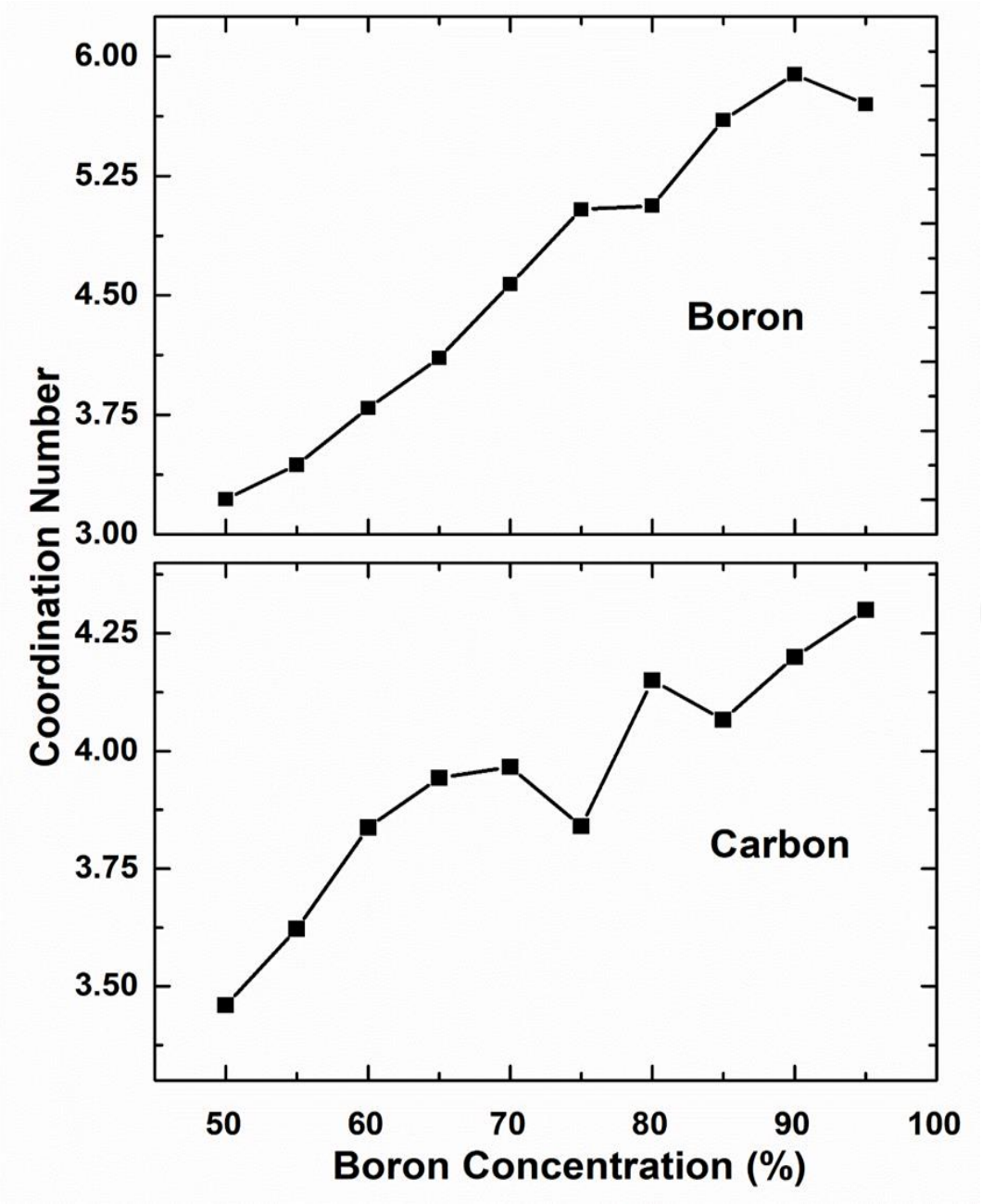

Figure 5.4 Modification of partial coordination numbers as a function of B concentration.

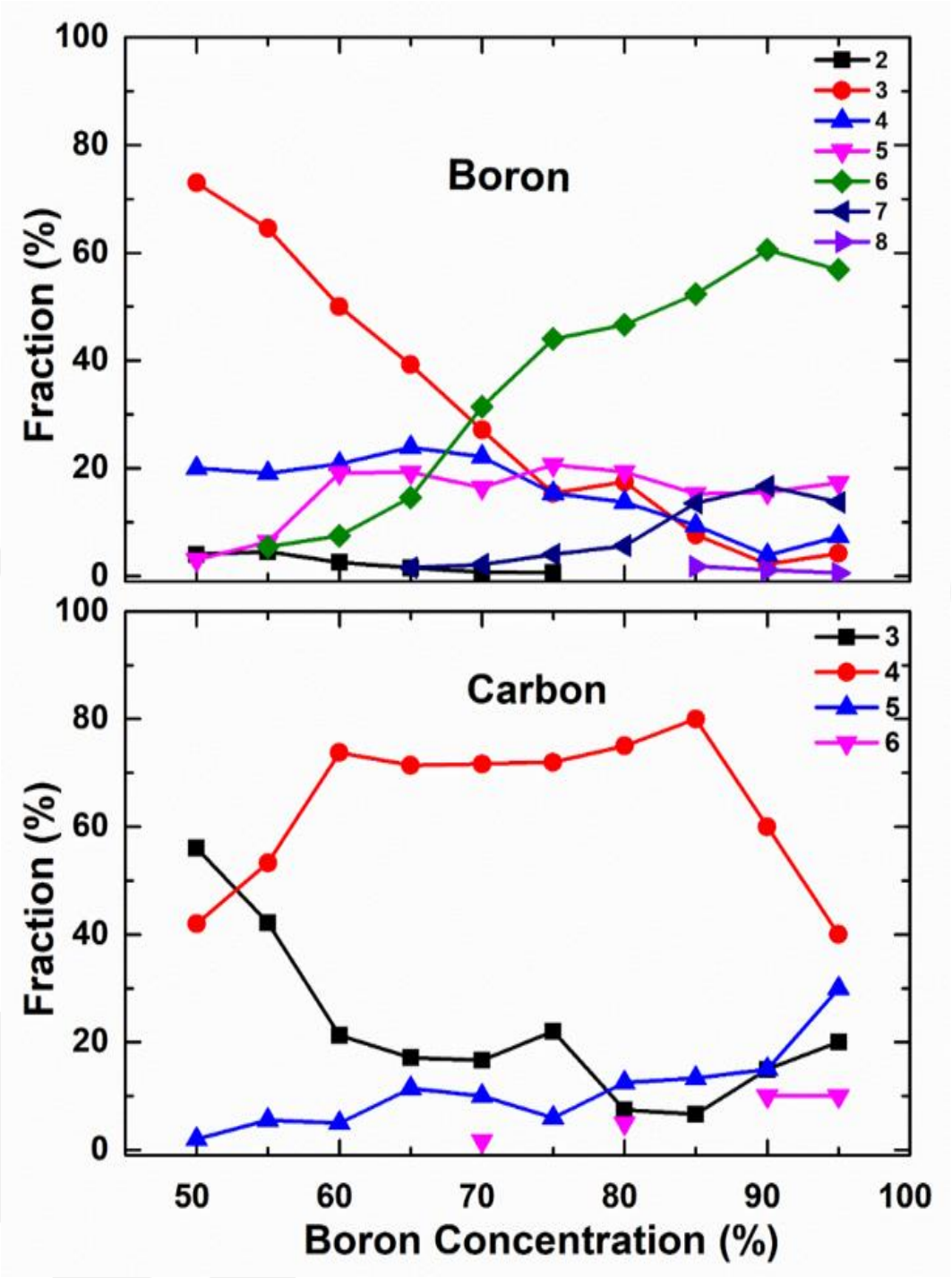

Figure 5.5 Coordination distribution of B and C atoms as a function of B concentration.

The bond angle distribution analysis (BADF) is performed to provide further information on the microstructure of amorphous boron carbide configurations. Figure 5.6 shows the B-B-B, B-C-B, C-B-C and C-C-C bond angle distributions of some amorphous models.

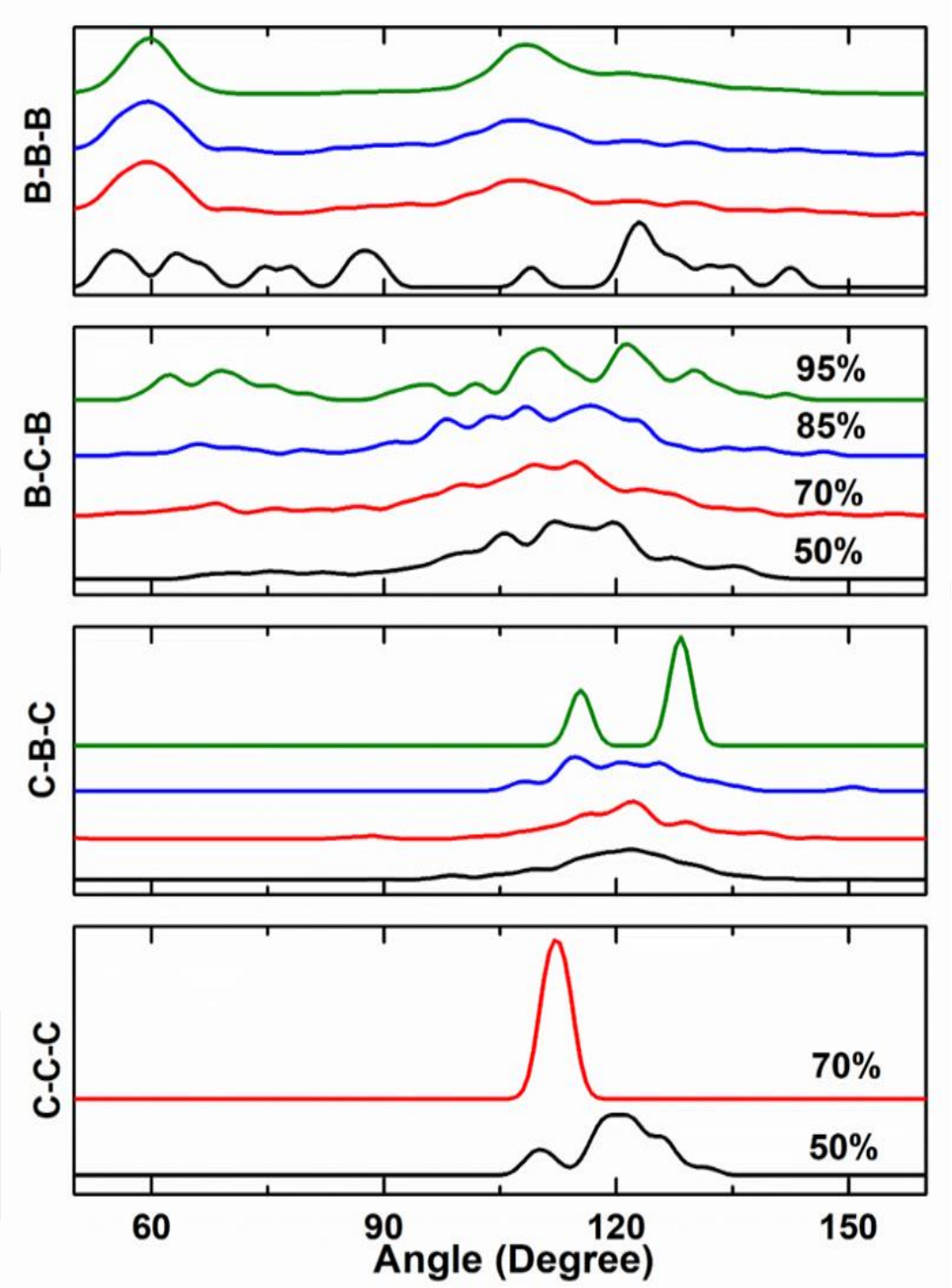

Figure 5.6 Bond angle distribution functions at some B concentrations.

The B-B-B angles possess a wide distribution with several peaks ranging from roughly 56º to 122º because of twofold-to-fivefold structures, respectively, at 50% B concentration. From 70% to 95% B content, the distribution has two clear peaks at roughly 60º and 107º, which are indeed related to intra-icosahedral bonds of the pentagonal pyramids. The B-C-B angles show a broad distribution nearly from 62º to

148º owing to forming of the different type of C motifs between 50% and 65% B contents. After 70% B range, the first peaks are placed at about 109º in view of tetrahedral angles while the second peak is due to the B-C-B zigzag-like motifs and it shifts from 114º to 121º with increasing B concentrations. On account of the existence of hexagonal angles in the disordered networks, the C-B-C distribution has a moderate peak at around 120º at 50-70% B concentrations. With increasing B content, the main peaks are sharpened, especially at 95% B content, at nearly115º and 128º, resulting from a structure like a bridge between incomplete pentagonal pyramid. The C-C-C angles of 50% B content possess two clear peaks at about 109º and 120º, related to ideal tetragonal and hexagonal angles, respectively. At 70% B concentration, there is a sharp peak at around 112º. The origin of this peak comes from the threefold coordinated structure similar to zigzag shape formed by only three C atoms. And lastly, two apparent peaks of the C-C-C angle distribution function are placed at around 120º and 131º at 75% B content.

Voronoi polyhedral method[221] is a powerful tool to examine the kind of clusters formed around an atom. According to this approach, a polyhedron is notated via several Voronoi index $<n_3, n_4, n_5, n_6>$, where n_i and $\sum n_i$ represent the number of *i*-edge faces of a cluster and its total coordination number, correspondingly. It is known that the main structure of ordered and disordered form of B and B-rich materials consists of quasimolecular B_{12} icosahedron, which comprises ideal pentagonal pyramids. Consequently, in order to further understand the microstructure of the amorphous models as well as to define the geometrical structures, the Voronoi polyhedral approach is used. For this analysis we concentrate mainly on <2,2,2,0> and <2,3,0,0> indices, presenting ideal and defective pentagonal pyramid-like geometries. Figure 5.7 displays their alternation as a function of B concentration. For B atoms, as the B concentration increases, the fraction of <2,2,2,0> type polyhedron raises from 5% to 55%. The frequency of <2,3,0,0> geometry alters from 3% to 16%.

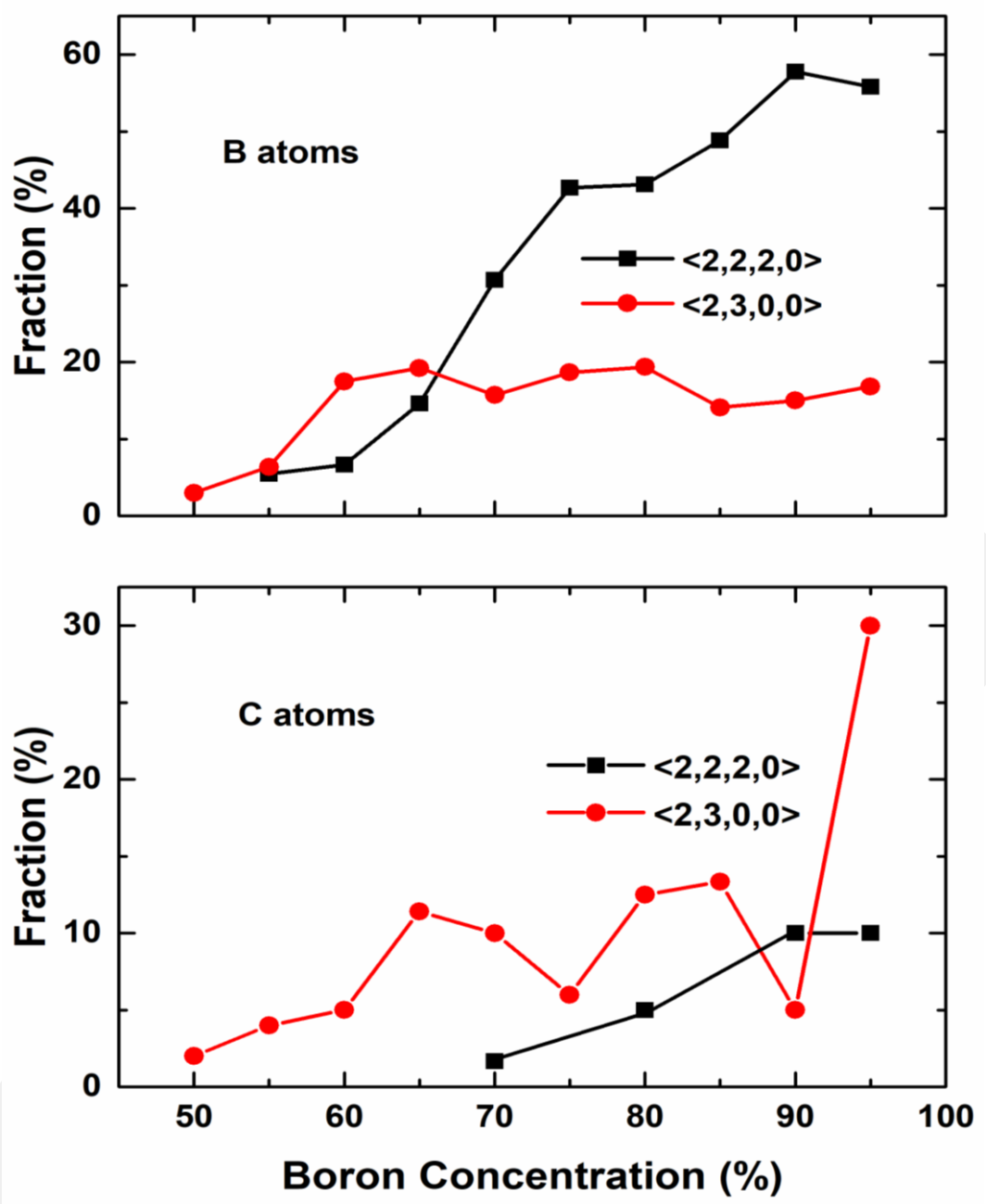

Figure 5.7 Fraction of ideal (<2,2,2,0>) and defective (<2,3,0,0>) pentagonal pyramids.

These analyses suggest that, as expected, the ideal and defective pentagonal pyramid-likes geometries develop around B atom. As for C atoms, the frequency of <2,2,2,0> type motif begins to form at 70% B content and its maximum fraction is 10 %. The portion of <2,3,0,0> structure ranges from 2% to 30%.The examination discloses that some C atoms have a tendency to form pyramid-like structures in amorphous boron carbides as well.

5.3.2. Electronic Properties

B compounds might possess the electronic structure such that they can offer some potential applications such as diodes and thermocouple consisting transistors and thus the analyzing of electronic properties of amorphous networks generated is mandatory in this study. We first focus on c-B_4C and found that its band gap defined as a difference between HOMO-LUMO state is nearly 2.9 eV based on the GGA calculation (Figure 5.8), comparable well with 2.6-3.0 eV[112,123,223–225] predicted in the earlier DFT-GGA/LDA studies but less than 3.84 eV based on a DFT-hybrid exchange functional (HEF) calculation[226]. In order to estimate more accurate band gap energy of the amorphous states, we perform GGA+U calculations by taking the DFT-HEF estimation as our reference. We change the Hubbard potential U (for B-p states because they are more dominant near the Fermi level for both valence and conduction bands) until the band gap energy of c-B_4C is close to the DFT-HEF prediction of 3.84 eV[226]. We find that U= 4.5 eV (for B-p state) yields a band gap of 3.85 eV for c-B_4C in our calculation and the same U is used for all amorphous configurations. The forbidden band gap of the amorphous models shows an increasing trend with increasing B content and is in the range of 0.2-1.47 eV as shown in Figure 5.8. It should be noted here that some mid-gap states near the Fermi level are observed for some amorphous configurations such that their band gap is projected by ignoring them. Considering the disordered nature of the models, one can see that our predictions are comparable with the values of 0.77-1.80 eV in the crystals with B/C=2.4-50[269].

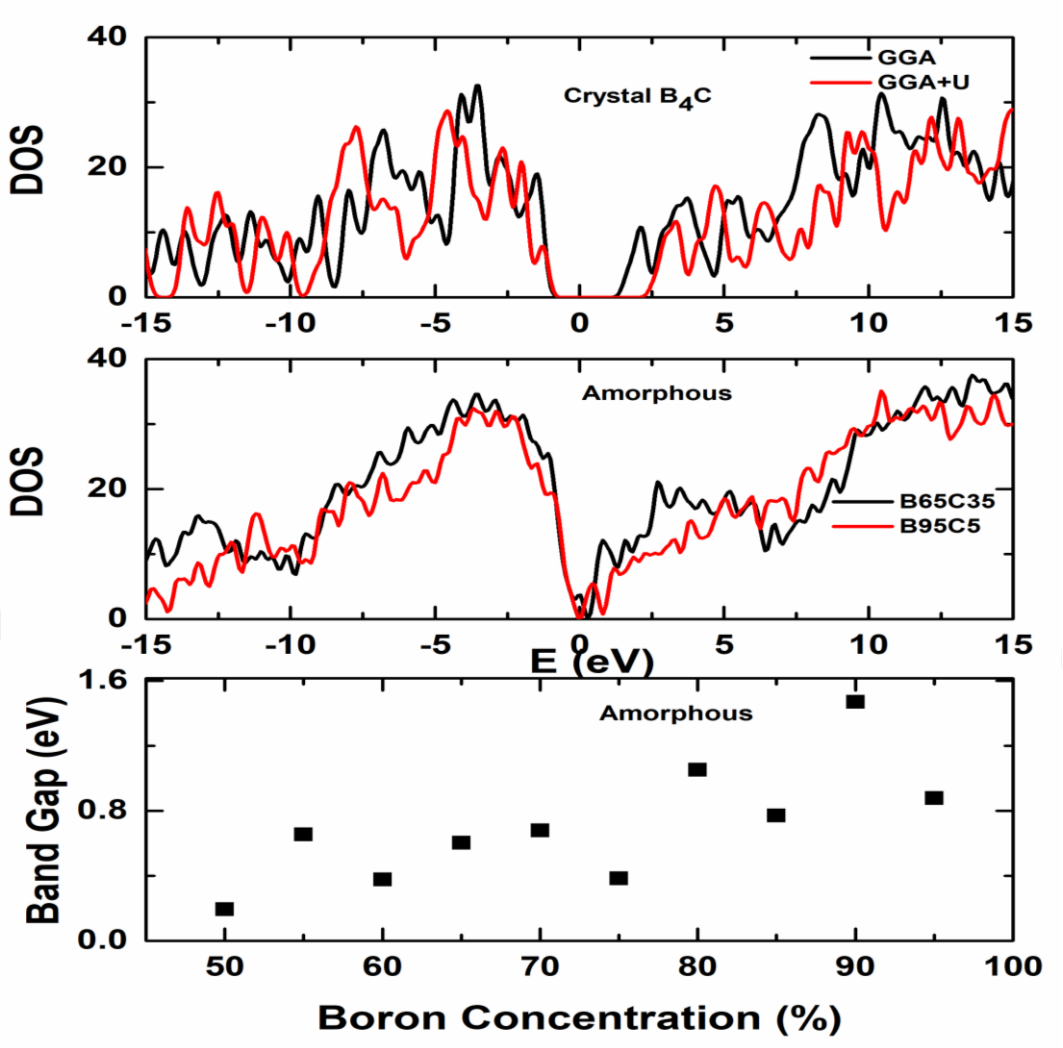

Figure 5.8 The band gap energy of B_4C crystal (top panel). The band gap energy of amorphous forms of $B_{65}C_{35}$ and $B_{95}C_5$ (middle panel). Variation in band gap energy of amorphous materials as a function of B content (bottom panel).

5.3.3 Mechanical Properties

The mechanical descriptions, including bulk modulus, Poisson's ratio, Young modulus, shear modulus, Vickers hardness and Pugh' ratio, are vital to the applications of a material in technology. Therefore, the mechanical features of the amorphous models are inclusively investigated. For comparison purposes, Table 5.1 gives the mechanical properties of some B concentrations in this study along with the data of some related crystal and amorphous materials in the literature.

Table 5.1 The mechanical properties of some B concentrations in this study along with the data of some crystal and amorphous materials in the literature.

	K (GPa)	E (GPa)	μ (GPa)	ν	H (GPa)	References
a-$B_{50}C_{50}$	105	142	56	0.27	~7-9	This study
g-graphite	38					[270]
				0.28		[275]
		23-32	10-13		~2-3	[278]
graphite				0.27		[276]
Amorphous C*		40-145		0.25	~5-15	[277]
a-$B_{80}C_{20}$	170	288	120	0.22	~18	This study
a-B_4C		255-351			~21-34	[220]
c-B_4C	248-274		188-200	0.17-0.18		[201, 230,232]
					~45	[229]
					~42	[220]
a-$B_{85}C_{15}$	193	326	135	0.21	~20	This study
c-$B_{85}C_{15}$			195-197	0.17		[228]
	245	466	197	0.18		[273]
a-$B_{90}C_{10}$	199	370	155	0.19	~23-25	This study
c-$B_{90}C_{10}$	130-183	319-348		0.16-0.21		[228]
	170-194	323-348	132-150	0.16-0.22		[273]
a-$B_{95}C_5$	183	332	139	0.20	~20-23	This study
a-B		320				[279]
γ-B	224		236	0.11		[274]

The bulk modulus (K), the compressibility of a material under pressure, are calculated by fitting the energy -volume relation of each model to the third order Birch-Murnaghan equation of states (Equation 2.44). In the equation, E and E_0 stand for the energy and the equilibrium energy, correspondingly while V and V_0 represent the volume and the equilibrium volume, respectively.K' is the derivative of K respect to pressure ($K' = dK/dP$). Figure 5.9 represents the change in K as a function of B content.

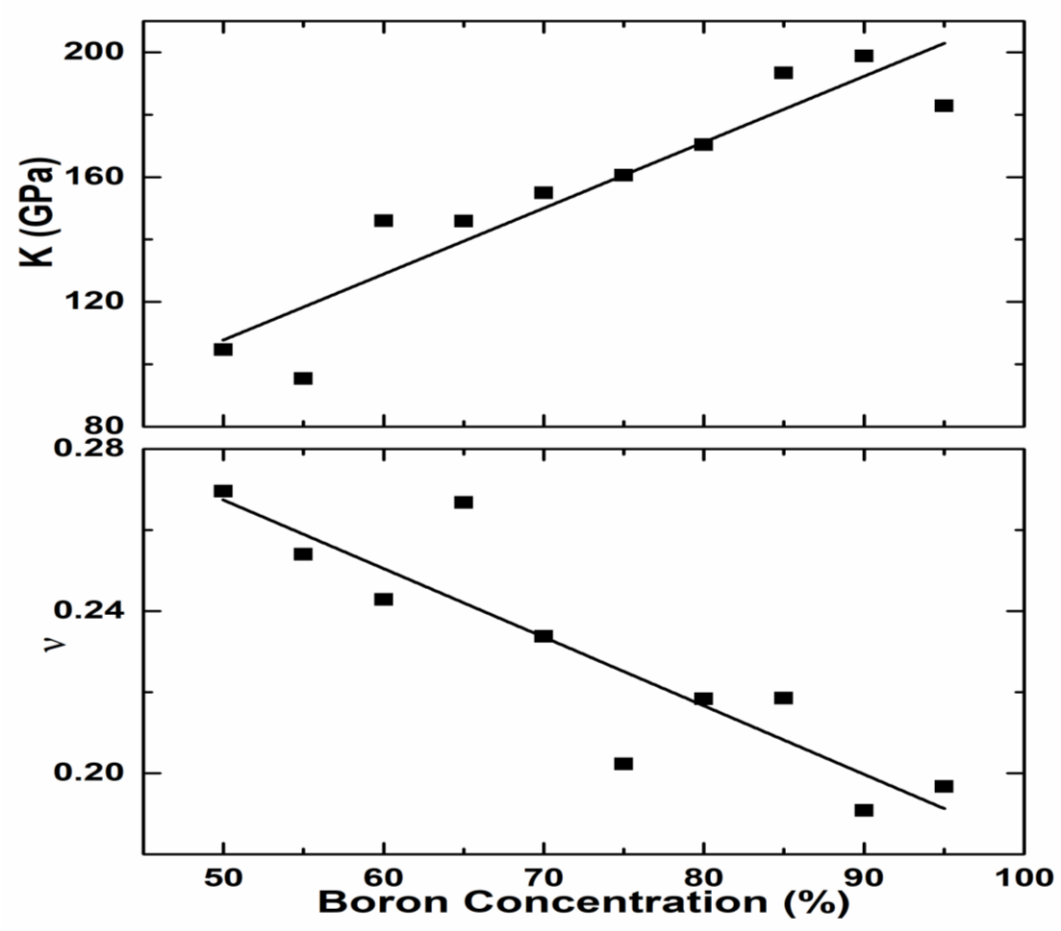

Figure 5.9 Variation in Bulk modulus (K) and Poisson's ratio (ν) as a function of B content.

As can be seen from the figure, it gradually increases. a-$B_{50}C_{50}$ has a value of nearly 105 GPa. The comparison with glassy graphite (g-graphite) (K=38 GPa)[270] suggests that a-$B_{50}C_{50}$ shows better incompressibility relative to g-graphite but it is considerably less than 363 GPa in the diamond-like amorphous carbon[271]. For c-B_4C, our estimation is 245 GPa, comparable with the previous data of 248-274 GPa[201,228–230,272]. On the other hand, its amorphous form has a value of 170 GPa, suggesting a noticeable softening by amorphization. Similar trend is also observed for 85% B concentration; namely, the bulk modulus of a-$B_{85}C_{15}$ (K=193 GPa) is again smaller than 245 GPa in its crystalline form[273]. The K value of a-$B_{90}C_{10}$, about 199 GPa, is larger than 130-183 GPa[228] and 170-194 GPa[273] in its crystalline counterpart. For a-$B_{95}C_5$, it is computed to be nearly 183 GPa. Since there is no data available in the literature for this composition, we compare it with a crystalline B phase (γ-B) whose K is 224GPa[274]. One can see that amorphization causes a decrease in bulk modulus.

Poisson's ratio (ν), described as the ratio of transverse strain to longitudinal strain computed by the application of a uniaxial strain along the principal axes, is estimated using Equation 2.46. As shown in Figure 5.9, ν decreases with increasing B content and lie in the range of nearly 0.27 to 0.20. For a-$B_{50}C_{50}$, it is found to be roughly 0.27, which is rather well overlap with 0.28, 0.27 and 0.25 reported for g-graphite, graphite and amorphous carbon with different sp^3/sp^2 ratios[275–277], respectively. For a-B_4C, ν is about 0.22 and slightly higher than experimental results of 0.17 and 0.18 in c-B_4C [228,229,272]. ν is 0.21 for a-$B_{85}C_{15}$ while its crystalline counterpart has the values of 0.17-0.18[228,273]. For the a-$B_{90}C_{10}$, the ratio is about 0.19, parallel to 0.16-0.22 in c-$B_{90}C_{10}$ [228,273].

Young modulus (E), in other words elastic modulus, stiffness of the material, is characterized with relationship between stress and strain in a material under a uniaxial deformation. E is related to both K and ν values and is practically obtained by way of Equation 2.47. Young modulus computed increases gradually from 140 to 370 GPa with increasing B content as seen in Figure 5.10.

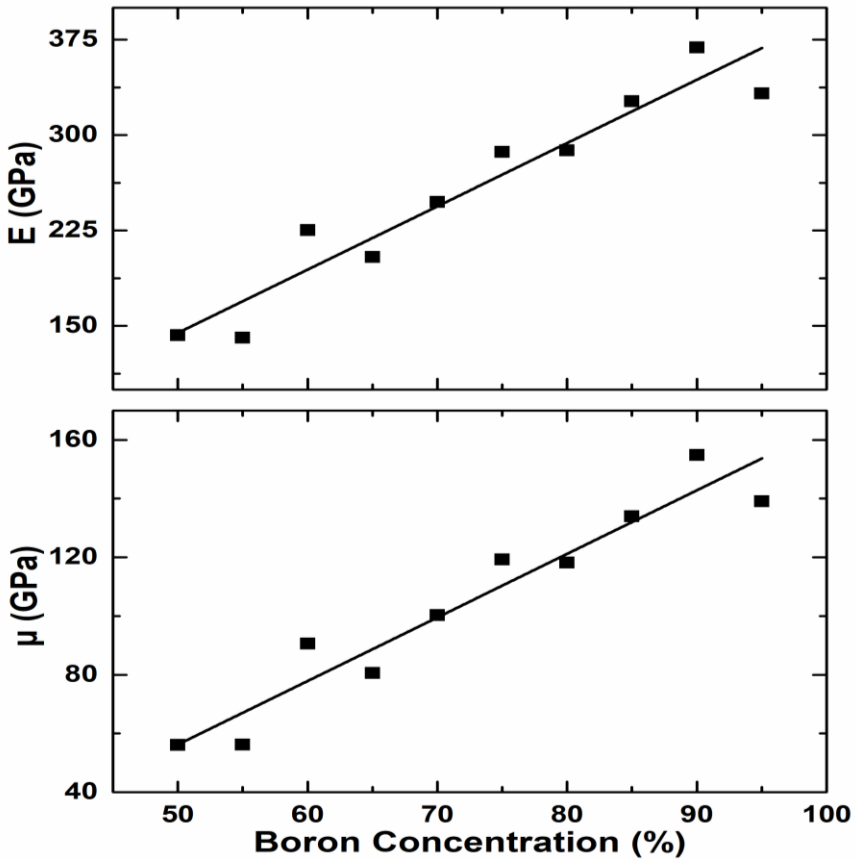

Figure 5.10 Variation in Young's modulus (E) and shear modulus (μ) as a function of B content.

For a-$B_{50}C_{50}$, E is projected to be about 142 GPa while it is 23-32 GPa for g-graphite[278], meaning that this material is more the stiffer than g-graphite. However, in an earlier study on amorphous carbon with different sp^3/sp^2 ratios[277], E is reported as 40-145 GPa, which are parallel to our result for a-$B_{50}C_{50}$. E is nearly 288 GPa in a-B_4C and it is comparable with experimental values of 255-351 GPa in a-B_4C[220]. When a-$B_{85}C_{15}$ is concerned, E is about 326 GPa, noticeably less than 466 GPa[273] in its crystalline form. a-$B_{90}C_{10}$ has the highest value of 370 GPa, as seen Table 5.1, in a good agreement with 319-348 GPa[228] and 323-348 GPa[273] in c-$B_{90}C_{10}$. E is ~332 GPa for a-$B_{95}C_5$, which is close to the experimental measurement of 320 GPa in a-B [279]. Eventually, the higher B content, the stiffer amorphous material forms.

Shear modulus (μ), the ability to resist shear deformation, can be defined as the ratio of shear stress to shear strain of the material within the restricted elastic deformation and can be achieved by using Equation 2.48.

As can be seen from Figure 5.10, μ exhibits a similar behavior with K and E. With increasing B content, μ progressively changes from ~56 GPa to 155 GPa. For a-$B_{50}C_{50}$, μ is computed as 56 GPa that is quite higher than 10-13GPa in g-graphite[278], implying that it shows more resistance to shear deformation, relative to g-graphite. The calculated μ of a-B_4C is about 120 GPa whilst it is about 188-200 GPa in c-B_4C [228,232,272]. Similarly, a noticeable decrease in μ is observed for $B_{85}C_{15}$ composition: it is about 135 GPa in a-$B_{85}C_{15}$ and 195-197 GPa in c-$B_{85}C_{15}$[228,273]. On the other hand, μ is projected as 155GPa for a-$B_{90}C_{10}$, comparable with 132-150 GPa in c-$B_{90}C_{10}$ [273]. Consequently, one can see that the estimated μ values are roughly equal to or less than that of their crystalline counterpart.

Vickers hardness (H_v), a measure of the resistance of a material to deformation, can be useful to determine the correlation between hardness and elastic properties. H_v can be approximately projected by different practical correlations (Equations 2.49-2.52) related to various mechanical properties of a material such as μ and E [173–176].

The alteration of the hardness is illustrated in Figure 5.11 and it rises from ~7 to 25 GPa with increasing B concentration.

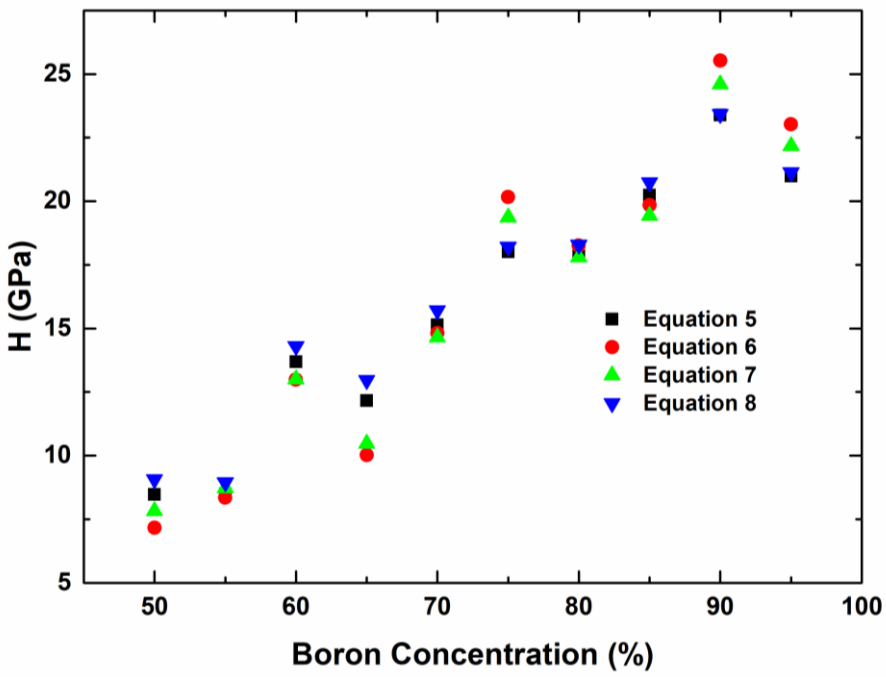

Figure 5.11 Variation in Vickers hardness (H_V) as a function of B content.

The computed H_v value for a-$B_{50}C_{50}$ is in the range of 7-9 GPa, as given in Table 5.1, apparently higher than 2-3 GPa in g-graphite[278] but relatively closer to 5-15 GPa in amorphous carbon having different sp^3/sp^2 ratios[277]. H_v is projected to be 18 GPa for a-B_4C whereas it is reported to be between 20.8 and 33.8 GPa for a-B_4C depending on the deposition temperature (25-900 °C)[220]. So, one can see that our estimation is fairly comparable with the lower limit of the experiment. For its crystalline counterpart, the reported values of 42-45 GPa[231,232,272] are higher than that of a-B_4C. The materials beyond 70% B content have hardness, higher than 20 GPa, indicating that these disordered structures can serve as hard materials.

Pugh ratio ($n=\mu/K$), is a method propounded by Lewandowski[280], to designate whether a material is brittle or ductile by using other mechanical properties. According to this method, if μ/K is higher (or lower) than 0.41-0.43, then material is called as brittle (or ductile). On the other way, ν can be also used to define ductile versus brittle nature of materials and ν value is lower (higher) than 0.31-0.32 is considered to be brittle (ductile). In the last part, Pugh ratio is calculated and presented in Figure 5.12. The computed Pugh ratio is in the range of 0.53-0.77, indicating that all amorphous models own brittle nature. Besides, ν values also support this finding.

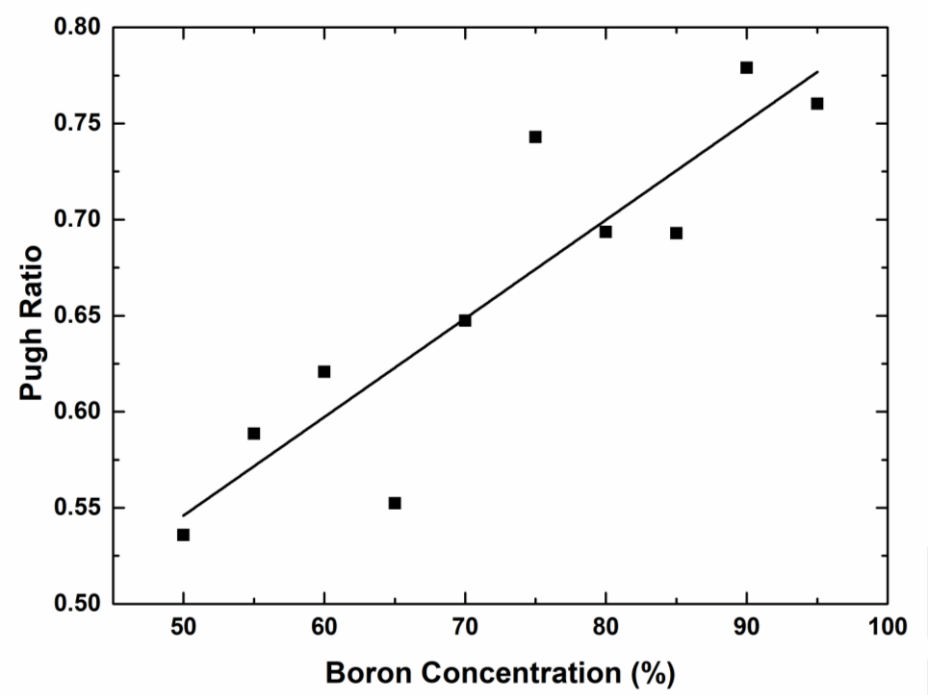

Figure 5.12 Variation of Pugh' ratio as a function of B concentration.

5.4 Discussion

a-$B_{50}C_{50}$ exhibits a mixed state of sp^2 and sp^3 hybridizations and its sp^3/sp^2 ratio is about 61% and hence we believe that a-$B_{50}C_{50}$ is structurally close to the low-density amorphous diamond. Indeed, the materials up to 65% B contents carry essentially the characteristic of amorphous diamond-like structure but it is slightly softer than amorphous diamond-like structure when its mechanical properties considered, which is probably associated with the presence of weaker B-B or B-C bonds in boron carbides, relative to C-C bond and a low sp^3/sp^2 ratio. Since the mechanical properties amorphous diamond strongly depend on the density (or sp^3/sp^2 ratio) and increase with increasing density, high density a-$B_{50}C_{50}$ material with different sp^3/sp^2 ratios, if they are fabricated under pressure, can show some superior properties, similar to amorphous-diamond, for example superhardness.

Beyond 65% contents, the materials show the characters of both amorphous diamond and a-B because sp^3 hybridization around C atoms is still the dominant one. At 70% B content, ideal pentagonal pyramid motifs (C-B_5) develop around C atoms and hence the formation of $B_{11}C$ molecules is expected to occur beyond 65% B concentration. Of course, there might be some uncertainties about this composition

because of the limitations in the simulations, such as time scale and size of the simulation box.

It is believed that c-B_4C consists of $B_{11}C$ icosahedrons with C-B-C intericosahedral chains rather than B_{12} icosahedrons and C-C-C linear chains [201]. It should be noted here that there exist the C-C-C (not linear chains) angles in the model up to 80% B concentration at which the motifs disappear while a few C-C bonds form in a-B_4C. Consequently, a-B_4C does not have C-C-C linear chains, similarly as proposed for its crystalline counterpart. Additionally, we witness the formation of C-B-C bond angles in the models but we do not observe the intericosahedral linear C-B-C chains since B-C_2 configuration does not exist in any model.

General trend in the mechanical properties of amorphous materials is to increase with increasing B content. When the amorphous and crystalline phases of materials having 10-20 C% concentrations (B/C>4) are compared, we notice an opposite trend in the mechanical properties. Namely, the maximum hardness was observed for the stoichiometric composition (c-B_4C) and its surprisingly decreased for nonstoichiometric B_4C (B/C>4 or B/C<4) compositions. For B/C>4 materials, the decrease was explained by the substitution of the stronger B–C bonds with weaker B–B bonds. For the amorphous phases, we believe that the increase in the coordination numbers and the development of more pentagonal pyramid-like topologies are probably responsible for such an increase in the mechanical properties. Note that twofold coordination does not exist in the amorphous forms in these composition ranges but in the crystal.

Via various Vickers hardness equations, it is seen that some B-rich amorphous materials beyond 70% B content have high hardness. Therefore, these materials can be referred to as hard materials. Also, it should be noted that these amorphous materials show semiconducting properties and hence they can offer some potential applications in harsh environments.

5.5 Conclusions

In the current study, for the first time, the structural, electrical and mechanical characters of B-rich amorphous boron carbides (B_xC_{1-x}, $0.50 \leq x \leq 0.95$) have been analyzed by the means of ab initio MD simulations. According to the result of CNs analyses, the mean CN of B atoms changes between 3.22 and 5.70 while that of C atoms

changes from 3.46 to 4.30. The materials up to 65% B content carry essentially the characteristic of amorphous diamond and beyond this content; the materials show the signature of both amorphous diamond and a-B because sp^3 hybridization around C atoms is still the major one in all compositions. The pentagonal pyramid motifs ($C\text{-}B_5$) and hence $B_{11}C$ clusters are expected to develop beyond 60% B concentration. There exist the C-C-C angles in the model up to 80% B concentration at which point they vanish. The intericosahedral linear C-B-C chains do not form in any model because $B\text{-}C_2$ configuration does not happen in any model. By means of four different Vickers hardness formulas, it is found that, some B-rich amorphous materials, specifically after 75% B concentration, own high Vickers hardness and thusly they can be called as hard materials. The HOMO-LUMO band gap calculations expose that all amorphous configurations are semiconductors. All these conclusions are based on 200 atoms amorphous configurations but some of our findings, specifically, the mechanical properties, are comparable with the available date in the literature and thus we believe that these amorphous structures generated offers accurate information about the local structure of these compositions. Nevertheless, the finite size effect and the time scale of simulation cannot be ignored and hence additional investigations on larger systems using reliable machine learning potentials are essential to expose their microstructures and properties in details.

Chapter 6

Conclusions and Future Prospects

6.1 Conclusions

In this thesis, different amorphous boron-based materials were modeled via DFT calculations.

In the first study (Chapter 3), *a*-BN:H models with four different hydrogen concentrations were created and the impression of hydrogenation on the microstructure and electronic features of *a*-BN was scrutinized for all models. When the comparing the *a* -BN:H and *a*-BN models, it was seen that they showed parallel properties locally, however, hydrogenation exhibited some considerable effects on the local arrangement of *a*-BN. For example, in the *a* -BN:H models, the twofold coordinated chain-like motifs did not occur owing to the H passivation of dangling (homopolar) bonds. Moreover, for similar reason, tetragonal-like rings extinguished. Considering the mechanical properties, *a* -BN:H models were exhibited better mechanical features than the pure structure due to the having more sp^3 bonding. However, hydrogenation did not show substantial weight on the electronic structure of *a*-BN.

In a second step (Chapter 4), the structural, mechanical and electrical characters of a-B_4C model were punctiliously assessed. The microstructure of the amorphous model was somewhat coherent with its crystalline counterpart. It was seen that the sixfold coordinated pentagonal pyramid-like structures for B atoms were the fundamental building motifs in a-B_4C. On the other side, for C atoms, the fourfold-coordinated motifs were the main configurations. The amorphous model exhibited semiconducting character and had an energy band gap of nearly 0.15 eV. The Vickers hardness estimation indicated that a-B_4C was a hard material.

And then, in the last study (Chapter 5), amorphous boron carbide compositions having high B contents (B_xC_{1-x}, $0.50 \leq x \leq 0.95$) were steadily constructed and their structural, electrical and mechanical properties were meticulously probed. The

coordination number of not only B but also C atoms increased gradually along with increasing B/C ratio. An amorphous diamond-like local structure was found to be dominant up to 65% B concentration and after which a mixed state of amorphous diamond- and B-like structures was perceived in the models because of the fact that sp^3 hybridization around C atoms was still dominant one for all compositions. The pentagonal pyramid motifs around C atoms were anticipated to appear beyond 65% content. All generated models were semiconducting materials. The mechanical properties gradually increased with increasing B content and some amorphous compositions were proposed to be hard materials by reason of their Vickers hardness estimation.

6.2 Societal Impact and Contribution to Global Sustainability

Materials science is categorized as an interdisciplinary field covering the design, create, and discovery of new and novel materials. Materials scientists generally focus on the comprehending the historical development of a material (processing), investigating and developing the various structures of materials, examining correlation between their structure and properties under different multi-disciplined field such as nanotechnology, biomaterials, metallurgy, and computational materials science etc. In order discover new materials, materials scientists can use different techniques such as various experimental protocols and theoretical methods. It is clear that experimental studies show a key role and are main building due to having tangible results, in materials science. However, certainly, it is accepted that computational researches are also of significant cruciality to define complicated structures, to examine the electronic character, to investigate mechanical properties and thus to develop new and novelty materials. Moreover, it is possible to make trustworthy estimations for the experimental studies by means of the theoretical techniques.

This thesis covers the computational studies of amorphous boron-based materials. In order to recognize local structures of amorphous boron-based materials, knowing relationships between physical features and crystal structure are necessary. Even though there are some experimental efforts as well as limited number of theoretical studies on their atomic structures, the correlation between their physical specialties and crystal structure is not completely clarified yet. Therefore, the studies presented in Chapter 3, 4,

and 5 in this thesis are important. In addition to contribution to the lacks of the literature, another important point of this thesis is that the presented studies are pretty coherent with the technology vision of project of TÜBİTAK having diverse targets (to create boron-based new materials, to enhance semiconducting technology, to product nanotechnology and advance ceramic materials and to develop materials technology etc.) as mentioned comprehensively in the overview section in Chapter 1.

The one of the major problems in the world is limited energy resources decreasing day by day. Boron-based materials, especially boron carbide and boron nitride and their amorphous forms, can play a key role in renewable development since they are the main materials in the semiconducting technology. It is known that semiconducting materials are the fundamental materials, which used in light emitting diodes (LEDs) that can be used in solar, wind or hydropowers.

The articles which emerged from the studies reported in this thesis, are presented in the 'Curriculum Vitae' section at the end of the thesis.

As a result of, the studies in this thesis in several ways can be contributed to global sustainability. To summarize, firstly, it can contribute to materials science as it generates new materials. Secondly, the materials can be used in semiconducting technology. Thirdly, the studies in this thesis are rather parallel to the technology vision of project of TÜBİTAK. And lastly, the thesis can be contributed to the literature by means of the reported articles.

6.3 Future Prospects

Amorphous boron based materials have received substantial attentions due to the superior characters. Hence, they have used various equipped with the latest technology applications ranging from electronic devices to medicine field. However, the essential questions regarding different boron-based materials with amorphous forms are still unsolved and current experimental processes cannot give certain verification at the atomistic level. In addition, there are still limited numbers of theoretical investigations, especially for disordered structures of boron-based materials, in the literature.

In the computational studies, the numbers of atoms in the simulation box and time scale are quite important parameters to obtain certain results. For this reason, by using different quenching rates and various sizes of supercells, different boron-based

materials and their amorphous arrangements can be created for future studies to discover innovative materials.

The main focus on this thesis is structural, mechanical and electrical characterizations boron carbide and boron nitride. However, the behavior of these materials at high pressure has not been investigated yet. According to the literature investigations, it is seen that the experimental enquiries mainly motivated on amorphous zones of boron carbide at high pressure, especially B_4C, whereas computational works were generally related to the underlying mechanism of the amorphization process. Moreover, different amorphous boron-based materials at high pressure have not been studied yet in detail. Therefore, in the future studies, amorphous boron-based materials at high pressure can be probed to understand its behavior under extreme conditions and to see whether a new form (high-density) of amorphous materials can be produced.

BIBLIOGRAPHY

[1] J. X. Prochaska, J. C. Howk, and A. M. Wolfe, “The elemental abundance pattern in a galaxy at z = 2.626,” Nature, 423, 57–59 (2003).

[2] Etimaden - Boron Mınerals, https://www.etimaden.gov.tr/en/boron-minerals (1 October 2022).

[3] N. S. Hosmane, “Boron Science” (2012).

[4] T. S. R. C. Murthy, J. K. Sonber, K. Sairam, S. Majumdar, and V. Kain, “Boron-Based Ceramics and Composites for Nuclear and Space Applications: Synthesis and Consolidation,”Handb. Advance Ceramic Composites, (2019).

[5] M. F. Hawthorne and A. Maderna, “Applications of Radiolabeled Boron Clusters to the Diagnosis and Treatment of Cancer,” Chemical Reviews, 99, 3421–3434 (1999).

[6] S. K. Mellerup and S. Wang, “Boron-Doped Molecules for Optoelectronics,” Trends in Chemistry, 1, 77–89 (2019).

[7] P. M. Georges Moussa, Romain Moury, Umut B. Demirci, Tansel Sener, “Boron-based hydrides for chemical hydrogen storage,” International Journal of Energy Research (2013).

[8] T. S. R. C. Murthy, J. K. Sonber, K. Sairam, R. D. Bedse, and J. K. Chakarvartty, “Development of Refractory and Rare Earth Metal Borides & Carbides for High Temperature Applications,” Materials Today Proceedings, 3, 3104–3113 Elsevier (2016).

[9] A. Paul, J. G. P. Binner, B. Vaidhyanathan, A. C. J. Heaton, and P. M. Brown, “Heat flux mapping of oxyacetylene flames and their use to characterise Cf-HfB2 composites,” Advances in Applied Ceramics, 115, 158–165 (2016).

[10] L. Silvestroni and D. Sciti, “Densification of ZrB2-TaSi2 and HfB 2-TaSi2 ultra-high-temperature ceramic composites,” Journal of the American Ceramic Society, 94, 1920–1930 (2011).

[11] J. K. Sonber, T. S. R. Murthy, C. Subramanian, R. C. Hubli, R. K. Fotedar, and A. K. Suri, “Effect of WSi2 addition on densification and properties of ZrB2,” Advances in Applied Ceramics, 113, 114–119 (2014).

[12] Boron - Element information, properties and uses | Periodic Table, https://www.rsc.org/periodic-table/element/5/boron (1 October 2022).

[13] Boron, https://www.chemeurope.com/en/encyclopedia/Boron.html#History (1 October 2022).

[14] Chemistry Explained, http://www.chemistryexplained.com/elements/A-C/Boron.html (1 October 2022).

[15] W. A. Haseltine, “Boron:Another Form,” 49–50 (1965).

[16] D. N. Sanz, P. Loubeyre, and M. Mezouar, “Equation of State and Pressure Induced Amorphization of [Formula presented]-Boron from X-Ray Measurements up to 100 GPa,” Physical Review Letters, 89, 9–12 (2002).

[17] A. R. Oganov and V. L. Solozhenko, “Boron: A hunt for superhard polymorphs,” Journal of Superhard Materials, 31, 285–291 (2009).

[18] R. M. Elrick, R. A. Sallach, and A. L. Ouellette, “Boron Carbide: Steam Reactions with Cesium Hydroxide and with Cesium Iodide at 1270K in an Inconel 600 System” (1987).

[19] X. Sun, X. Liu, J. Yin, J. Yu, Y. Li, Y. Hang, X. Zhou, M. Yu, J. Li, et al., “Two-Dimensional Boron Crystals: Structural Stability, Tunable Properties, Fabrications and Applications,” Advanced Functional Materials, 27 (2017).

[20] T. Ogitsu, E. Schwegler, and G. Galli, “β-Rhombohedral boron: At the crossroads of the chemistry of boron and the physics of frustration,” Chemical Reviews, 113, 3425–3449 (2013).

[21] D. E. Sands and J. L. Hoard, “Rhombohedral elemental boron,” Journal of the American Chemical Society, 79, 5582–5583 (1957).

[22] A. E. J. McCarty, L. V., Kasper, J. S., Horn, F. H., Decker, B. F., Newkirk, “A new crystalline modification of boron,” 6410 (1957).

[23] B. F. Decker and J. S. Kasper, “The crystal structure of a simple rhombohedral form of boron,” Acta Crystallographica, 12, 503–506(1959).

[24] F. H. Horn, “Zone-refined boron [2],” Journal of Applied Physics, 30, 1612–1613 (1959).

[25] A. R. Oganov, J. Chen, C. Gatti, Y. Ma, Y. Ma, C. W. Glass, Z. Liu, T. Yu, O. O. Kurakevych, et al., “Ionic high-pressure form of elemental boron,” Nature, 457, 863–867(2009).

[26] E. Y. Zarechnaya, L. Dubrovinsky, N. Dubrovinskaia, Y. Filinchuk, D. Chernyshov, V. Dmitriev, N. Miyajima, A. El Goresy, H. F. Braun, et al., “Superhard semiconducting optically transparent high pressure phase of boron,” Physical Review Letters, 102, 8–11 (2009).

[27] M. Vlasse, R. Naslain, J. S. Kasper, and K. Ploog, “Crystal structure of tetragonal boron related to α-AlB12,” Journal of Solid State Chemistry, 28, 289–301 (1979).

[28] B. Albert and H. Hillebrecht, “Boron: Elementary challenge for experimenters and theoreticians,” Angewandte Chemie International Edition, 48, 8640–8668 (2009).

[29] M. J. Van Setter, M. A. Uijttewaal, G. A. De Wijs, and R. A. De Grout, “Thermodynamic stability of boron: The role of defects and zero point motion,” Journal of the American Chemical Society, 129, 2458–2465 (2007).

[30] R. J. Nelmes, J. S. Loveday, D. R. Allan, J. M. Besson, G. Hamel, P. Grima, and S. Hull, “Neutron- and X-ray-diffraction measurements of the bulk modulus of boron,” Physical Review B, 47, 7668–7673 (1993).

[31] W. Gao, “Crystal growth of alpha-rhombohedral boron,” krex.k-state.edu/dspace/handle/2097/4171 (2010).

[32] F. H. Horn, “Boron, Synthesis Structure and Properties,” in Proceeding Conf. Boron, (1960).

[33] S. O. Shalamberidze, G. I. Kalandadze, D. E. Khulelidze, and B. D. Tsurtsumia, “Production of α-rhombohedral boron by amorphous boron crystallization,” Journal of Solid State Chemistry, 154, 199–203 (2000).

[34] F. H. LV McCarty, J.S. Kasper, “A new crystalline modification of boron,” Chemical Society Reviews, 5582, 6410 (1957).

[35] B. Kolakowski, “The space group is R3m. From the macroscopic,” Acta Physica Polonica, 22, 439–440 (1962).

[36] H. F. D. Geist, R. Kloss, “Verfeinerung des β-rhomboedrischen bors” Acta Crystallographica Section B, 26, 1800–1802 (1970).

[37] J. L. Hoard, D. B. Sullenger, C. H. L. Kennard, and R. E. Hughes, “The structure analysis of β-rhombohedral boron,” Journal of Solid State Chemistry, 1, 268–277 (1970).

[38] V. I. Matkovich, “Boron and Refractory Borides,” Springer (1977).

[39] T. Kobayashi, “Icosahedral Boron Frameworks,” Journal of the American Chemical Society, 5507–5508 (1977).

[40] H. Matsuda, T. Nakayama, K. Kimura, Y. Murakami, H. Suematsu, M. Kobayashi, and I. Higashi, “Structural and electronic properties of Li- and Cu-doped β-rhombohedral boron constructed from icosahedral and truncated icosahedral clusters,” Physical Review B, 52, 6102–6110 (1995).

[41] A. Masago, K. Shirai, and H. Katayama-Yoshida, “Crystal stability of α - andβ - boron,” Physical ReviewB, 73, 104102 (2006).

[42] V. L. Solozhenko, O. O. Kurakevych, and A. R. Oganov, “On the hardness of a new boron phase, orthorhombic γ-B28,” Journal of Superhard Materials, 30, 428–429 (2008).

[43] E. Yu Zarechnaya, L. Dubrovinsky, N. Dubrovinskaia, N. Miyajima, Y. Filinchuk, D. Chernyshov, and V. Dmitriev, “Synthesis of an orthorhombic high pressure boron phase,” Science and Technology of Advanced Materials, 9, 044209 (2008).

[44] S. Mondal, S. Van Smaalen, A. Schönleber, Y. Filinchuk, D. Chernyshov, S. I. Simak, A. S. Mikhaylushkin, I. A. Abrikosov, E. Zarechnaya, et al., “Electron-deficient and polycenter bonds in the high-pressure γ-B 28 phase of boron,” Physical Review Letters, 106, 1–4 (2011).

[45] W. H. Han, Y. J. Oh, D. H. Choe, S. Kim, I. H. Lee, and K. J. Chang, “Three-dimensional buckled honeycomb boron lattice with vacancies as an intermediate phase on the transition pathway from α-B to γ-B,” NPG Asia Mater, 9, e400-7 ,Nature Publishing Group, (2017).

[46] J. L. H. A. W. Laubengayedr., T. Hurd, A. E. New Kirk, “Boron. I. Preparation and Properties of Pure Crystalline Boron,” Journal of the American Chemical Society, 65, 1924–1931 (1943).

[47] R. H. JL Hoard, S Geller, “On The Structure of Elementary Boron,” Journal of the American Chemical Society, 73, 1892–1893 (1951).

[48] D. S. JL Hoard, RE Hughes, “The Structure of Tetragonal Boron,” Journal of the American Chemical Society, 80, 4507–4515 (1958).

[49] E. Amberger and K. Ploog, “Bildung der gitter des reinen bors,” Journal of the Less Common Metals, 23, 21–31 (1971).

[50] C. P. Talley, S. La Placa, and B. Post, “A new polymorph of boron,” Acta Crystallographica, 13, 271–272 (1960).

[51] M.VlasseR.NaslainJ.S.KasperK.Ploog, “The crystal structure of tetragonal boron,” Journal of the Less Common Metals, 67, 1–6 (1979).

[52] C. S. Park, J. S. Yoo, and J. S. Chun, “The deposition characteristics and the structural nature of the deposit in the chemical vapour deposition of boron,” Thin Solid Films, 131, 205–214 (1985).

[53] Y. Ma, C. T. Prewitt, H. K. Mao, R. J. Hemley, and G. Zou, “High-pressure high-temperature x-ray diffraction of β-boron to 30 GPa,” Physical Review B, 67, 17, 174116 (2003).

[54] J. Qin, T. Irifune, H. Dekura, H. Ohfuji, N. Nishiyama, L. Lei, and T. Shinmei, “Phase relations in boron at pressures up to 18 GPa and temperatures up to 2200 °c,” Physical Review B, 85, 1, 014107 (2012).

[55] W. Hayami and S. Otani, “Surface energy and growth mechanism of β-tetragonal boron crystal,” The Journal of Physical Chemistry, C111, 10394–10397 (2007).

[56] W. Hayami, “Structural stability and electronic properties of β-tetragonal boron: A first-principles study,” Journal of Solid State Chemistry, 221, 378–383 (2015).

[57] H. Werheit, M. Laux, and U. Kuhlmann, “Interband and Gap State Related Transitions in β-Rhombohedral Boron,” Physica Status Solidi, 176, 415–432 (1993).

[58] D. S. Williams, “Elastic stiffness and thermal expansion coefficient of boron nitride films,” Journal of Applied Physics, 57, 2340–2342 (1985).

[59] R. W. Trice and J. W. Halloran, “Hot-Pressed Boron Nitride / Oxide Ceramic Composites,” Journal of the American Ceramic Society, 65, 2563–2565 (1999).

[60] O. O. Kurakevych and V. L. Solozhenko, “High-pressure design of advanced bn-based materials,” Molecules, 21, 1–16 (2016).

[61] K. Watanabe, T. Taniguchi, and H. Kanda, “Direct-bandgap properties and evidence for ultraviolet lasing of hexagonal boron nitride single crystal,” Nature Materials, 3, 404–409 (2004).

[62] W. Lei, H. Zhang, Y. Wu, B. Zhang, D. Liu, S. Qin, Z. Liu, L. Liu, Y. Ma, et al., “Oxygen-doped boron nitride nanosheets with excellent performance in hydrogen storage,” Nano Energy, 6, 219–224.

[63] D. S. McGregor, T. C. Unruh, and W. J. McNeil, “Thermal neutron detection with pyrolytic boron nitride,” Nucl. Instruments Methods Phys. Res. Sect. A Accel. Spectrometers, Detect. Assoc. Equip, 591, 530–533, (2008).

[64] M. Zheng, Y. Liu, P. Wang, and Y. Xiao, “Synthesis and formation mechanism of cubic boron nitride nanorods in lithium bromide molten salt,” Materials Letters, 91, 206–208, (2013).

[65] S. Noor Mohammad, “Electrical characteristics of thin film cubic boron nitride,” Solid-State Electronics, 46, 203–222 (2002).

[66] J. Eichler and C. Lesniak, “Boron nitride (BN) and BN composites for high-temperature applications,” Journal of the European Ceramic Society, 28, 1105–1109 (2008).

[67] T. Taniguchi, T. Teraji, S. Koizumi, K. Watanabe, and S. Yamaoka, “Appearance of n-type semiconducting properties of cBN single crystals grown at high pressure,” Japanese J.ournal of Applied Physics, Part 2: Letters, 41, 39–42 (2002).

[68] A. N. Caruso, “The physics of solid-state neutron detector materials and geometries,” Journal of Physics: Condensed Matter, 22 (2010).

[69] X. Zhang, J. Meng, “Ultra-wide Bandgap Semiconductor Materials,” Materials Today, 347-419 (2019).

[70] R. T. Paine and C. K. Narula, “Synthetic Routes to Boron Nitride,” Chemical Reviews, 90, 73–91 (1990).

[71] J. D. Caldwell, I. Aharonovich, G. Cassabois, J. H. Edgar, B. Gil, and D. N. Basov, “Photonics with hexagonal boron nitride,” Nature Reviews Materials, 4, 552–567 (2019).

[72] L. Song, L. Ci, H. Lu, P. B. Sorokin, C. Jin, J. Ni, A. G. Kvashnin, D. G. Kvashnin, J. Lou, et al., “Large scale growth and characterization of atomic hexagonal boron nitride layers,” Nano Letters, 10, 3209–3215 (2010).

[73] M. Durandurdu, “Hexagonal nanosheets in amorphous BN: A first principles study,” Journal of Non-Crystalline Solids, 427, 41–45 (2015).

[74] H. P. R. Lide, D. R., & Frederikse, “CRC Handbook of Chemistry and Physics” CRC Press(2005).

[75] A. Lipp, K. A. Schwetz, and K. Hunold, “Hexagonal boron nitride: Fabrication, properties and applications,” Journal of the European Ceramic Society, 5, 3–9 (1989).

[76] Y. Zhang, X. He, J. Han, and S. Du, “Combustion synthesis of hexagonal boron-nitride-based ceramics,” Journal of Materials Processing Technology, 116, 161–164 (2001).

[77] B. J. Choi, “Chemical vapor deposition of hexagonal boron nitride films in the reduced pressure,” Materials Research Bulletin, 34, 2215–2220 (1999).

[78] S. Dai, Z. Fei, Q. Ma, A. S. Rodin, M. Wagner, A. S. McLeod, M. K. Liu, W. Gannett, W. Regan, et al., “Tunable phonon polaritons in atomically thin van der Waals crystals of boron nitride,” Science, 343, 1125–1129 (2014).

[79] J. D. Caldwell, A. V. Kretinin, Y. Chen, V. Giannini, M. M. Fogler, Y. Francescato, C. T. Ellis, J. G. Tischler, C. R. Woods, et al., “Sub-diffractional volume-confined polaritons in the natural hyperbolic material hexagonal boron nitride,” Nature Communications, 5, 1–9 (2014).

[80] A. Woessner, M. B. Lundeberg, Y. Gao, A. Principi, P. Alonso-González, M. Carrega, K. Watanabe, T. Taniguchi, G. Vignale, et al., "Highly confined low-loss plasmons in graphene-boron nitride heterostructures," Nature Materials, 14, 421–425 (2015).

[81] S. Dai, Q. Ma, M. K. Liu, T. Andersen, Z. Fei, M. D. Goldflam, M. Wagner, K. Watanabe, T. Taniguchi, et al., "Graphene on hexagonal boron nitride as a tunable hyperbolic metamaterial," Nature Nanotechnology, 10, 682–686 (2015).

[82] T. T. Tran, K. Bray, M. J. Ford, M. Toth, and I. Aharonovich, "Quantum emission from hexagonal boron nitride monolayers," Nature Nanotechnology, 11, 37–41 (2016).

[83] N. Ooi, A. Rairkar, L. Lindsley, and J. B. Adams, "Electronic structure and bonding in hexagonal boron nitride," Journal of Physics: Condensed Matter, 18, 97–115 (2006).

[84] A. Abdellaoui, A. Bath, B. Bouchikhi, and O. Baehr, "Structure and optical properties of boron nitride thin films prepared by PECVD," Materials Science and Engineering, B47, 257–262 (1997).

[85] V. L. Solozhenko, A. G. Lazarenko, J. P. Petitet, and A. V. Kanaev, "Bandgap energy of graphite-like hexagonal boron nitride," Journal of Physics and Chemistry of Solids, 62, 1331–1334 (2001).

[86] K. P. Loh, I. Sakaguchi, M. N. Gamo, S. Tagawa, T. Sugino, and T. Ando, "Surface conditioning of chemical vapor deposited hexagonal boron nitride film for negative electron affinity," Applied Physics Letters, 74, 28–30 (1999).

[87] Y. Matsui, Y. Sekikawa, T. Sato, T. Ishii, S. Isakosawa, and K. Shii, "Formations of rhombohedral boron nitride, as revealed by TEM-electron energy loss spectroscopy," Journal of Materials Science, 16, 1114–1116 (1981).

[88] Y. Le Godec, D. Martinez-Garcia, V. L. Solozhenko, M. Mezouar, G. Syfosse, and J. M. Besson, "Compression and thermal expansion of rhombohedral boron nitride at high pressures and temperatures," Journal of Physics and Chemistry of Solids, 61, 1935–1938 (2000).

[89] R. M. Kosanke, "Preparation et structure du nitrure de bore," Comptes Rendus de, Academic des Science, 246 (2019).

[90] T. Ishii, T. Sato, Y. Sekikawa, and M. Iwata, “Growth of whiskers of hexagonal boron nitride,” Journal of Crystal Growth, 52, 285–289 (1981).

[91] R. H. Wentorf, “Cubic form of boron nitride,” The Journal of Chemical Physics, 26, 956 (1957).

[92] R. H. Wentorf, “Synthesis of the cubic form of boron nitride,” The Journal of Chemical Physics, 34, 809–812 (1961).

[93] L. Vel, G. Demazeau, and J. Etourneau, “Cubic boron nitride: synthesis, physicochemical properties and applications,” Materials Science and Engineering: B, 10, 149–164 (1991).

[94] D. Litvinov, C. A. Taylor, and R. Clarke, “Semiconducting cubic boron nitride,” Diamond and Related Materials, 7, 360–364 (1998).

[95] D. J. Kester and R. Messier, “Phase control of cubic boron nitride thin films,” Journal of Applied Physics, 72, 504–513 (1992).

[96] F. P. Bunby and R. H. Wentorf, “Direct transformation of hexagonal boron nitride to denser forms,” The Journal of Chemical Physics, 38, 1144–1149 (1963).

[97] N. L. Coleburn and J. W. Forbes, “Irreversible transformation of hexagonal boron nitride by shock compression,” The Journal of Chemical Physics, 48, 555–559 (1968).

[98] V. N. I. N. Dulin, L. V. Al’tshuler, V. Ya. Vashchenko and Zubarev, “Phase Transformation in boron nitride caused by dynamic compression,” Soviet Physics Solid State, 11, 1016 (1969).

[99] A. Onodera, H. Miyazaki, and N. Fujimoto, “Phase transformation of wurtzite-type boron nitride at high pressures and temperatures,” The Journal of Chemical Physics, 74, 5814–5816 (1981).

[100] B. P. Singh, “Characterization of wurtzitic boron nitride compacts,” Journal of Materials Science, 22, 495–498 (1987).

[101] T. Akashi, H. R. Pak, and A. B. Sawaoka, “Structural changes of wurtzite-type and zincblende-type boron nitrides by shock treatments,” Journal of Materials Science, 21, 4060–4066 (1986).

[102] M. Deura, K. Kutsukake, Y. Ohno, I. Yonenaga, and T. Taniguchi, “Nanoindentation measurements of a highly oriented wurtzite-Type boron nitride bulk crystal,” Japanese Journal of Applied Physics, 56 (2017).

[103] A. Onodera, K. Inoue, H. Yoshihara, H. Nakae, T. Matsuda, and T. Hirai, “Synthesis of cubic boron nitride from rhombohedral form under high static pressure,” Journal of Materials Science, 25, 4279–4284 (1990).

[104] R. F. Zhang, S. Veprek, and A. S. Argon, “Anisotropic ideal strengths and chemical bonding of wurtzite BN in comparison to zincblende BN,” Physical ReviewB ,77, 17, 172103 (2008).

[105] S. Yixi, J. Xin, W. Kun, S. Chaoshu, H. Zhengfu, S. Junyan, D. Jie, Z. Sheng, and C. Yuanbin, “Vacuum-ultraviolet reflectance spectra and optical properties of nanoscale wurtzite boron nitride,” Physical ReviewB, 50, 18637–18639 (1994).

[106] N. E. Christensen, “Optical and structural properties of III-V nitrides under pressure,” Physical ReviewB, 50, 4397–4415 (1994).

[107] Z. Pan, H. Sun, Y. Zhang, and C. Chen, “Harder than diamond: Superior indentation strength of wurtzite BN and lonsdaleite,” Physical Review Letters, 102, 1–4 (2009).

[108] Y. Liu, G. (David) Zhan, Q. Wang, D. He, J. Zhang, A. Liang, T. E. Moellendick, L. Zhao, and X. Li, “Hardness of Polycrystalline Wurtzite Boron Nitride (wBN) Compacts,” Scientific Reports, 9, 1–7 (2019).

[109] C. Pallier, J. M. Leyssale, L. A. Truflandier, A. T. Bui, P. Weisbecker, C. Gervais, H. E. Fischer, F. Sirotti, F. Teyssandier, et al., “Structure of an amorphous boron carbide film: An experimental and computational approach,” Chemistry of Materials, 25, 2618–2629 (2013).

[110] S. V. Konovalikhin and V. I. Ponomarev, “Carbon in boron carbide: The crystal structure of B11.4C 3.6,” Russian J.ournal of Inorganic Chemistry, 54, 197–203 (2009).

[111] F. Thévenot, “Boron carbide-A comprehensive review,” Journal of the European Ceramic Society, 6, 205–225 (1990).

[112] V. I. Ivashchenko, V. I. Shevchenko, and P. E. A. Turchi, “First-principles study of the atomic and electronic structures of crystalline and amorphous B4C,” Physical ReviewB, 80, 23, 235208 (2009).

[113] F. De. H. Wöhler, “Du Bore,” Annales de Chimmie et de Physique, 52, 63–92 (1858).

[114] F. and B. M. Thevenot, “Le carbure de bore: matériau industriel performant. 1ère partie: le point des connaissances physico-chimiques,” L’industrie céramique, 732, 655–661 (1979).

[115] R. R. Ridgway, “Boron carbide A new crystalline abrasive and wear-resisting product.,” J Electrochem Soc, 66, 117–133 (1934).

[116] A. I. . Samsonov, G.N, Zhuravlev N.N, “Physicochemical properties of boron-carbon alloys.,” Fiz. Met. i Met. Akad. Nauk SSSR3, 309–313 (1956).

[117] G. S. Zhuravlev, N N; Makarenko, G N; Samsonov, G V; Sinel’nikova, V S; Tsebulya, “Properties and phase studies of boron and carbon systems,” Izvest. Akad. Nauk S.S.S.R., Otd. Tekh. Nauk. Met. i Topl, (1961).

[118] A. W. Weimer, W. G. Moore, R. P. Roach, J. E. Hitt, R. S. Dixit, and S. E. Pratsinis, “Kinetics of Carbothermal Reduction Synthesis of Boron Carbide,” Journal of the American Ceramic Society, 75, 2509–2514 (1992).

[119] O. Conde, A. J. Silvestre, and J. C. Oliveira, “Influence of carbon content on the crystallographic structure of boron carbide films,” Surface and Coatings Technology, 125, 141–146 (2000).

[120] A. K. Suri, C. Subramanian, J. K. Sonber, and T. S. R. Ch Murthy,“ Synthesis and consolidation of boron carbide: A review,”International Materials Reviews, 55 (2010).

[121] V. Domnich, S. Reynaud, R. A. Haber, and M. Chhowalla, “Boron carbide: Structure, properties, and stability under stress,” JJournal of the American Ceramic Society, 94, 3605–3628 (2011).

[122] N. Vast, J. Sjakste, and E. Betranhandy, “Boron carbides from first principles,” Journal of Physics: Conference Series, 176 (2009).

[123] K. Shirai, “Electronic structures and mechanical properties of boron and boron-rich crystals (Part I),” Journal of Superhard Materials, 32, 205–225 (2010).

[124] K. Shirai, “Electronic structures and mechanical properties of boron and boron-rich crystals (Part 2),” Journal of Superhard Materials, 32, 336–345 (2010).

[125] H. Werheit, V. Filipov, U. Kuhlmann, U. Schwarz, M. Armbrüster, A. Leithe-Jasper, T. Tanaka, I. Higashi, T. Lundström, et al., “Raman effect in icosahedral boron-rich solids,” Science and Technology of Advanced Materials, 11 (2010).

[126] N. S. Hosmane, J. A. Maguire, and Z. Yinghuai, “Polyhedral boron cage compounds: An account,” Main Group Chemistry, 5, 251–265 (2006).

[127] M. Bouchacourt and F. Thevenot, “The melting of boron carbide and the homogeneity range of the boron carbide phase,” Journals of the Less-Common Metals, 67, 327–331 (1979).

[128] M. Bouchacourt and F. Thevenot, “Analytical investigations in the BC system,” Journals of the Less-Common Metals, 82, 219–226 (1981).

[129] A. C. O. Ekbom L.B., “Microstructural evaluation of sintered boron carbides with different compositions,” in Proc. 11 th Int. Conf. Sci. Ceram. held Stenungsund, K. S. Carlsson R., Ed., Swedish Ceram. Soc, Gothenburg, Sweden, (1981).

[130] M. Beauvy, “Stoichiometric limits of carbon-rich boron carbide phases,” Journals of the Less-Common Metals, 90, 169–175 (1983).

[131] K. A. Schwetz and P. Karduck, “Investigations in the boron-carbon system with the aid of the electron probe microanalysis,”Journals of the Less-Common Metals, 1, 1–11 (1991).

[132] D. Gosset and M. Colin, “Boron carbides of various compositions: An improved method for X-rays characterisation,” Journal of Nuclear Materials, 183, 161–173 (1991).

[133] TUBITAK, Vizyon 2023, https://www.tubitak.gov.tr/tubitak_content_files/vizyon2023/kimya/kimya_son_surum.pdf (10 October 2022)

[134] J. Thijssen, “Computational physics,”Cambridge University Press (2007).

[135] T. Pang, “An Introduction to Computation Physics,” Cambridge University Press (2006).

[136] R. L. McGreevy, “Reverse Monte Carlo modelling,” Journal of Physics: Condensed Matter, 13 (2001).

[137] L. M.B., “Model creation and electronic structure calculation of amorphous hydrogenated boron carbide,” University of Missouri(2015).

[138] T. Van Mourik, M. Bühl, and M. P. Gaigeot, “Density functional theory across chemistry, physics and biology,” Philosophical Transactions of the Royal Society A: Mathematical, Physical and Engineering Sciences,372, 20120488 (2011).

[139] N. Argaman and G. Makov, “Density functional theory: An introduction,” American Journal of Physics, 68, 69–79 (2000).

[140] W. Kohn, “Nobel lecture: Electronic structure of matter - Wave functions and density functional,” Reviews of Modern Physics, 71, 1253–1266 (1999).

[141] O. R. Born M., “Zur quantentheorie der molekeln.,” Annals of Physics, 389, 714–733 (1927).

[142] B. F., “Über die quantenmechanik der elektronen in kristallgittern.,” Zeitschrift für Physics, 52, 555–600 (1929).

[143] P. Hohenberg and W. Kohn, “Inhomogeneous Electron Gas,” Physical Review, 136, B864–B871 (1964).

[144] R. M. Martin, “Electronic structure, basic theory and pratical methods,” Cambridge University Press (2004).

[145] J. A. Sholl, D.S., Steckel, “Density functional theory: a practical introduction,” John Wiley & Sons(2011).

[146] W. Kohn and L. J. Sham, “Self-Consistent Equations Including Exchange and Correlation Effects,” Physical Review, 140, A1133–A1138 (1965).

[147] D. M. Ceperley and B. J. Alder, “Ground state of the electron gas by a stochastic method,” Physical Review Letters, 45, 566–569 (1980).

[148] S. H. Vosko, L. Wilk, and M. Nusair, “Accurate spin-dependent electron liquid correlation energies for local spin density calculations: a critical analysis,” Canadian Journal of Physics, 58, 1200–1211 (1980).

[149] A. D. Becke, “Density-functional exchange-energy approximation with correct asymptotic behavior,” Physical Review A, 38, 3098–3100 (1988).

[150] Y. Wang and J. P. Perdew, “Correlation hole of the spin-polarized electron gas, with exact small-wave-vector and high-density scaling,” Physical Review B, 44, 13298–13307 (1991).

[151] J. P. Perdew, K. Burke, and M. Ernzerhof, “Generalized gradient approximation made simple,” Physical Review Letters, 77, 3865–3868 (1996).

[152] C. Lee, W. Yang, and R. G. Parr, “Development of the Colle-Salvetti correlation-energy formula into a functional of the electron density,” Physical Review B, 37, 785–789 (1988).

[153] B. J. Alder and T. E. Wainwright, “Phase Transition for a Hard Sphere System,” The Journal of Chemical Physics, 27, 1208–1209 (1957).

[154] B. J. Alder and T. E. Wainwright, “Studies in Molecular Dynamics. I. General Method,” The Journal of Chemical Physics, 31, 459–466 (1959).

[155] A. Rahman, “Correlations in the Motion of Atoms in Liquid Argon,” Physical Review, 136, A405–A411 (1964).

[156] A. Rahman, “Liquid Structure and SelfDiffusion,” The Journal of Chemical Physics, 45, 7, 2585-2592 (1966).

[157] D. C. Rapaport, “The Art of Molecular Dynamics”Cambridge University Press (1995).

[158] R. Iftimie, P. Minary, and M. E. Tuckerman, “Ab initio molecular dynamics: Concepts, recent developments, and future trends,” Proceedings of Natinonal Academy of Science, 102, 6654–6659 (2005).

[159] R. Car and M. Parrinello, “Unified Approach for Molecular Dynamics and Density-Functional Theory,” Physical Review Letters, 55, 2471–2474 (1985).

[160] R. Iftimie, P. Minary, and M. E. Tuckerman, “Ab initio molecular dynamics: Concepts, recent developments, and future trends,” Proceedings of Natinonal Academy of Science, 102, (2005).

[161] M. E. Tuckerman, “Ab initio molecular dynamics: basic concepts, current trends and novel applications,” Journal of Physics: Condensed Matter, 14, R1297–R1355 (2002).

[162] J. Hutter, “Car-Parrinello molecular dynamics,” Wiley Interdisciplinary Reviews: Computational Molecular Science,2, 604–612 (2012).

[163] H. J. Marx, Dominik, “Ab initio molecular dynamics: basic theory and advanced methods.“ ,Cambridge University Press (2009).

[164] H. C. Andersen, “Molecular dynamics simulations at constant pressure and/or temperature,” The Journal of Chemical Physics, 72, 2384–2393 (1980).

[165] M. Parrinello and A. Rahman, “Crystal Structure and Pair Potentials: A Molecular-Dynamics Study,” Physical Review Letters, 45, 1196–1199 (1980).

[166] M. Parrinello and A. Rahman, “Polymorphic transitions in single crystals: A new molecular dynamics method,” Journal of Applied Physics, 52, 7182–7190 (1981).

[167] Amorphous Solid, https://en.wikipedia.org/wiki/Amorphous_solid (24 October 2022)

[168] W. H. Zachariasen, “The atomic arrangements in glass,” Journal of the Ameican Chemical Society, 54, 3841–3851 (1932).

[169] J. M. Soler, E. Artacho, J. D. Gale, A. García, J. Junquera, P. Ordejón, and D. Sánchez-Portal, “The SIESTA method for ab initio order- N materials simulation,” Journal of Physics: Condensed Matter, 14, 2745–2779 (2002).

[170] J. R. Chelikowsky, “Comprehensive Semiconductor Science and Technology”, Elsevier (2011).

[171] J. M. Seminario, “Theoretical and Computational Chemistry”, Elsevier (1999).

[172] N. Troullier and J. L. Martins, “Efficient pseudopotentials for plane-wave calculations,” Physical Review B, 43, 1993–2006 (1991).

[173] D. M. Teter, “Computational alchemy: the search for new superhard materials,” Materials Research Society Bulletin, 23, 22–27 (1998).

[174] X. Q. Chen, H. Niu, D. Li, and Y. Li, “Modeling hardness of polycrystalline materials and bulk metallic glasses,” Intermetallics, 19, 1275–1281, Elsevier (2011).

[175] Y. Tian, B. Xu, and Z. Zhao, “Microscopic theory of hardness and design of novel superhard crystals,” International Journal of Refractory Metals and Hard Materials, 33, 93–106 (2012).

[176] X. Jiang, J. Zhao, A. Wu, Y. Bai, and X. Jiang, “Mechanical and electronic properties of B12-based ternary crystals of orthorhombic phase,” Journal of Physics: Condensed Matter, 22 (2010).

[177] B. T. T. Kelly, “Physics of Graphite,” J. Nucl. Mater, 114, 1983 (1983).

[178] K. K. Kim, A. Hsu, X. Jia, S. M. Kim, Y. Shi, M. Hofmann, D. Nezich, J. F. Rodriguez-Nieva, M. Dresselhaus, et al., “Synthesis of monolayer hexagonal boron nitride on Cu foil using chemical vapor deposition,” Nano Letters, 12, 161–166 (2012).

[179] G. Cassabois, P. Valvin, and B. Gil, “Hexagonal boron nitride is an indirect bandgap semiconductor,” Nature Photonics, 10, 262–266 (2016).

[180] V. L. Solozhenko, I. A. Petrusha, and A. A. Svirid, “Thermal phase stability of rhombohedral boron nitride,” High Pressure Research, 15, 95–103 (1996).

[181] R. Ahmed, F.-E. -Aleem, S. Javad Hashemifar, and H. Akbarzadeh, “First principles study of structural and electronic properties of different phases of boron nitride,” Physica B, 400, 297–306 (2007).

[182] F. P. Bundy and R. H. Wentorf, “Direct Transformation of Hexagonal Boron Nitride to Denser Forms,” The Journal of Chemical Physics, 38, 1144–1149 (1963).

[183] J. Y. Huang, H. Yasuda, and H. Mori, “HRTEM and EELS studies on the amorphization of hexagonal boron nitride induced by ball milling,” Journal of the American Ceramic Society, 83, 403–409 (2000).

[184] S. -I Hirano, T. Yogo, S. Asada, and S. Naka, “Synthesis of Amorphous Boron Nitride by Pressure Pyrolysis of Borazine,” Journal of the American Ceramic Society, 72, 66–70 (1989).

[185] R. Zedlitz, M. Heintze, and M. B. Schubert, “Properties of amorphous boron nitride thin films,” Journal of Non-Crystalline Solids, 198–200, 403–406 (1996).

[186] E. J. M. Hamilton, S. E. Dolan, C. M. Mann, H. O. Colijn, C. A. McDonald, and S. G. Shore, “Preparation of Amorphous Boron Nitride and Its Conversion to a Turbostratic, Tubular Form,” Science, 260, 659–661 (1993).

[187] H. Lorenz and I. Orgzall, “In situ observation of the crystallization of amorphous boron nitride at high pressures and temperatures,” Scripta Materialia, 52, 537–540 (2005).

[188] D. R. Ketchum, A. L. DeGraffenreid, P. M. Niedenzu, and S. G. Shore, “Synthesis of amorphous boron nitride from the molecular precursor ammonia-monochloroborane,” Journal of Materials Research, 14, 1934–1938 (1999).

[189] A. Werbowy, J. Szmidt, A. Sokolowska, A. Olszyna, and S. Mitura, “Fabrication and properties of Mo contacts to amorphous cubic boron nitride (a-cBN) layers,” Diamond and Related Materials, 5, 1017–1020 (1996).

[190] T. Taniguchi, K. Kimoto, M. Tansho, S. Horiuchi, and S. Yamaoka, “Phase Transformation of Amorphous Boron Nitride under High Pressure,” Chemistry of Materials, 15, 2744–2751 (2003).

[191] S. K. Singhal and J. K. Park, “Synthesis of cubic boron nitride from amorphous boron nitride containing oxide impurity using Mg–Al alloy catalyst solvent,” Journal of Crystal Growth, 260, 217–222 (2004).

[192] M. Legesse, M. Nolan, and G. Fagas, “A first principles analysis of the effect of hydrogen concentration in hydrogenated amorphous silicon on the formation of strained Si-Si bonds and the optical and mobility gaps,” Journal of Applied Physics, 115, 203711 (2014).

[193] S. W. King, M. French, J. Bielefeld, M. Jaehnig, M. Kuhn, and B. French, “X-ray photoelectron spectroscopy investigation of the Schottky barrier at a-BN:HCu interfaces,” Electrochemical and Solid-State Letters, 14 (2011).

[194] S. W. King, M. French, J. Bielefeld, M. Jaehnig, M. Kuhn, G. Xu, and B. French, “Valence band offset at the amorphous hydrogenated boron nitride-silicon (100) interface,” Applied Physics Letters, 101 (2012).

[195] D. G. McCulloch, D. R. McKenzie, and C. M. Goringe, “Ab initio study of structure in boron nitride, aluminum nitride and mixed aluminum boron nitride amorphous alloys,” Journal of Applied Physics, 88, 5028–5032 (2000).

[196] Y. Kumashiro, Ed., “Electric Refractory Materials,” Taylor&Francis(2000).

[197] W. T. Klooster, T. F. Koetzle, P. E. M. Siegbahn, T. B. Richardson, and R. H. Crabtree, “Study of the N-H···H-B dihydrogen bond including the crystal structure of BH3NH3 by neutron diffraction,” Journal of American Chemical Society, 121, 6337–6343 (1999).

[198] R. J. Yeo, “Overview of Amorphous Carbon Films,”Ultrathin Carbon-Based Overcoats for Extremely High Density Magnetic Recording, Springer(2017).

[199] M. Topsakal, E. Aktürk, and S. Ciraci, “First-principles study of two- and one-dimensional honeycomb structures of boron nitride,” Physical Review B, 79, 115442 (2009).

[200] B.B. Darwent, “Bond Dissociation Energies in Simple Molecules,” National Standard Reference Data System (1970).

[201] R. Lazzari, N. Vast, J. M. Besson, S. Baroni, and A. Dal Corso, “Atomic structure and vibrational properties of icosahedral B4C boron carbide,” Physical Review Letters, 83, 3230–3233 (1999).

[202] S. Lee, J. Mazurowski, G. Ramseyer, and P. A. Dowben, “Characterization of boron carbide thin films fabricated by plasma enhanced chemical vapor deposition from boranes,” Journal of Applied Physics, 72, 4925–4933 (1992).

[203] A. W. Weimer, “Thermochemistry and Kinetics,” Carbide, nitride and boride materials synthesis and processing, 79-113, Springer(1997).

[204] M. W. Mortensen, P. G. Sørensen, O. Björkdahl, M. R. Jensen, H. J. G. Gundersen, and T. Bjørnholm, “Preparation and characterization of Boron carbide nanoparticles for use as a novel agent in T cell-guided boron neutron capture therapy,” Applied Radiation and Isotopes, 64, 315–324 (2006).

[205] A. Lipp, “Boron Carbide: Production, Properties, Application.,” Technical Rundschau, 58, 1–47 (1966).

[206] R. E. Hoard, J.L., Hughes, “Elemental boron and compounds of high boron content: structure, properties, and polymorphism.,” Chemistry Boron and its Compounds, Wiley (1967).

[207] H. K. Clark and J. L. Hoard, “The Crystal Structure of Boron Carbide,” Journal of the American Chemical Society, 65, 2115–2119 (1943).

[208] N. G. Zhdanov, G.S., Sevast’yanov, “X-ray investigations of boron carbide structure,” ZhFH, 326–335 (1943).

[209] D. Simeone, C. Mallet, P. Dubuisson, G. Baldinozzi, C. Gervais, and J. Maquet, “Study of boron carbide evolution under neutron irradiation by Raman spectroscopy,” Journal of Nuclear Materials, 277, 1–10 (2000).

[210] M. Chen, J. W. McCauley, and K. J. Hemker, “Shock-Induced Localized Amorphization in Boron Carbide,” Science, 80, 299, 1563–1566 (2003).

[211] V. Domnich, Y. Gogotsi, M. Trenary, and T. Tanaka, “Nanoindentation and Raman spectroscopy studies of boron carbide single crystals,” Applied Physics Letters, 81, 3783–3785 (2002).

[212] D. Ge, V. Domnich, T. Juliano, E. . Stach, and Y. Gogotsi, “Structural damage in boron carbide under contact loading,” Acta Materialia, 52, 3921–3927 (2004).

[213] G. Fanchini, V. Gupta, A. B. Mann, and M. Chhowalla, “In Situ Monitoring of Structural Changes in Boron Carbide Under Electric Fields,” Journal of the American Ceramic Society, 91, 2666–2669 (2008).

[214] X. Q. Yan, Z. Tang, L. Zhang, J. J. Guo, C. Q. Jin, Y. Zhang, T. Goto, J. W. McCauley, and M. W. Chen, “Depressurization Amorphization of Single-Crystal Boron Carbide,” Physical Review Letters, 102, 075505 (2009).

[215] Q. An, W. A. Goddard, and T. Cheng, “Atomistic Explanation of Shear-Induced Amorphous Band Formation in Boron Carbide,” Physical Review Letters, 113, 095501 (2014).

[216] Q. An and W. A. Goddard, “Atomistic Origin of Brittle Failure of Boron Carbide from Large-Scale Reactive Dynamics Simulations: Suggestions toward Improved Ductility,” Physical Review Letters, 115, 105501 (2015).

[217] K. Shirai, S. Emura, S. I. Gonda, and Y. Kumashiro, “Infrared study of amorphous B1-xCx films,” Journal of Applied Physics, 78, 3392–3400 (1995).

[218] M. J. Zhou, S. F. Wong, C. W. Ong, and Q. Li, “Microstructure and mechanical properties of B4C films deposited by ion beam sputtering,” Thin Solid Films, 516, 336–339 (2007).

[219] L. G. Jacobsohn and M. Nastasi, “Sputter-deposited boron carbide films: Structural and mechanical characterization,” Surface and Coatings Technology, 200, 1472–1475 (2005).

[220] V. Kulikovsky, V. Vorlicek, P. Bohac, R. Ctvrtlik, M. Stranyanek, A. Dejneka, and L. Jastrabik, “Mechanical properties and structure of amorphous and crystalline B4C films,” Diamond and Related Materials, 18, 27–33 (2009).

[221] N. Medvedev, “The algorithm for three-dimensional voronoi polyhedra,” Journal of Computational Physics, 67, 223–229 (1986).

[222] A. Ö. Çetin and M. Durandurdu, “Hard boron rich boron nitride nanoglasses,” Jounal of the American Ceramic Society, 101, 1929–1939 (2018).

[223] A. Ektarawong, S. I. Simak, and B. Alling, “Effect of temperature and configurational disorder on the electronic band gap of boron carbide from first principles,” Physical Review Materials, 2, 104603 (2018).

[224] D. M. Bylander, L. Kleinman, and S. Lee, “Self-consistent calculations of the energy bands and bonding properties of B12C3,” Physical Review B, 42, 1394–1403 (1990).

[225] A. Ektarawong, S. I. Simak, L. Hultman, J. Birch, and B. Alling, “First-principles study of configurational disorder in B4C using a superatom-special quasirandom structure method,” Physical Review B, 90, 024204 (2014).

[226] H. Wang and Q. An, “Band-Gap Engineering in High-Temperature Boron-Rich Icosahedral Compounds,” TheJournal of Physical Chemistry, C123, 12505–12513 (2019).

[227] W. Manghnani, M. H., Wang, Y., Li, F., Zinin, P., Rafaniello, “Elastic and vibrational properties of B4C to 21 GPa.,” International Conference Science and Technology High Pressure(2000).

[228] J. H. Gieske, T. L. Aselage, and D. Emin, “Elastic properties of boron carbides,” in AIP Conference Proceeding, 231 (1991).

[229] S. Aydin and M. Simsek, “Hypothetically superhard boron carbide structures with a B11C icosahedron and three-atom chain,” Physica Status Solidi: Basic Research, 246, 62–70 (2009).

[230] Y. Shen, G. Li, and Q. An, “Enhanced fracture toughness of boron carbide from microalloying and nanotwinning,” Scripta Materialia, 162, 306–310 (2019).

[231] S. R. Murthy, “Elastic properties of boron carbide,” Journals of Materials Science Letters, 4, 603–605 (1985).

[232] K. A. Schwetz and W. Grellner, “The influence of carbon on the microstructure and mechanical properties of sintered boron carbide,” Journal of the Less Common Metals, 82, 37–47 (1981).

[233] Q. An and W. A. Goddard, “Microalloying boron carbide with silicon to achieve dramatically improved ductility,” The Journal of Physical Chemistry Letters, 5, 4169–4174 (2014).

[234] S. Han, J. Ihm, S. G. Louie, and M. L. Cohen, “Enhancement of Surface Hardness: Boron on Diamond (111),” Physical Review Letters, 80, 995–998 (1998).

[235] M.-L. Wu, J. D. Kiely, T. Klemmer, Y.-T. Hsia, and K. Howard, “Process–property relationship of boron carbide thin films by magnetron sputtering,” Thin Solid Films, 449, 120–124 (2004).

[236] O. A. Golikova, “Boron and boron-based semiconductors.,” Physica Status Solidi (A), Applied Research, 51, 11–40 (1979).

[237] R. Schmechel and H. Werheit, “Correlation between structural defects and electronic properties of icosahedral boron-rich solids,” Journal of Physics: Condensed Matter, 11, 6803–6813 (1999).

[238] D. Emin, “Unusual properties of icosahedral boron-rich solids,” Journal of Solid State Chemistry, 179, 2791–2798 (2006).

[239] D. Emin, “Icosahedral Boron-Rich Solids as Refractory Semiconductors,” Materials Research Society Proceeding, 97, 3 (1987).

[240] J. E. Zorzi, C. A. Perottoni, and J. A. H. da Jornada, “Hardness and wear resistance of B4C ceramics prepared with several additives,” Materials Letters, 59, 2932–2935 (2005).

[241] H. Werheit, “Boron-rich solids: A chance for high-efficiency high-temperature thermoelectric energy conversion,” Materials Science and Engineering, B29, 228–232 (1995).

[242] T. L. Aselage, D. Emin, C. Wood, I. Mackinnon, and I. Howard, “Anomalous Seebeck Coefficient in Boron Carbides,” Materials Research Society Proceeding, 97, 27 (1987).

[243] M. Carrard, D. Emin, and L. Zuppiroli, “Defect clustering and self-healing of electron-irradiated boron-rich solids,” Phys. Rev. B, 51, 11270–11274 (1995).

[244] A. N. Caruso, R. B. Billa, S. Balaz, J. I. Brand, and P. A. Dowben, “The heteroisomeric diode,” Journal of Physics: Condensed Matter, 16, L139–L146 (2004).

[245] N. Hong, J. Mullins, K. Foreman, and S. Adenwalla, “Boron carbide based solid state neutron detectors: the effects of bias and time constant on detection efficiency,” Journal of Physics D: Applied Physics, 43, 275101 (2010).

[246] K. Osberg, N. Schemm, S. Balkir, J. I. Brand, M. S. Hallbeck, P. A. Dowben, and M. W. Hoffman, “A Handheld Neutron-Detection Sensor System Utilizing a New Class of Boron Carbide Diode,” IEEE Sensors Journal, 6, 1531–1538 (2006).

[247] E. Day, M. J. Diaz, and S. Adenwalla, “Effect of bias on neutron detection in thin semiconducting boron carbide films,” Journal of Physics D: Applied Physics, 39, 2920–2924 (2006).

[248] A. N. Caruso, P. A. Dowben, S. Balkir, N. Schemm, K. Osberg, R. W. Fairchild, O. B. Flores, S. Balaz, A. D. Harken, et al., “The all boron carbide diode neutron

detector: Comparison with theory," Materials Science and Engineering: B, 135, 129–133 (2006).

[249] D. E. Grady, "Hugoniot equation of state and dynamic strength of boron carbide," Journal of Applied Physics, 117, 165904 (2015).

[250] R. Bao and D. B. Chrisey, "Chemical states of carbon in amorphous boron carbide thin films deposited by radio frequency magnetron sputtering," Thin Solid Films, 519, 164–168 (2010).

[251] T. Csákó, J. Budai, and T. Szörényi, "Property improvement of pulsed laser deposited boron carbide films by pulse shortening," Applied Surface Science, 252, 4707–4711 (2006).

[252] F. Kokai, M. Taniwaki, K. Takahashi, A. Goto, M. Ishihara, K. Yamamoto, and Y. Koga, "Laser ablation of boron carbide: thin-film deposition and plume analysis," Diamond and Related Materials, 10, 1412–1416 (2001).

[253] F. Kokai, M. Taniwaki, M. Ishihara, and Y. Koga, "Effect of laser fluence on the deposition and hardnessof boron carbide thin films," Applied Physics A: Materials Science and Processing, 74, 533–536 (2002).

[254] C. Ronning, D. Schwen, S. Eyhusen, U. Vetter, and H. Hofsäss, "Ion beam synthesis of boron carbide thin films," Surface Coatings Technology, 158–159, 382–387 (2002).

[255] K. Y. Xie, V. Domnich, L. Farbaniec, B. Chen, K. Kuwelkar, L. Ma, J. W. McCauley, R. A. Haber, K. T. Ramesh, et al., "Microstructural characterization of boron-rich boron carbide," Acta Materialia, 136, 202–214(2017).

[256] C. Cheng, K. M. Reddy, A. Hirata, T. Fujita, and M. Chen, "Structure and mechanical properties of boron-rich boron carbides," Journal of the European Ceramic Society, 37, 4514–4523(2017).

[257] A. Chauhan, M. C. Schaefer, R. A. Haber, and K. J. Hemker, "Experimental observations of amorphization in stoichiometric and boron-rich boron carbide," Acta Materialia, 181, 207–215 (2019).

[258] D. E. Taylor, J. W. McCauley, and T. W. Wright, "The effects of stoichiometry on the mechanical properties of icosahedral boron carbide under loading," Journal of Physics: Condensed Matter, 24 (2012).

[259] M. Ishimaru, R. Nakamura, Y. Zhang, W. J. Weber, G. G. Peterson, N. J. Ianno, and M. Nastasi, “Electron diffraction radial distribution function analysis of amorphous boron carbide synthesized by ion beam irradiation and chemical vapor deposition,” Journal of the European Ceramic Society, 42, 376–382 (2022).

[260] B. J. Nordell, S. Karki, T. D. Nguyen, P. Rulis, A. N. Caruso, S. S. Purohit, H. Li, S. W. King, D. Dutta, et al., “The influence of hydrogen on the chemical, mechanical, optical/electronic, and electrical transport properties of amorphous hydrogenated boron carbide,” Journal of Applied Physics, 118, 035703 (2015).

[261] B. J. Nordell, T. D. Nguyen, A. N. Caruso, S. S. Purohit, N. A. Oyler, W. A. Lanford, D. W. Gidley, J. T. Gaskins, P. E. Hopkins, et al., “Carbon-Enriched Amorphous Hydrogenated Boron Carbide Films for Very-Low- k Interlayer Dielectrics,” Advanced Electronic Materials, 3, 1700116 (2017).

[262] K. Momma and F. Izumi, “VESTA 3 for three-dimensional visualization of crystal, volumetric and morphology data,” Journal of Applied Crystallography, 44, 1272–1276 (2011).

[263] R. Khadka, N. Baishnab, G. Opletal, and R. Sakidja, “Study of amorphous boron carbide (a-BxC) materials using Molecular Dynamics (MD) and Hybrid Reverse Monte Carlo (HRMC),” Journal of Non-Crystalline Solids, 530, 119783 (2020).

[264] S. Krishnan, S. Ansell, J. J. Felten, K. J. Volin, and D. L. Price, “Structure of Liquid Boron,” Physical Review Letters, 81, 586–589 (1998).

[265] R. G. Delaplane, U. Dahlborg, B. Granéli, P. Fischer, and T. Lundström, “A neutron diffraction study of amorphous boron,” Journal of Non-Crystalline Solids, 104, 249–252 (1988).

[266] D. W. Bullett, “Structure and bonding in crystalline boron and B 12 C 3,” Journal of Physics C: Solid State Physics, 15, 415–426 (1982).

[267] M. M. Balakrishnarajan, P. D. Pancharatna, and R. Hoffmann, “Structure and bonding in boron carbide: The invincibility of imperfections,” New Journal of Chemistry, 31, 473 (2007).

[268] D. W. Brenner, “Empirical potential for hydrocarbons for use in simulating the chemical vapor deposition of diamond films,” Physical Review B, 42, 9458–9471 (1990).

[269] A. O. Sezer and J. I. Brand, “Chemical vapor deposition of boron carbide,” Materials Science and Engineering, B79, 191–202 (2001).

[270] X. Wang, Z. X. Bao, Y. L. Zhang, F. Y. Li, R. C. Yu, and C. Q. Jin, “High pressure effect on structural and electrical properties of glassy carbon,” Journal of Applied Physics, 93, 1991–1994 (2003).

[271] L. Tan, H. Sheng, H. Lou, B. Cheng, Y. Xuan, V. B. Prakapenka, E. Greenberg, Q. Zeng, F. Peng, et al., “High-Pressure Tetrahedral Amorphous Carbon Synthesized by Compressing Glassy Carbon at Room Temperature,” TheJournal of Physical Chemistry, C124, 5489–5494 (2020).

[272] W. Manghnani, M.H, Wang, Y., Li, F., Zinin, P., Rafaniello, “Elastic and vibrational properties of B4C to 21 GPa.,” High Press. Sci. Technol., M. F. Manghnani, M.H., Nellis, W.J., Nicol, Ed., 945–948, Universities Press (2000).

[273] T. L. Aselage, D. R. Tallant, J. H. Gieske, S. B. Deusen, and R. G. Tissot, “Preparation and Properties of Icosahedral Borides,” The Physics and Chemistry of Carbides, Nitrides and Borides, Springer(1990).

[274] C. Jiang, Z. Lin, J. Zhang, and Y. Zhao, “First-principles prediction of mechanical properties of gamma-boron,” Applied Physics Letters, 94, 191906 (2009).

[275] X. Jiang, J. W. Zou, K. Reichelt, and P. Grünberg, “The study of mechanical properties of a -C:H films by Brillouin scattering and ultralow load indentation,” Journal of Applied Physics, 66, 4729–4735 (1989).

[276] J.-L. Tsai and J.-F. Tu, “Characterizing mechanical properties of graphite using molecular dynamics simulation,” Materials and Design, 31, 194–199 (2010).

[277] X. Jiang, K. Reichelt, and B. Stritzker, “The hardness and Young’s modulus of amorphous hydrogenated carbon and silicon films measured with an ultralow load indenter,” Journal of Applied Physics, 66, 5805–5808 (1989).

[278] H. M. Hawthorne, “The microindentation hardness behaviour of carbon filaments, glassy carbons, and pyrolytic graphites,” Carbon, 13, 215–223 (1975).

[279] J. M. Maita, G. Song, M. Colby, and S.-W. Lee, “Atomic arrangement and mechanical properties of chemical-vapor-deposited amorphous boron,” Materials and Design, 193, 108856 (2020).

[280] J. J. Lewandowski, W. H. Wang, and A. L. Greer, “Intrinsic plasticity or brittleness of metallic glasses,” Philosophical Magazine Letters, 85, 77–87 (2005).

APPENDIX

Copyrights and Permissions

- Figure 1.5: ‘Reprinted with permission from [*Angew. Chemie - Int. Ed.*48, 8640–8668 (2009)]’. Copyright 2009 John Wiley and Sons
- Figure 1.6: ‘Reprinted with permission from [*Angew. Chemie - Int. Ed.*48, 8640–8668 (2009)]. Copyright 2009 John Wiley and Sons
- Figure 1.7: ‘Reprinted with permission from [*Phys. Rev. Lett.*106, 1–4 (2011)]’. Copyright 2011 American Physical Society
- Figure 1.8: ‘Reprinted with permission from [*J. Solid State Chem.*221, 378–383]’. Copyright 2015 Elsevier
- Figure 1.9: ‘Reprinted with permission from [*J. Mater Today.*, 347-419 (2019)]. Copyright 2019 Elsevier
- Figure 1.10: ‘Reprinted with permission from [*J. Am. Ceram. Soc.*94, 3605–3628 (2011)]’. Copyright 2011 John Wiley and Sons
- Figure 1.11: ‘Reprinted with permission from [*J. Am. Ceram. Soc.*94, 3605–3628 (2011)]’. Copyright 2011 John Wiley and Sons

CURRICULUM VITAE

EDUCATION

2007-2011	**B.Sc.,** Erciyes University, Physics, Kayseri/TURKEY
2011-2013	**M.Sc.,** Erciyes University, Institute of Science and Technology, Atoms and Molecules Physics Department, Kayseri/TURKEY
2017-2023	**Ph.D.**, Abdullah Gül University, Institute of Science and Technology, Materials and Mechanical Engineering Department, Kayseri/TURKEY

SUPPORTED PROJECTS

2017-2020	'B-Rich Amorphous Materials', TÜBİTAK 1001 Project, 117M372, Scholar.

SCHOLARSHIP/GRANT

Scholarships

2018-2021	**TÜBİTAK**, 2211-C National PhD Scholarship Program in the Priority Field in Science and Technology
2017-2021	**YÖK**, 100/2000 Priority Areas Doctorate
2007-2010	**Higher Education Student Loans and Dormitories Institution**, Undergraduate Scholarship

Awards

2010-2011	First Place Graduation, Department of Physics, Erciyes University

PUBLICATIONS

Journals That Entered SCI and SSCI Indexes

J1) T. A. Üçhöyük, M. Durandurdu, Hydrogenated amorphous boron nitride: A first principles study published in Journal of Non-Crystalline Solids (Aug. 2018)

J2) T. A. Yıldız, M. Durandurdu, Amorphous boron carbide from ab initio simulations published in Computational Materials Science (Jan. 2020)

J3) T. A. Yıldız, M. Durandurdu, Stoichiometric amorphous boron carbide (BC) published in Journal of Materials Science (July 2020)

J4) T. A. Yıldız, M. Durandurdu, Ab-initio study of boron-rich amorphous boron carbides published in Journal of the American Ceramic Society (Jan. 2023)

Refereed Congress / Symposium Publications in Proceedings

C1) T. A. Üçhöyük, M. Durandurdu, Amorphous Boron Carbide From Ab-initio Simulations, 34th Turkish Physical Society International Physical Congress, Bodrum, Muğla, Turkey (Sep. 2018)

C2) M. Durandurdu, A. Ö. Çetin, T. A. Üçhöyük, CMCM Intermediate Phase For The HCP-To-BCC Phase Transition in Magnesium, IMSTEC 2018: 3rd International Conference on Material Science and Technology in Cappadocia, Nevşehir, TURKEY (Sep. 2018)

C3) T. A. Yıldız, M. Durandurdu, Hydrogenated Amorphous Boron Nitride: A First Principles Study, CSC2018: International Computational Science Congress, Amasya, Turkey (Oct. 2018)

C4) T. A. Yıldız, M. Durandurdu, Atomic Structure of Amorphous B_9C, CSC2018: International Computational Science Congress, Amasya, Turkey (Oct. 2018)

C5) T. A. Yıldız, M. Durandurdu, Amorphous Phase of Boron Carbide, MSNG2019: 6th International Conference on Materials Science and Nanotechnology for Next Generation, Niğde, Turkey (Oct. 2019)